CHALMERS

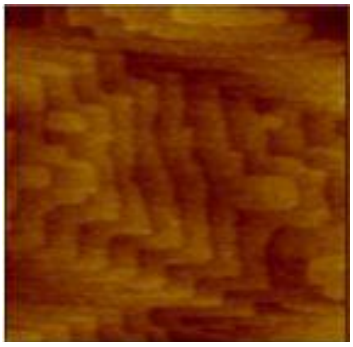
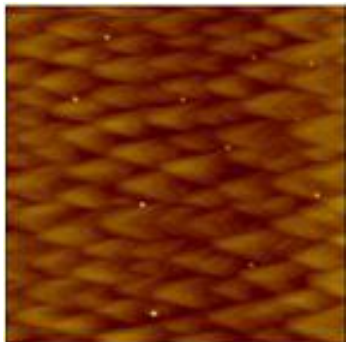

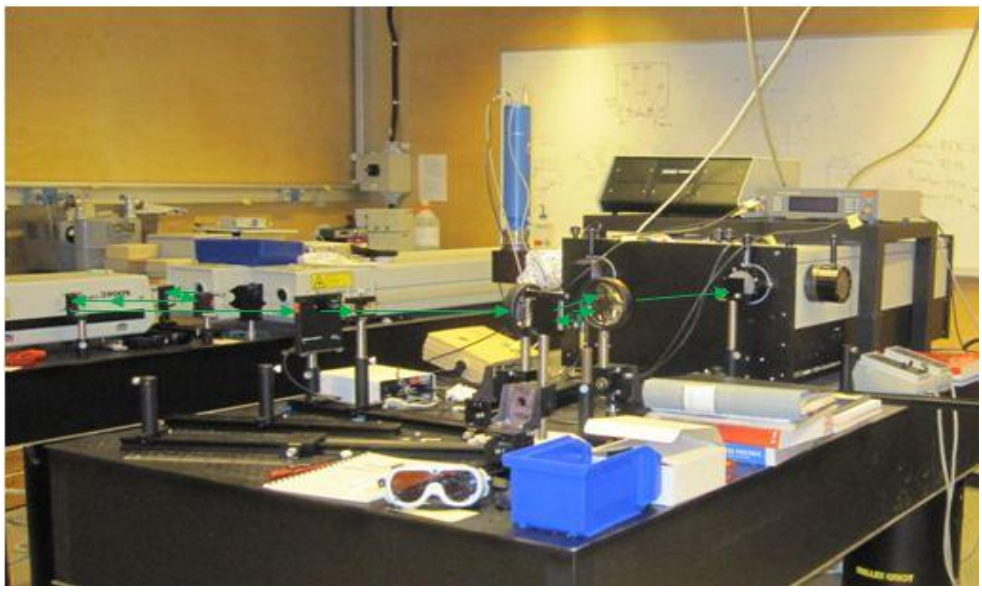

Characterization of Bismuth Containing Compounds

Master of Science Thesis in Wireless and Photonics Engineering

IVY SAHA ROY

Photonics Laboratory
Department of Microtechnology and Nanoscience – MC2
CHALMERS UNIVERSITY OF TECHNOLOGY
Gothenburg, Sweden, 2012

Thesis for the degree of Master of Science in Wireless and Photonics Engineering

Characterization of Bismuth Containing Compounds

Ivy Saha Roy

(আইভী সাহা রায়)

Photonics Laboratory

Department of Microtechnology and Nanoscience – MC2

CHALMERS UNIVERSITY OF TECHNOLOGY

Gothenburg, Sweden 2012

Characterization of Bismuth Containing Compounds

Ivy Saha Roy

Photonics Laboratory
Department of Microtechnology and Nanoscience – MC2
CHALMERS UNIVERSITY OF TECHNOLOGY
SE-412 96, Gothenburg, Sweden
Telephone: +46 (0) 31 772 1000

Cover: Atomic force microscopy (AFM) height images of GaSbBi from mirror-like surface for 1x1 μm^2 (top-left), 10x10 μm^2 (top-right) scan size, and Photoluminescence (PL) system with Room Temperature components set-up (bottom).

Printed by Reproservice, Chalmers University of Technology
Gothenburg, Sweden, June 2012

To:

My Parents

(Anjana Rani Saha &

Nepal Chandra Ray)

Abstract

New semiconductor materials with more beneficial properties are continuously demanding for device applications. The heaviest group V and least studied bismuth containing compounds have potential applications in electronics, optoelectronics, thermoelectric field and also in fundamental physics. Dilute bismides offer large bandgap bowing in valence band by shifting up the valence band edge. This property offers a grand freedom to engineer band structure of semiconductors for potential high-speed electronic and infrared optoelectronic applications. Also it provides a large spin orbit coupling effect which is useful to suppress inter-valence band Auger recombination processes in 1.55 μm lasers. The potential applications for dilute bismides alloys are expected in heterostructure bipolar transistors, light emitting devices, laser diodes and solar cells. Another Bi-containing material Bi_2Te_3 has great thermoelectric property; this property can be used for the applications of cooling different types of devices and for power generation from waste heat.

In this research project, different features have been found and studied for different Bi containing compounds. The samples were grown by a Riber Compact21 MBE system with varying growth temperatures and Bi flux. MBE grown Bismuth containing compounds GaSbBi, GaAsBi, InGaAsBi QW, InSbBi and also Bi_2Te_3 are investigated by atomic force microscopy (AFM), X-ray diffraction (XRD) and Photoluminescence (PL) techniques and then surface morphologies, structural and optical properties are explored from these characterizations, respectively. The MBE grown $GaSb_{1-x}Bi_x$ thin films are established for the first time. Strategies have been taken care of to avoid the formation of Bi droplets and enhance Bi incorporation. From XRD and AFM, maximum Bi incorporation with smooth surface has been obtained for growth temperature of 370 °C and then saturation occurs. InGaAsBi QW samples are characterized by PL at room temperature (RTPL) and also at low temperature (LTPL) for different sample positions and temperatures, respectively. When Bi is incorporated, 10 times higher PL intensity has been achieved comparing with the reference InGaAs QW sample. For Bi_2Te_3 samples grown on Si substrates, growth temperature of 240°C showed the best feature both in AFM and XRD characterizations.

Since this project on Bi-containing compounds is still under experimental demonstration, there is a lot to do for improving the material quality. One important future goal of this project is to establish the relation between the fundamental physical parameters such as lattice constant, bandgap and effective mass etc and the Bi composition. Getting hold of improved quality Bi containing QWs at 1.55 μm is another goal of this research in future. The future Bi containing compounds research is expected to be accelerated at a much fast pace.

Keywords: molecular beam epitaxy, atomic force microscopy (AFM), photoluminescence (PL), X-ray diffraction (XRD), dilute bismide, band gap bowing effect, GaSbBi, GaAsBi, InSbBi, InGaAsBi, Bi_2Te_3.

Acknowledgement

First of all, I would like to announce my biggest gratitude to my examiner, Professor Shumin Wang, to accept me for this challenging project and to give me opportunity to work on this excellent research field. His kind discussion and suggestions made my thesis work possible to be well-wrapped.

A very special and big gratitude goes to my supervisor Yuxin Song. It's a real great pleasure for having such a kind person as my supervisor. During my thesis work, he kept infinite patience to answer my hundreds of silly queries and questions. I am forever appreciative for his nice helps and discussions of every difficulties and guidance throughout the project. I learnt a lot from him.

I love to thank Professor Anders Larsson for his warm welcome to Photonics Lab. I also like to thank all other Professors, PhD students, and rest of the members of Photonics lab to fashion such a comfortable and friendly working environment for me.

My deepest gratitude goes to my parents and all of my family members for their love, well wish and encouragement that helped me all time to move forward, even staying far from them in abroad.

Last but not least, I owe my cordial thank to all of my friends for mental supports that they have given to me all time and for all fun.

Ivy Saha Roy

Gothenburg, Sweden

January, 2012

Publications

The thesis is end up with the following publications:

Journal Papers:

[A] Y. X. Song, S. M. Wang, I. S. Roy, P. X. Shi, and A. Hallen, "Growth of $GaSb_{1-x}Bi_x$ by molecular beam epitaxy", *J. Vac. Sci. Technol.*, B **30** (2), 02B114-7 (2012).

[B] Y. X. Song, S. M. Wang, I. S. Roy, P. X. Shi, and A. Hallen, "MBE growth and lattice contraction of $GaSb_{1-x}Bi_x$ thin films", *Journal Manuscript*.

Other papers not included in this thesis:

International conference papers:

[I] S. M. Wang, Y. X. Song, and I. S. Roy, "Bismuth incorporation and lattice contraction in GaSbBi and InSbBi", *13th International Conference on Transparent Optical Networks (ICTON 2011)*, Stockholm, Sweden, June 2011 (invited talk).

[II] Y. X. Song, S. M. Wang and I. S. Roy, "Molecular Beam Epitaxy Growth of $GaSb_{1-x}Bi_x$", *18th North American Molecular Beam Epitaxy Conference (NAMBE)*, San Diego, USA (2011).

List of Acronyms and Abbreviations

AFM	Atomic Force Microscopy
Ar^+	Argon Ion
BEP	Beam Equivalent Pressure
Bi	Bismuth
Bi_2Te_3	Bismuth Telluride
CCD	Charge-Coupled Device
eV	Electron Volt
FWHM	Full width Half Maximum
Ga	Gallium
GaAs	Gallium Arsenide
GaAsBi	Gallium Arsenide Bismide
GaSb	Gallium Antimonide
GaSbBi	Gallium Antimonide Bismide
Ge	Germanium
HBT	Heterojunction Bipolar Transistor
InGaAsBi	Indium Gallium Arsenide Bismide
InP	Indium Phosphide
InSb	Indium Antimonide
InSbBi	Indium Antimonide Bismide
LTPL	Low Temperature Photoluminescence
MBE	Molecular Beam Epitaxy
MOVPE	Metal Organic Vapor Phase Epitaxy
PL	Photoluminescence
QL	Quintuple Layer
QW	Quantum Well

RHEED	Reflective High-Energy Electron Diffraction
RMS	Root Mean Square
RTPL	Room Temperature Photoluminescence
Sb	Antimony
SFM	Scanning Force Microscopy
Si	Silicon
SI	Semi-Insulating
SPM	Scanning Probe Microscopy
STM	Scanning Tunneling Microscopy
T_g	Growth Temperature
UHV	Ultra High Vacuum
UV	Ultra Violet
XRD	X-Ray Diffraction

Contents

Chapter 1

1. Introduction

Because of a number of interesting material properties, striking interests have been observed on Bismuth containing compounds in last few years. Bismuth is the heaviest group V, non-toxic, non-radioactive and least-electronegative element, which has a large atomic radius. Bismuth containing compounds have potential applications in electronics, optoelectronics, thermoelectric field and also in fundamental physics. The interesting properties of Bi are the surfactant effect, large bandgap bowing effect [1] and strong spin-orbit coupling [2] for its incorporation into normal III/V materials. For dilute Bismides, only the large bandgap bowing effect and the strong spin-orbit coupling property are considered. By adding a small amount of Bi atoms in conventional III-Vs, large bandgap bowing effect, i.e. lower bandgap between conduction band and valence band, can be achieved. Incorporation of Bi is predicted for initiating large spin-orbit split for suppressing Auger recombination in 1.55 μm lasers [3]. A schematic view of group V elements of periodic table is shown in Figure 1.1.

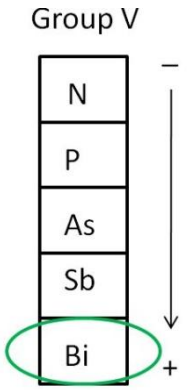

Figure 1.1: Group V elements in periodic table; the marked one is, 'Bismuth', the last and least studied element in this group.

By using the above discussed properties, it is possible to improve material quality and wavelength extension of lasers and photo-detectors, and also less temperature dependent device performances are expected. Other Bi containing materials such as Bi_2Te_3 are predicted for having a great blow on thermoelectric cooling and power generation because of its superior thermoelectric performance at room temperature [4] [5]. The very recent predicted application of Bi_2Te_3 is topological insulator, which is under experimental demonstration

now. Dilute bismides e.g., GaAsBi, InGaAsBi, GaSbBi and InSbBi have been grown for optoelectronic devices; whereas, Bi_2Te_3 bulk structures have been grown for the application of thermoelectric cooling.

Because of ultra high vacuum growth environment and possible low growth temperature (Tg), molecular beam epitaxy (MBE) method is used to produce bismuth containing compound materials. The samples were grown by a Riber Compact21 MBE system with varying growth temperatures and Bi flux. Atomic force microscopy (AFM) is used to characterize surface morphology of both dilute bismides and Bi_2Te_3 materials and photoluminescence (PL) measurement technique has been operated to characterize optical properties of dilute bismides quantum wells (QWs).

The potential application for dilute bismides alloys are expected in transistors, light emitting devices and solar cells. Normally the output amplifiers of portable wireless devices have relatively high power consumption [6]. Bandgap bowing effect of incorporated dilute Bi into normal III/V materials can be utilized to reduce power consumption of heterojunction bipolar transistors (HBTs) [7] [8] [9]. 0.9 – 1.1 eV band gap layer in four junction solar cells grown on Ge substrates is another potential application of the dilute bismides [6]. Both the electronic properties and the surface morphology of the deposited layers can be improved by using Bi as a surfactant. Many promising device applications of Bi containing compounds have already been recognized [6]. In future, the Bi containing compounds research can be divided into different areas including materials science, electronic properties and devices. The large increase in spin orbit splitting for electrons is attractive to make spintronic devices feasible [6].

1.1 Motivations

Both dilute nitrides and bismides have large bandgap bowing effect. Dilute nitride is renowned for its large bandgap bowing effect by lowering the conduction band edge and providing better confinement for electrons, whereas, dilute bismides offer large bandgap bowing in valence band by lowering the valence band edge and provides large valence band offset to confine holes. A schematic illustration of band gap bowing property for a dilute bismide, GaAsBi, is shown in Figure 1.2. This property offers a grand freedom to engineer band structure of semiconductors for potential applications. Dilute bismide provides a large spin orbit coupling effect and this property is useful to suppress inter-valence band Auger recombination processes [3]. Moreover, only gas source can be used to grow dilute nitride

containing materials in MBE. On the other hand, both solid and gas sources can be used for growing dilute Bi containing materials by MBE system. The motivation to work on Bi_2Te_3 material is its great thermoelectric property, which has a handsome number of applications for cooling different types of devices and for power generation from waste heat.

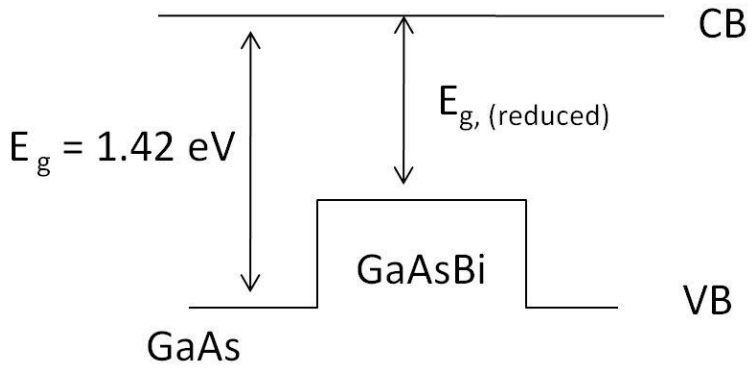

Figure 1.2: Schematic illustration of band gap bowing property for GaAsBi.

Chapter 2

2. Molecular beam epitaxy (MBE) growth and property of Bismuth (Bi) containing compounds

2.1 MBE growth system

Molecular beam epitaxy (MBE) is a sophisticated and finely controlled multipurpose technique to grow thin epitaxial films, such as metal, semiconductor and insulator structures [10]. The meaning of epitaxy is the preparation of atoms on a well-arranged substrate. The three important factors to define MBE technique are the thermal energy molecular or atomic beams, substrate with elevated temperature or growth temperature and high vacuum (typical range for background pressure 10^{-6} to 10^{-9} torr) or ultra-high vacuum environment (typical range for background pressure up to 10^{-11} torr) [11]. At an appropriate temperature for chemical reaction and epitaxy, thin films are grown by gradually evaporating materials on single-crystal in MBE [10]. Because of the low growth rate (generally around 1 monolayer per second), it is possible to grow thin films epitaxially up to the sub-monolayer level with a precise thickness control [11]. Since MBE has practiced enormously rapid growth on many applications, such as electronics, optoelectronics, ferromagnetics etc., over the past few years, it is now one of the most advanced and well-known epitaxial techniques to grow state-of-the-art devices [10] [11]. During the growth, the *in-situ* characterization can be considered by using reflective high-energy electron diffraction (RHEED) to examine the surface reconstruction process and to calibrate the growth rate. This is a big advantage of using MBE over other technologies [11]. Other advantages of MBE Technique are the clean growth environment, precise control of the beam fluxes and growth conditions, and compatibility with other high vacuum thin-film processing methods.

Figure 2.1: A Riber Compact21 MBE system model

Figure 2.1 shows a Riber Compact21 MBE system model, which is a very flexible and affordable MBE system designed for materials research. It has *in-situ* characterization abilities and all other essential MBE tools to grow high quality semiconductor materials. This system consists of the growth chamber, pumping system and wafer handling system. Everything starts from the wafer handling system. The in-between step before epitaxy is the buffer or preparation chamber, which is a comprehensive and self-governing chamber with its own control and pumping system. The growth chamber, a vertical UHV reactor, is situated in the heart of the system and is designed for use with solid, gas, or special sources. In order to eliminate any type of contamination during growth, facing down wafers are planned. To reach high level of layer performances, the effusion cells have been improved for this MBE system model [10].

2.2 Dilute Bi containing compounds

From the late 1970s, research has been carried out to reach the narrowest possible band gap of III-V materials for long wavelength infrared detectors by growing InSbBi bulk materials [12] [13] [14]. Strong research has also been employed after realizing the epitaxial growth of GaAsBi and related materials by metal organic vapor phase epitaxy (MOVPE) in 1998 [15] and by molecular beam epitaxy (MBE) in 2003 [16]. Dilute GaAsBi pioneers a large spin-orbit split property that is recommended to use for suppressing Auger recombination for 1.55

μm lasers on GaAs [3]. The schematic illustration for spin-orbit coupling is shown in Figure 2.2. The first time demonstrated $GaSb_xBi_{1-x}$ material has huge potentials for near and mid wavelength infrared optoelectronics applications [17] [18]. Some examples of applications, such as high performance solar cells, light emitting materials with temperature-insensitive output wavelengths, low power consumption transistors for wireless devices etc. have need of semiconductor materials with new properties [6]. Dilute Bismuth containing compounds are supposed to have potential applications in transistors, light emitting devices and solar cells. If dilute Bi alloys are incorporated into the base of a heterojunction bipolar transistor (HBT), it is expected that it will reduce power consumption of devices with the help of bandgap bowing property of dilute Bi [7] [8] [9].

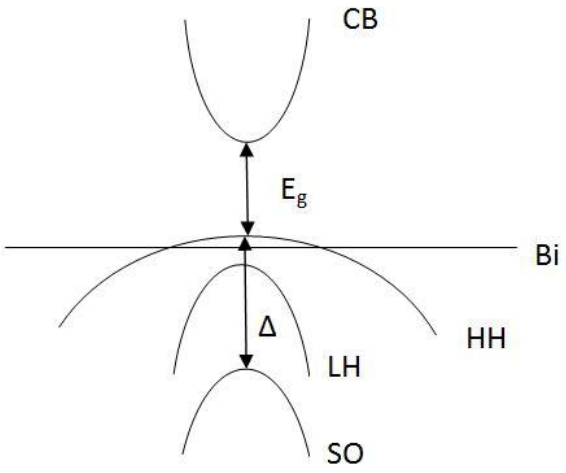

Figure 2.2: Schematic illustration for spin-orbit split property describing the anticrossing of the valence band of Bi-containing III-V materials.

Bi can be considered as an ideal surfactant due to its strong tendency to surface segregation during MBE growth [19] [20] [21] [22]. As Bi can stay on the surface without incorporating into materials, it is an excellent surfactant for III-V semiconductor growth and thus the electronic properties and the surface morphology of the deposited layers can be improved [6]. It is predictable that the lattice constant of III-V-Bi should be higher than that of III-V compounds. This prediction is because Bi is the last column V element with the largest atomic radius [17] [18]. Because of the large size and low electronegativity of Bi (i.e., exactly the opposite of the small size and high electronegativity of nitrogen) compared with other conventional group V element, the III-V-Bi compounds have unusual electronic properties. Also the required growth conditions are rather different than standard III-V growth processes [1] [16] [23]. According to bandgap bowing effect, only the valence band structures have some affects, when Bi is incorporated. In other word, the giant bandgap reduction, which is about 88 meV/%Bi in GaAsBi, happens only in the valence band and has very small

influence on electrons [9] [17] [18]. Bi alloying are expected for making stronger scattering of holes than electrons. Consequently, the hole mobility would be decreased more than the electron mobility [6]. In case of Bi incorporation, the electron mobility of dilute GaAsBi is much less affected compared with the case of dilute nitrides incorporation [18]. For dilute Bi, photoluminescence intensity increases with the Bi incorporation [18]. In the field of spintronics, it would be an important and great development if a large increase in spin orbit splitting for electrons occurs [6].

In this thesis, dilute Bi containing thin films grown by MBE are inspected in order to optimize the growth conditions. The effects of different parameters, growth rate, growth temperature and Bi flux (i.e., V/III ratio) were examined to achieve maximum Bi incorporation. Samples were grown on undoped (100) GaSb, undoped (100) GaAs and InP substrates for dilute Bi alloys in the Riber MBE system. During the growth, sample surface was *in-situ* observed by RHEED to examine the growth front of the samples. For having effective Bi incorporation, a large Bi flux is required for the slightly weak bonding of III-Bi compared with conventional other III-V alloys. Due to the weak bonding of III-Bi, there are possibilities for Bi atoms not to be incorporated or to be segregated to the growth front at high growth temperature [17] [18].

2.3 Bi_2Te_3 for thermoelectric cooling

Bismuth telluride (Bi_2Te_3) is likely for having application in thermoelectric devices, particularly for cooling of electronics because of their greater thermoelectric performance at room temperature [4] [5]. The thermoelectric cooling system is an ideal system when precise temperature control is needed [24]. The potential applications are in electronic systems and computers to cool sensitive components, in a satellite or space probe to modest the excessive temperatures, in digital cameras and also in charge-coupled devices (CCDs) to minimize thermal noise [25]. Some other applications are in laser diodes, laboratory instruments, temperature baths, refrigerators, and telecommunications equipments etc. [24]. This cooling system, which is also known as Peltier heat pump, is a way to take out thermal energy from a device by applying a constant polarity voltage to a junction between two different conductors or semiconductors [25] [26]. Bi_2Te_3 is sandwiched between these two conductors [24]. Because of its relatively high figure of merit, Bi_2Te_3 is the most common semiconductor for electronics cooling applications. But, the performance of this material is still quite low [27].

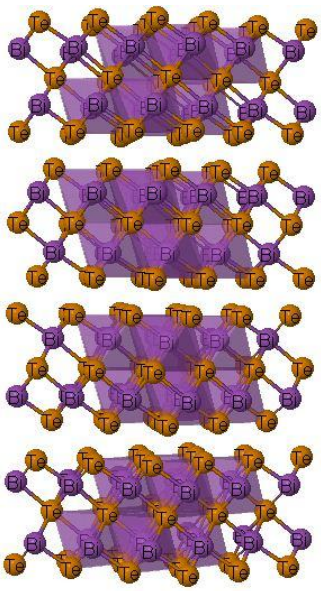

Figure 2.3: The schematic crystal structure of Bi_2Te_3

Figure 2.3 shows the schematic view of rhombohedral crystal structure of Bi_2Te_3 material, a narrow gap layered semiconductor with a trigonal unit cell [28] [29]. According to above shown structure, Bi_2Te_3 along its [111] crystallographic direction has five atomic layers with a stacking sequence of Te(1)-Bi-Te(2)-Bi-Te(1) , which forms a quintuple layer (QL) [29]. Since the interaction between two neighboring tellurium atoms are actually weak van der Waals bonding, the QLs are easily cleaved by the Te(1) atomic layers on both sides [29] [30]. Because of its too low surface energy, this material always confirms a Te-terminated surface [29].

A very promising way to obtain a true bulk structure with high quality is to grow the Bi_2Te_3 films by MBE [29]. With the MBE technique, Bi_2Te_3 thin films for thermoelectric cooling have been successfully grown on Si(111)N+ and Si(111)SI substrates. In this case, the critical growth parameters are the flux ratios (i.e., Bi/Te ratios), growth temperatures and differences in step-by-step growth methods. In this thesis, MBE grown Bi_2Te_3 materials are investigated with help of different characterization techniques and discussed with consider of different growth conditions.

Chapter 3

3. Measurement Techniques

Atomic Force Microscopy (AFM) and Photoluminescence (PL) measurement techniques have to be implemented for the MBE grown samples. AFM has been used to characterize surface morphology of both dilute bismides and Bi_2Te_3 materials; while PL has been performed to characterize optical properties of dilute bismides. The mechanisms of AFM and PL are explained below.

3.1 Atomic Force Microscopy (AFM)

Scanning Probe Microscopy (SPM) consists of a sharp probe with a cantilever that can scan across a surface and from the probe-sample interactions the surface morphologies are monitored on computer screen. Two primary forms of SPM are Scanning Tunneling Microscopy (STM) and Atomic Force Microscopy (AFM). AFM is also known as Scanning Force Microscopy (SFM). Three primary modes of AFM are Contact Mode, Non-contact Mode and Tapping Mode AFM. Tapping Mode AFM is considered to characterize the surface morphology of bismuth containing compound samples. The advantages of Tapping Mode AFM are higher lateral resolution on most samples, minor forces, negligible damage to soft samples and no scraping. The only demerit is slightly slower scan speed compare to Contact Mode AFM.

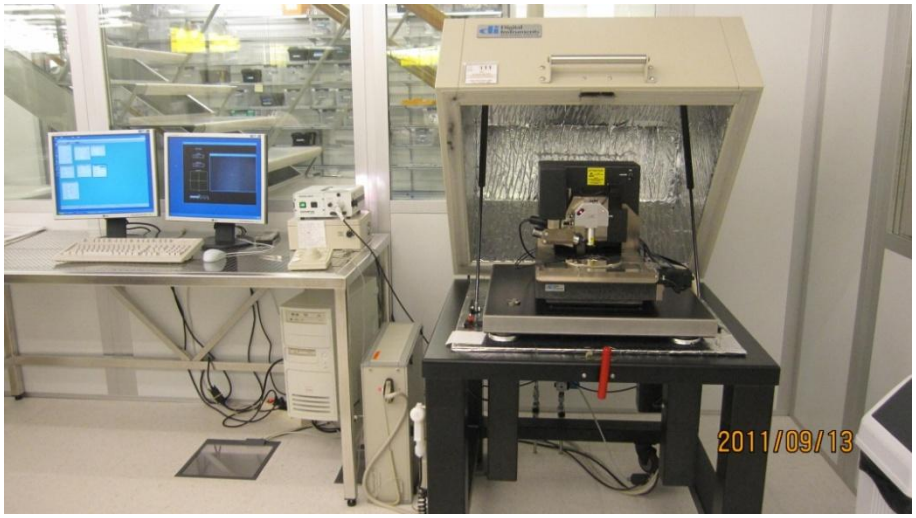

Figure 3.1: SPM- Veeco Dimension 3000 SPM (Model: Dimension 3000/Nanoscope IIIa)

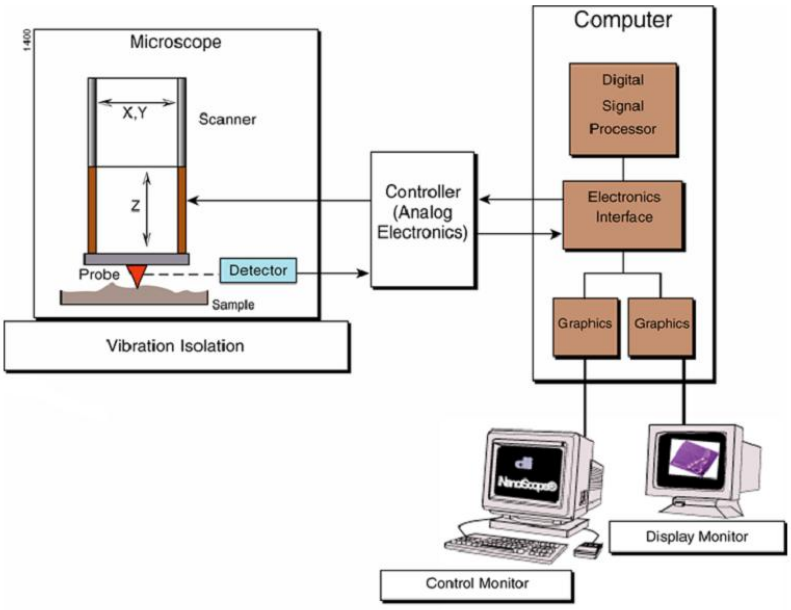

Figure 3.2: Schematic diagram of basic SPM components

Figure 3.1 shows a SPM tool (Model: 'SPM-Veeco Dimension 3000 SPM') and Figure 3.2 shows a schematic diagram of the SPM tool with its basic components. In these figures, the left monitor is for controlling the scanning and the right one is 'Nanoscope image' for monitoring surface morphology of the sample. Tapping Mode AFM characterization has been performed for different scan sizes (normally for 1x1 μm^2 and 10x10 μm^2) and for different scan directions (usually 0°, 45° and 90°). Nanoscope software is used to control sample scanning and post data analysis.

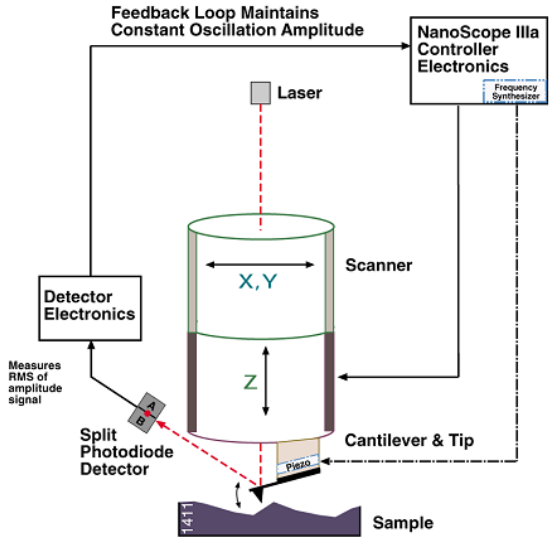

Figure 3.3: Schematic diagram of a Tapping Mode AFM with basic components

Figure 3.3 shows the schematic diagram of a Tapping Mode AFM with basic components, where a tip is attached to the end of an oscillating cantilever so that the tip can scan across the sample surface. The resonant frequency of the oscillated cantilever follows amplitude, ranging from 20 nm to 100 nm. Split photodiode detector helps to keep a constant RMS of the oscillation signal and then the feedback loop maintains constant oscillation amplitude. Thus during the scanning, a constant tip-sample interaction is maintained. In order to form the image of the sample surface, the vertical position of the scanner (i.e., each (x, y) data point) maintains a constant amplitude, which is stored by the computer.

3.2 Photoluminescence (PL)

Two different types of Photoluminescence (PL) measurement techniques have been considered to characterize optical properties of dilute bismides. One technique was 'Room-Temperature PL' or RTPL for examining different positions on the samples and the other one was 'Low-Temperature PL' or LTPL by varying temperature starting from a very low temperature (e.g., 45 Kelvin). MATLAB (with configured PLtool) software was required to perform these PL measurements. One typical example during an ongoing measuring process is shown in Figure 3.4. Bandgap changing with different Bi concentrations of the samples, in another word, material quality for different Bi containing samples can be judged from this kind of amplitude vs. wavelength graph shown in Figure 3.4.

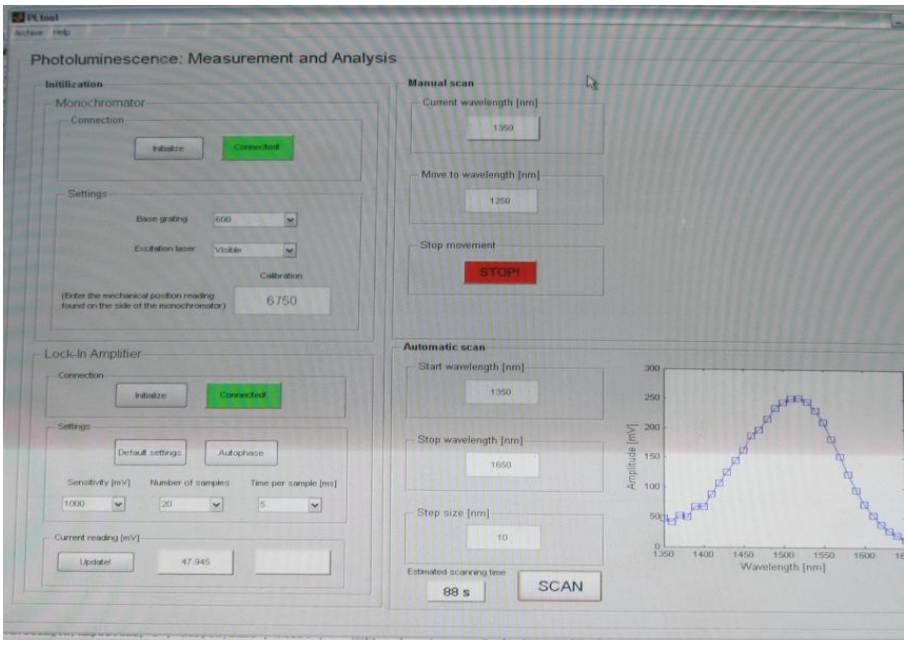

Figure 3.4: Configured PLtool in MATLAB software showing 'Photoluminescence: Measurement and Analysis' during an ongoing measuring process

The Room Temperature PL (RTPL) and Low Temperature PL (LTPL) are explained shortly with their own set-up components below.

3.1.1 Room Temperature PL

The four basic components for a PL system are a light source, a sample, a light filtering system and a photo detector. When the light from the light source (here, an Ar^+ laser) hits the sample, it generates electron-hole pairs and also interactions among the electrons. Because of these interactions, emission of light occurs. And the emitted light is then filtered to its different energies, or in other word, in different wavelengths by a monochromator, which is then recorded by the photo detector.

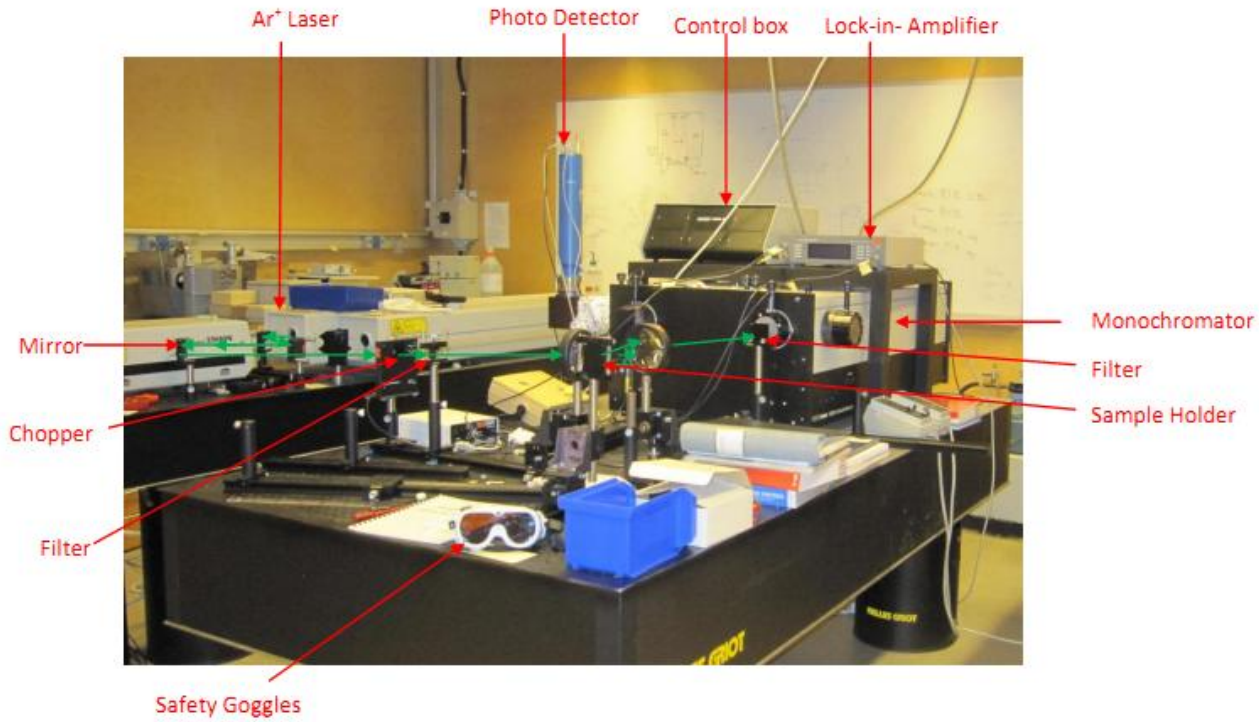

Figure 3.5: Photoluminescence (PL) system with Room Temperature components set-up

Figure 3.5 shows the room-temperature Photoluminescence (RTPL) system for Bi samples. The light beam can be followed by the direction of green arrows showing in the figure above. The system contains an Ar^+ laser as the light source, a water cooling circulation system for the laser, a photo detector (need to be cooled by liquid nitrogen), some adjustable aligned mirrors to guide the light beam in a required path, a chopper to chop the laser light up to higher frequencies, a filter to filter out visible and ultra-violet (UV) light, two lenses: first one for focusing the light on the sample and second one for focusing the light into the monochromator, an attenuator to prevent the monochromator from damaging, a small mirror helping to shine the light on to the sample from the laser, a bismuth containing sample mounted on a sample holder, a lock-in-amplifier, a control box for linking the whole process with a controlling computer and a monochromator as the light filtering system. When the light finally goes into the monochomator, it splits into different energies or in other word, wavelengths and then detected by the detector. Then the data goes to the lock-in amplifier and this component is responsible to make sure that frequency of the chopper is matched. Then the data is sent back through the control-box to the controlling computer and program (MATLAB with configured PLtool).

3.1.2 Low Temperature PL

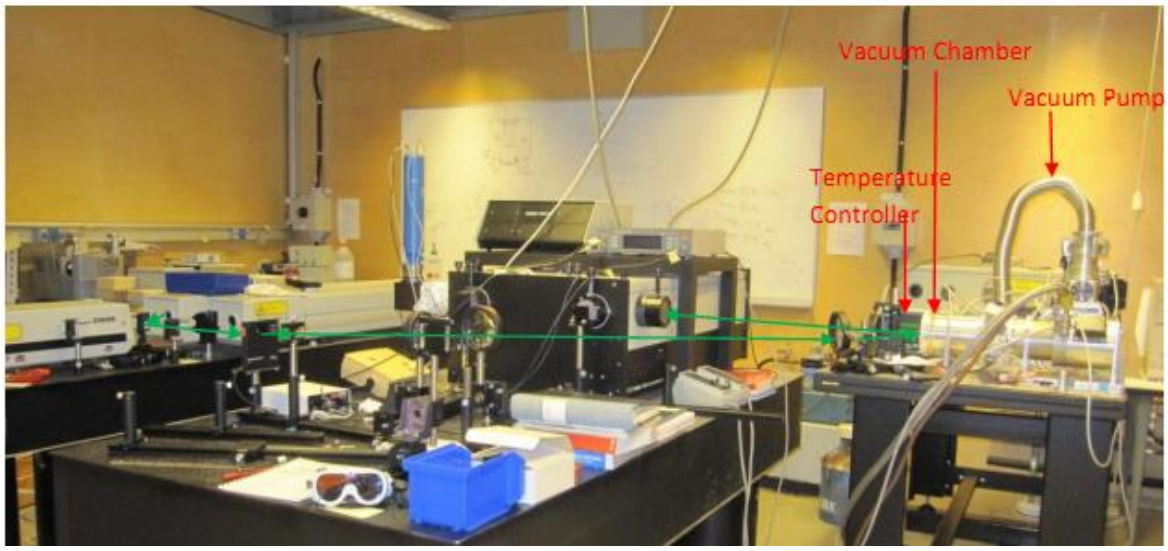

Figure 3.6: Photoluminescence (PL) system with low temperature components set-up

Figure 3.6 shows a Low-Temperature Photoluminescence (LTPL) system with Cryo Temperature components for Bi samples. The light beam can be followed by the direction of green arrows showing in the figure above. The set-up is similar to RTPL; the only difference is that LTPL includes Cryo Temperature PL components, which consist of a vacuum pump, a compressor, a temperature controller, a vacuum chamber for the sample and two valves for water cooling circulations. The sample has to be mounted inside the vacuum chamber and the vacuum chamber is used as a sample holder to keep the temperature at a desired value. The vacuum pump is responsible to make the chamber totally vacuumed. The compressor works for decreasing temperature inside the vacuum chamber as low as possible. Temperature controller takes a vital role in order to scan the sample at different temperatures.

Chapter 4

4. Characterizations, results and analysis on dilute bismides

AFM characterization has been implemented on MBE grown different dilute bismide materials to investigate the surface morphologies. Room temperature and also low temperature Photoluminescence (PL) techniques have been implemented only on InGaAsBi QW samples to determine the optical properties. The characterization results and analysis on different dilute bismide materials are discussed below.

4.1 Analysis with AFM and XRD

Below are the discussions of MBE grown dilute bismides GaSbBi, GaAsBi, InGaSbBi QW and InSbBi, which are investigated by AFM and also X-ray diffraction (XRD) techniques. XRD was considered to study structural properties of the samples.

4.1.1 Analysis of GaSbBi material (grown on GaSb Substrate)

Sample Name	Project	Growth Temperature, Tg [°C]	Top layer thickness [nm]	Growth Rate [µm/h]	RMS Surface Roughness (in nm)	
					For 1x1 µm	For 10x10 µm
R0371	GaSbBi	330	200	0.1	0.4	0.8
R0373	GaSb (Reference)	370	200	0.1	0.11	0.6
R0374	GaSbBi	360	200	0.1	0.19	0.64
R0375	GaSbBi	370	200	0.1	3.93	2.86
R0376	GaSbBi	380	200	0.1	0.27	0.93
R0380	GaSbBi	390	200	0.1	4.71	5.43
R0388	GaSbBi	380	500	0.1	0.12	0.68

Table 4.1: GaSbBi (on GaSb substrate) samples grown at different growth temperatures with 0.1 µm/h growth rate. Different RMS roughness of surface is achieved for different growth conditions.

In GaSbBi, Bi is incorporated with Sb and GaSb is used as substrate. The thickness of GaSbBi was 200 nm in most cases and the Bi samples were grown by varying Bi flux and growth temperature (Tg) from 330 °C to 390 °C. The growth rate was 0.1 µm/h. Since the III-Bi has slightly weak bonding compared to III-Sb, it requires a large Bi/Sb flux ratio for capable Bi incorporation.

Figure 4.1 shows the AFM images of GaSbBi from mirror-like surface for (a) 1x1 μm² and (b) 10x10 μm² scan size. In this case, the growth temperature was 360˚C. The atomic steps can be observed from the Mirror-like flat surface for 1x1 μm² scan size. Triangle shaped feature with small droplets are found during large scale AFM characterization. The surface roughness for this sample are 0.185 nm and 0.635 nm for 1x1 μm² and 10x10 μm² scan size, respectively. For the sample shown in Figure 4.1 (the mirror-like flat surface), the Bi flux is set to the calculated vapor pressure are same at the corresponding Tg. The Sb flux is a bit higher than the transition point for the Ga droplet formation.

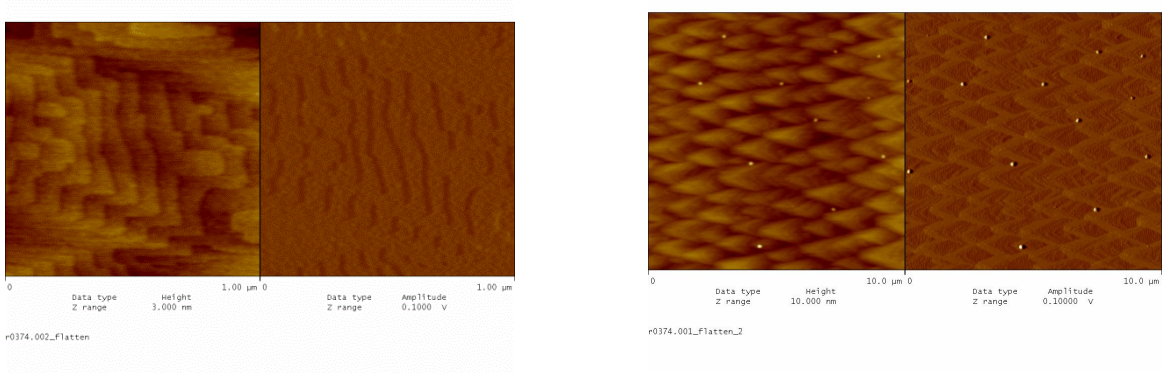

(a) (b)

Figure 4.1: AFM images of GaSbBi from mirror-like surface for (a) 1x1 μm² and (b) 10x10 μm² scan size

Figure 4.2 shows AFM images of sample surface from the hazy regions for different growth temperatures. For Figure 4.2 (a), Tg was 360 °C and for Figure 4.2 (b), Tg was 370 °C. In Figure 4.2 (a), the clearly observable Bi droplets are ring shaped with facets while in Figure 4.2 (b), common spherical shaped Ga droplets are monitored from the hazy region of the sample grow at a higher temperature.

The reason for forming these droplets is of having excess of Bi atoms on the growth front, which were neither incorporated nor evaporated. Corresponding to the growth temperature (Tg), the Bi flux should be preferred closed to its vapor pressure to avoid Bi droplets. Higher Bi flux has need of higher Tg, which may cause non-incorporation of Bi. Sb flux should be kept as low as possible to facilitate Bi incorporation but not to have any Ga droplet. Because of this trade-off, an optimal growth temperature for Bi incorporation should be chosen.

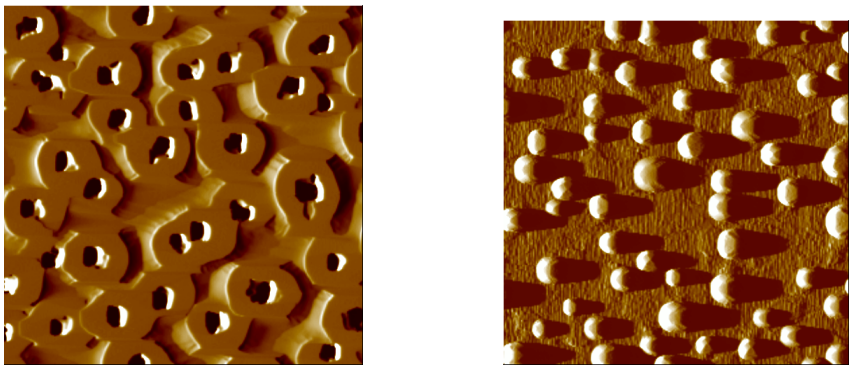

(a) (b)

Figure 4.2: AFM images of GaSbBi from (a) surface with Bi droplets and (b) Ga droplets

Figure 4.3 shows the surface roughness (in nm) of GaSbBi samples on GaSb substrates for different growth temperatures (Tg in °C) for 1x1 μm² (indicated by blue) and 10x10 μm² (indicated by red) scan size. Surface RMS roughness of reference sample is also shown separately in this figure. From the below graph, it can easily be seen that the surface roughness is relatively lower in the range between 330 ˚C and 380 ˚C temperature variation. For 1x1 μm² scan size, roughness varies from 0.10 nm to 0.40 nm and for 10x10 μm² scan size, roughness varies from 0.60 to 0.95 nm for almost flat sample surfaces. But for one sample, there is a surprising exception in roughness at T_g=370 ˚C, which has a relatively higher roughness of surface (3.9 nm for 1x1 μm² scan size) shown in Figure 4.4. For this sample, the surface pattern is very different and interesting than others. The reason of having it is not known yet.

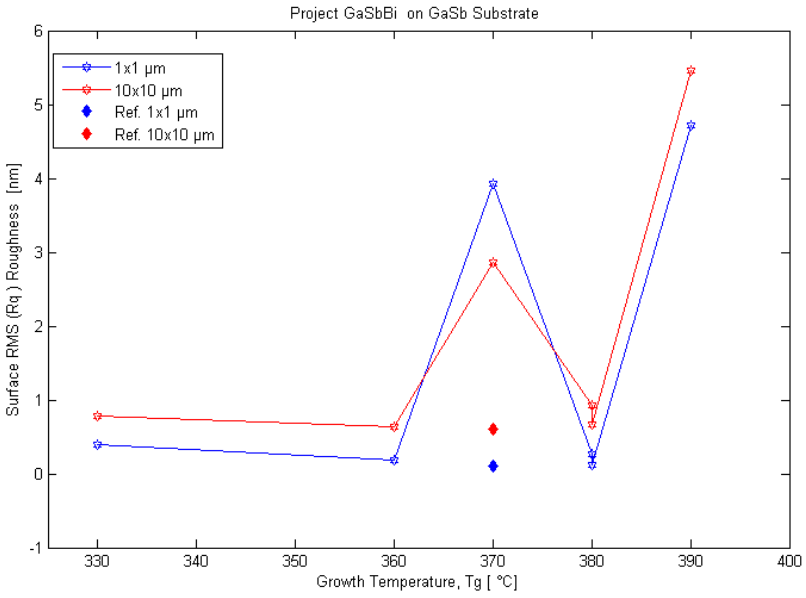

Figure 4.3: Surface RMS roughness (in nm) of GaSbBi samples on GaSb substrates for different growth temperature (T_g in °C) for 1x1 μm² (blue) and 10x10 μm² (red) scan size. Surface RMS roughness of reference sample is also shown separately in above figure.

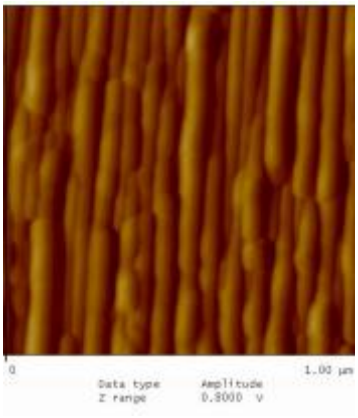

Figure 4.4: 1x1 µm² AFM amplitude image of a GaSbBi material showing very different and rough surface morphology at growth temperature 370 ˚C.

High quality surfaces with observable atomic steps and a little higher RMS roughness compare to that of the reference sample have been obtained for the GaSbBi samples grown at 330 °C, 360 °C and 380 °C. But, for a higher growth temperature i.e., at 390 ˚C, the sample surface became very rough with elongated dots. The possible reason for this could be the relaxation of layers.

Figure 4.5 (a) shows XRD (004) rocking curves of GaSbBi samples grown at different temperatures and Bi beam equivalent pressures (BEPs). The graph is shown in logarithmic scale. Figure 4.5 (b) shows the separation between the GaSbBi peak and the GaSb substrate peak vs. the Bi BEP. At growth temperature 370 °C or lower, interference fringes can be observed from the samples. But no interference pattern can be seen at higher T_g due to inferior GaSbBi/GaSb interface. Though the lattice constant of III-V-Bi should be larger than that of III-V, in this case, it is very surprising that the 0^{th} peak of the top layer GaSbBi appears at the higher angle than the diffraction angle of the GaSb substrate indicating a smaller lattice constant for GaSbBi than that of GaSb substrate. It can be realized from Figure 4.5 (b) that the difference in angle relative to the GaSb peak increases with increasing T_g up to 380 °C and then suddenly decreases. Lattice constants can also be figured out from this peak separation vs. Bi BEP curve.

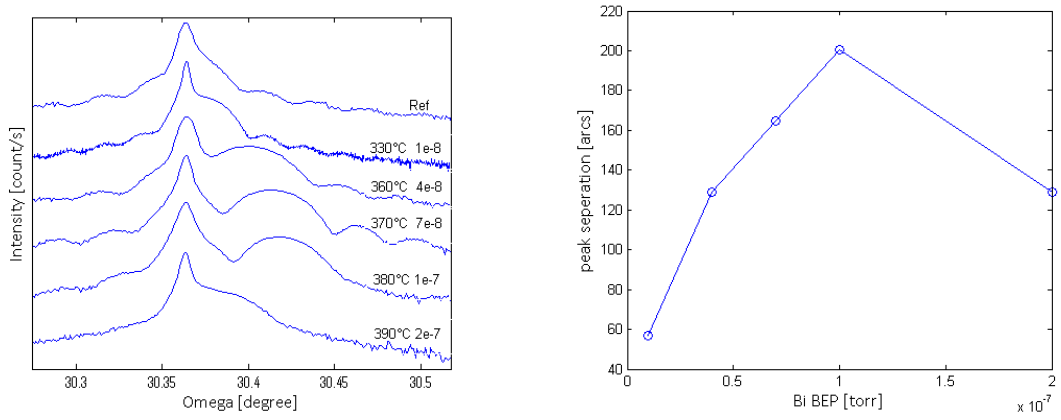

(a) (b)

Figure 4.5: a) XRD (004) rocking curves of GaSbBi samples grown at different temperatures and Bi beam equivalent pressures (BEPs), which are mentioned to the right side of each curve. The graph is shown in logarithmic scale. (b) The separation between the GaSbBi peak and the GaSb substrate peak vs. the Bi BEP.

4.1.2 Analysis of GaSbBi material (grown on GaAs Substrate)

In order to compare the GaSbBi samples grown on GaSb substrate, a good number of samples were grown on GaAs substrate maintaining unchanged growth condition. Table 4.2 describes how the RMS surface roughness of the samples differs for different growth conditions applied on different GaSbBi (grown on GaAs substrate) samples.

Sample Name	Project	Growth Temperature, Tg [°C]	Top layer thickness [nm]	Growth Rate [µm/h]	RMS Surface Roughness (in nm)	
					For 1x1 µm	For 10x10 µm
R0390	GaSbBi/GaAs	360	200	0.1	1.2	1.11
R0391	GaSbBi/GaAs	370	200	0.1	4.12	5.2
R0394	GaSb/GaAs (Reference)	370	200	0.1	0.62	0.8
R0401	GaSbBi/GaAs	380	200	0.1	2.47	5.36
R0402	GaSbBi/GaAs	390	200	0.1	2.42	5.7

Table 4.2: GaSbBi (on GaAs substrate) samples grown at different growth temperatures with 0.1 µm/h growth rate. Different RMS roughness of surface is achieved for different growth conditions.

By comparing Table 4.1 and Table 4.2, it can be noticed that surface RMS roughness is relatively higher for samples grown on GaAs substrate; this is due to the strain relaxation. Surface morphologies for these samples are shown in small scale (i.e., 1x1 µm²) and also in large scale (i.e., 10x10 µm²) in Figure 4.6 and Figure 4.7, respectively. Though from Table 4.2, it is understandable that surface roughness is similar for all samples except R0390 (T_g 360 °C) in large scale (i.e., 10x10 µm²), but the morphologies are different to each other which can be observed from morphology figures in large scale.

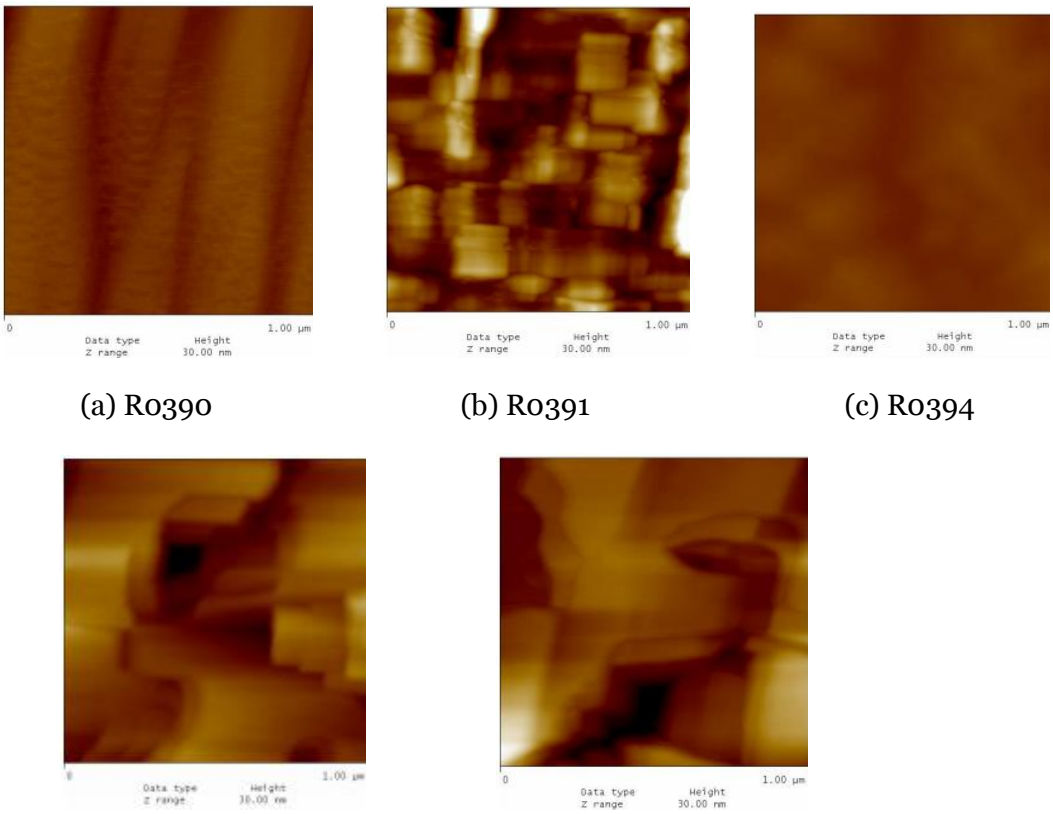

(a) R0390 (b) R0391 (c) R0394

(d) R0401 (e) R0402

Figure 4.6: 1x1 µm² AFM height images of GaSbBi (on GaAs substrate) materials grown at different growth temperatures showing different surface morphology with 0.1 µm/h growth rate. Sample names are mentioned below each image (from (a) to (e)).

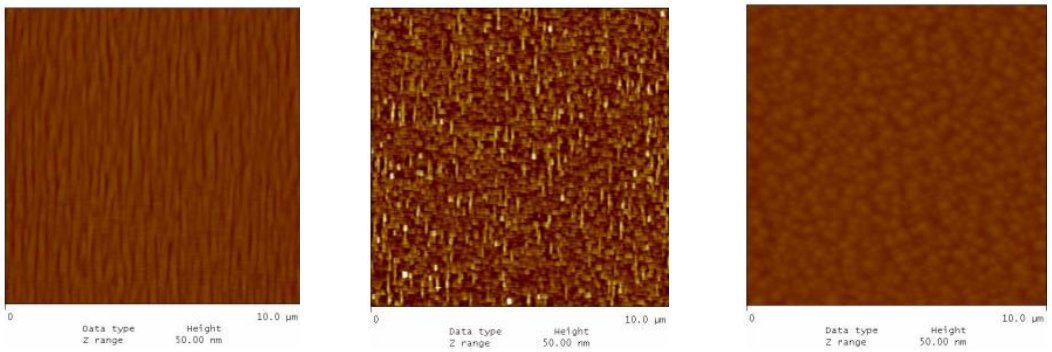

(a) R0390 (b) R0391 (c) R0394

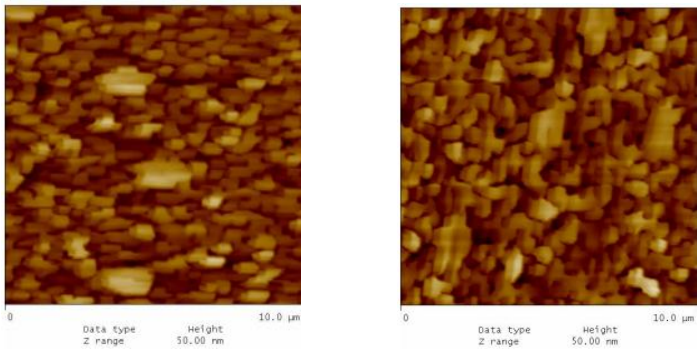

(d) R0401 (e) R0402

Figure 4.7: 10x10 µm² AFM height images of GaSbBi (on GaAs substrate) materials grown at different growth temperatures showing different surface morphology with 0.1 µm/h growth rate. Sample names are mentioned below each image (from (a) to (e)).

Sample 'R0390' has elongated feature with a little higher roughness in surface compare to round shape featured reference sample 'R0394'. Otherwise in all other samples, discrete platform-like features have been originated and the individual area of platforms increases with growth temperature, T_g.

Figure 4.8 shows the surface roughness (in nm) of GaSbBi samples on GaAs substrates for different growth temperatures (Tg in °C) for 1x1 μm² (indicated by blue) and 10x10 μm² (indicated by red) scan size. Surface RMS roughness of reference sample is also shown separately in this figure. From the below graph, it can easily be seen that the surface RMS roughness is much lower at T_g = 360 ˚C. For this set of samples, the highest RMS roughness is obtained from the sample 'R0391' grown at T_g = 370 ˚C for small scale AFM characterization. Otherwise, roughness varies from 1.2 nm to 2.5 nm for 1x1 μm² scan size. For 10x10 μm² scan size, RMS roughness is higher and similar for all samples except R0390 at T_g = 360 ˚C. Much rougher surface morphologies have been obtained for GaSbBi samples grown on GaAs substrates comparing to samples grown on GaSb substrates.

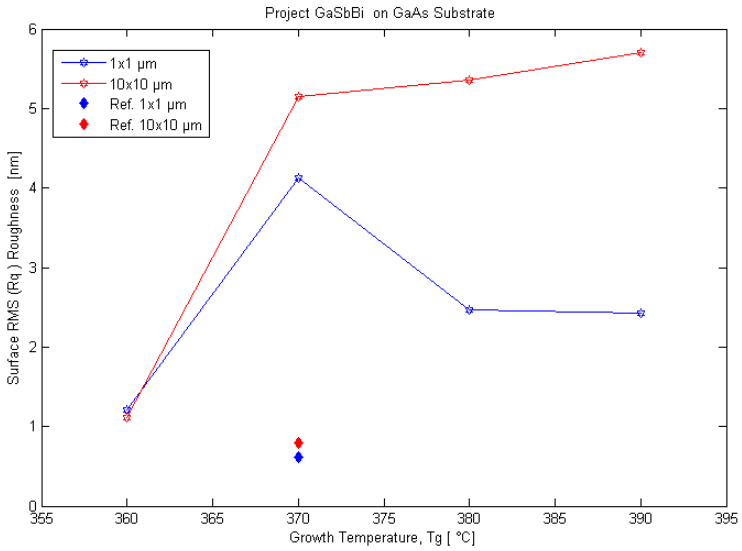

Figure 4.8: Surface RMS roughness (in nm) of GaSbBi samples on GaAs substrates for different growth temperature (T_g in °C) for 1x1 μm² (blue) and 10x10 μm² (red) scan size. Surface RMS roughness of reference sample is also shown separately in above figure.

4.1.3 Analysis of GaAsBi material (grown on GaAs Substrate)

Table 4.3 describes how the RMS surface roughness of the samples differs for different growth conditions applied on different GaAsBi samples grown on GaAs substrate.

Sample Name	Project	Growth Temperature, Tg [°C]	Top layer thickness [nm]	Growth Rate [µm/h]	RMS Surface Roughness (in nm)	
					For 1x1 µm	For 10x10 µm
R0356	GaAsBi	380	500	1	0.09	0.13
R0357	GaAsBi	360	500	1	0.26	0.46
R0358	GaAsBi	340	500	1	5.87	30.7

Table 4.3: GaAsBi (on GaAs substrate) samples grown at different growth temperatures with 1 µm/h growth rate. Different RMS roughness of surface is achieved for different growth conditions.

In Figure 4.9 and 4.10, much rougher surface morphology with very many big non-uniformed droplets has been obtained for sample R0358 at lower T_g, 340 °C. Though no atomic steps have been observed, the morphologies are very flat for two other samples grown at comparatively higher T_g i.e., 360 °C and 380 °C. The RMS roughness of surface decreases with increasing growth temperature, T_g.

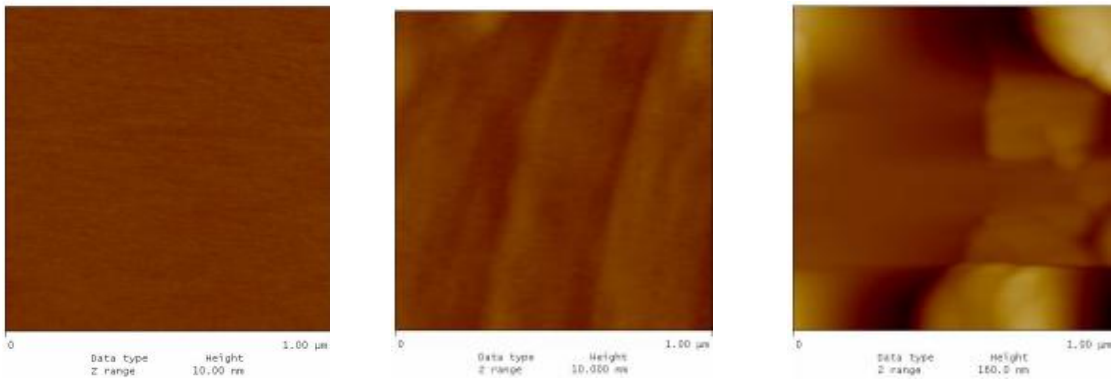

(a) R0356 (b) R0357 (c) R0358

Figure 4.9: 1x1 µm² AFM height images of GaAsBi (on GaAs substrate) materials grown at different growth temperatures showing different surface morphology with 1 µm/h growth rate. Sample names are mentioned below each image (from (a) to (c)).

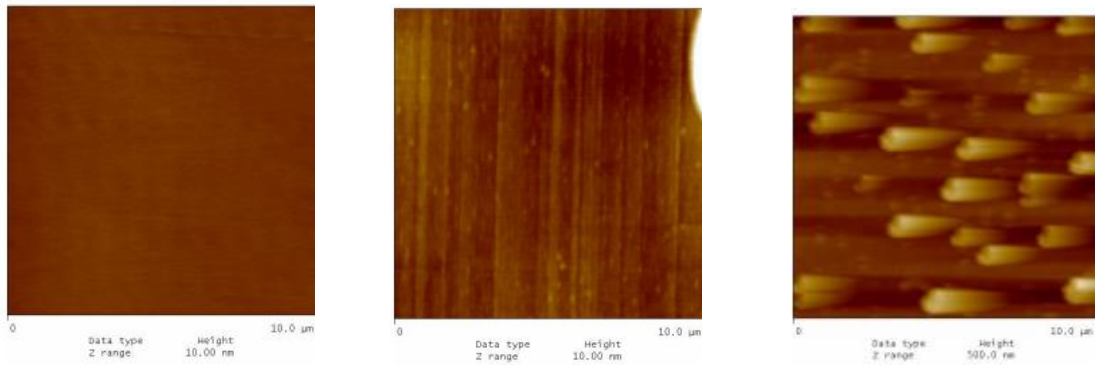

(a) R0356 (b) R0357 (c) R0358

Figure 4.10: 10x10 µm² AFM height images of GaAsBi (on GaAs substrate) materials grown at different growth temperatures showing different surface morphology with 1 µm/h growth rate. Sample names are mentioned below each image (from (a) to (c)).

Figure 4.11 shows the surface roughness (in nm) of GaAsBi samples on GaAs substrates for different growth temperatures (Tg in °C) for 1x1 µm² (indicated by blue) and 10x10 µm² (indicated by red) scan size. From the below graph, it is clearly observable that the surface RMS roughness is much lower at T_g = 360 °C and 380 °C. For this set of samples, the highest RMS roughness is obtained from the sample 'R0358' grown at T_g = 340 °C for both small and large scale AFM characterization.

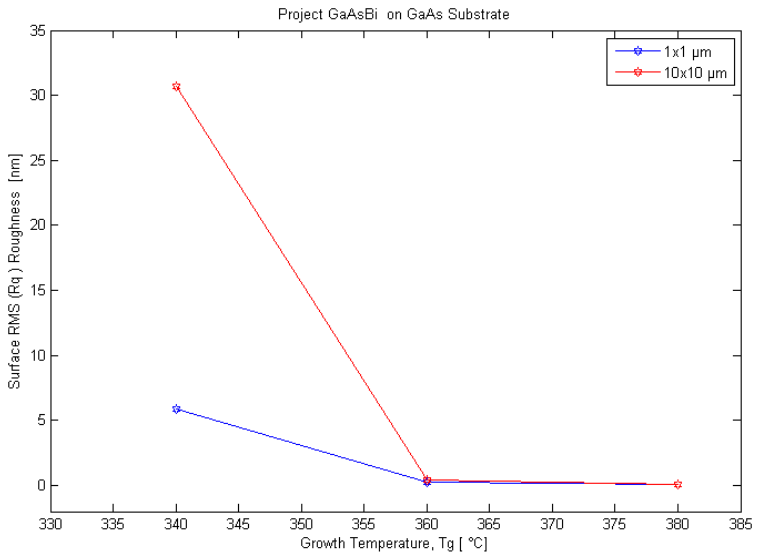

Figure 4.11: Surface RMS roughness (in nm) of GaAsBi samples on GaAs substrates for different growth temperature (T_g in °C) for 1x1 µm² (blue) and 10x10 µm² (red) scan size.

4.1.4 Analysis of InGaAsBi QW (grown on InP Substrate)

Table 4.4 describes how the RMS surface roughness of the samples differs for different growth conditions applied on an InGaAsBi QW sample grown on InP substrates.

Sample Name	Project	Growth Temperature, Tg [°C]	RMS Surface Roughness (in nm)	
			For 1x1 µm	For 10x10 µm
R0296	InGaAs QW (Ref.)	400	0.29	0.36
R0297	InGaAsBi QW	400	0.43	1.13
R0301	InGaAs QW (Ref. at high Tg)	510	0.3	0.48

Table 4.4: An InGaAsBi QW sample grown on InP substrate. Different RMS roughness of surface is achieved for different conditions.

Figure 4.12 and Figure 4.13 show 1x1 µm² and 10x10 µm² AFM height images of InGaAsBi QW samples on InP substrate, respectively. The growth temperature is 400 °C for both R0296 and R0297. From the large scale AFM characterization, it is found that the surface RMS roughness is higher for the reference sample 'R0301' grown at higher T_g comparing to reference 'R0296' sample. Also R0301 has almost flat but elongated feature with very many different shaped small droplets compared to R0296. It can be observed from the large scale AFM height image that because of Bi incorporation with InGaAs QW, 'R0297' has three times rougher surface with some non-uniformed and almost round shaped islands or droplets.

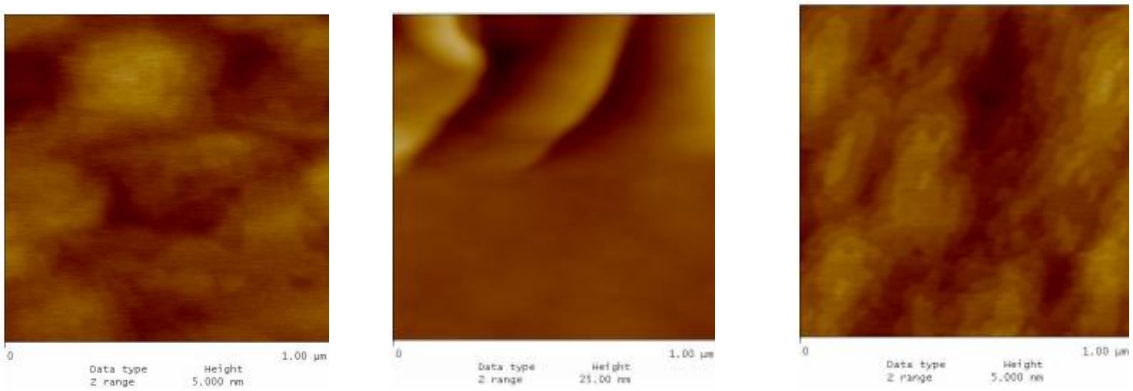

(a) R0296 (b) R0297 (c) R0301

Figure 4.12: 1x1 µm² AFM height images of InGaAsBi QW materials grown on InP substrate. Sample names are mentioned below each image (from (a) to (c)).

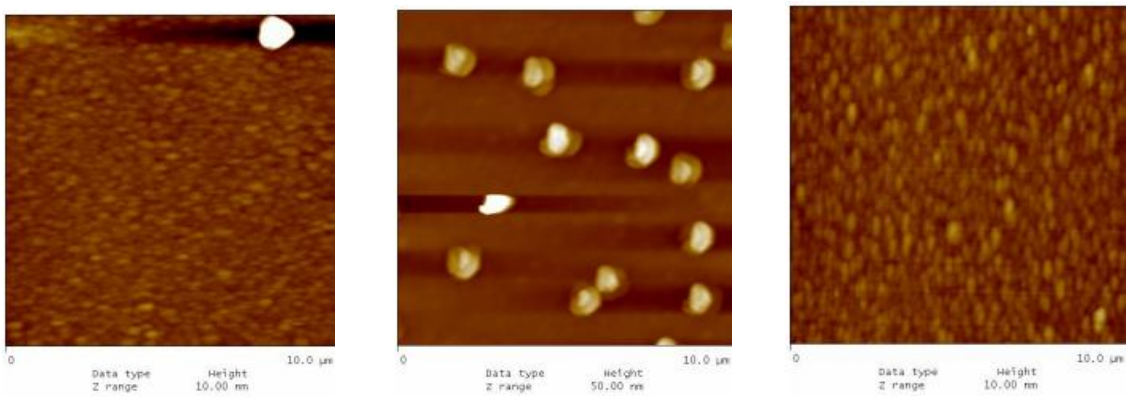

(a) R0296 (b) R0297 (c) R0301

Figure 4.13: 10x10 µm² AFM height images of InGaAsBi QW materials grown on InP substrate. Sample names are mentioned below each image (from (a) to (c)).

Figure 4.14 shows the XRD (004) rocking curves for InGaAsBi QW reference 'R0296' (red) and 'R0297' (blue) samples grown at the same temperature. Here, the highest peaks are obtained from the InP substrate. The peaks from Bi containing top layers are found at the left shoulder of substrate peaks. It can be found from the figure that the diffraction angles of InGaAsBi QW samples are lower than their substrate (InP) peaks, which means the Bi containing QW layers have higher lattice constants compare to their substrates. The interference patterns can be observed both in the left and right sides of the XRD curves. These interferences occur due to the reflections from sample interface.

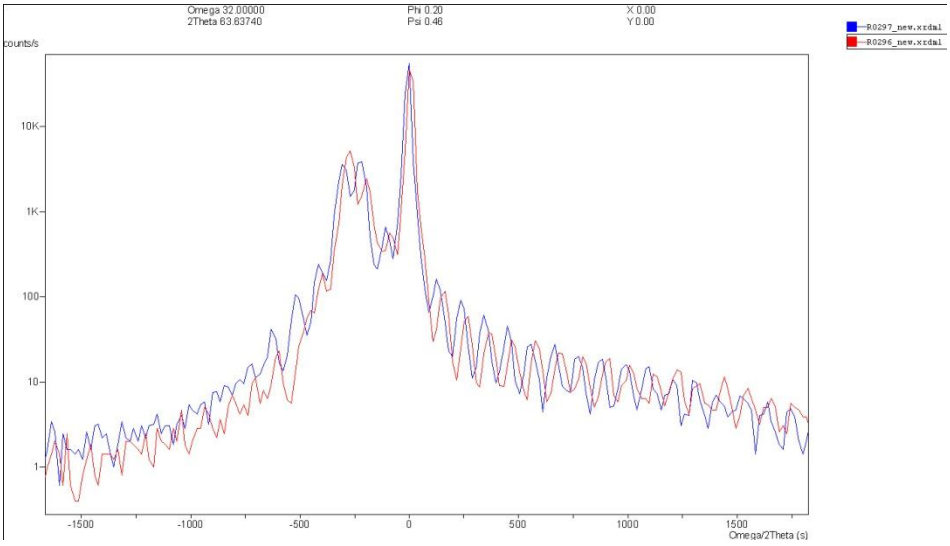

Figure 4.14: XRD (004) rocking curves for InGaAsBi QW reference 'R0296' (red) and 'R0297' (blue) samples grown at the same temperature.

Optical properties of these InGaAsBi QW samples are discussed in the next section of the current chapter, where Photoluminescence measurement technique has been considered.

4.1.5 Analysis of InSbBi material (grown on GaAs Substrate)

Table 4.5 describes how the RMS surface roughness of the samples differs for different growth conditions applied on some InSbBi (grown on GaAs substrate) samples. The growth rate was 0.2 µm/h for InSbBi samples. A buffer layer of 200 nm thick GaSb is introduced in between the GaAs substrate and the Bi containing 200 nm thick top InSbBi layer.

Sample Name	Project	Growth Temperature, Tg [°C]	Top layer thickness [nm]	Growth Rate [µm/h]	RMS Surface Roughness (in nm)	
					For 1x1 µm	For 10x10 µm
R0384	InSb (Reference)	360	200	0.2	0.34	1.22
R0386	InSbBi	360	200	0.2	1.93	11.07
R0387	InSbBi	370	200	0.2	2.86	23.48
R0389	InSbBi	350	200	0.2	1.89	2.01
R0396	InSbBi	355	200	0.2	0.26	1.17
R0398	InSbBi	385	200	0.2	4.88	16.82
R0400	InSbBi	395	200	0.2	7.56	35.44

Table 4.5: InSbBi (on GaAs substrate) samples grown at different growth temperatures with 0.2 µm/h growth rate. Different RMS roughness of surface is achieved for different growth conditions.

Figure 4.15 and Figure4.16 show 1x1 μm^2 and 10x10 μm^2 AFM height images of InSbBi (on GaAs substrate) samples, respectively, grown at different growth temperatures featuring different surface morphologies with 0.2 µm/h growth rate. R0384 is the reference sample grown at 360°C. Sample grown at 350°C (R0389) has almost flat surface and elongated feature with no observable atomic steps, which can be noticed from the small scale AFM image, Fig. 4.15 (d). From Fig. 4.15 (e), the atomic steps can clearly be seen for sample grown at 355°C (R0396). The lowest RMS surface roughness has been obtained from this sample (listed in Table 4.5), which ensures a high quality material. In Figure 4.15 (b) and Figure 4.16 (b), when a sample was grown at 360°C (R0386), a discrete platform-like feature has been found in large scale. From the small scale AFM image, atomic steps with some different shaped holes can be pointed out. In large scale, the RMS roughness is higher (11.07 nm) for 'R0386' sample. From Figure 4.15 (c) and Figure 4.16 (c), it is understandable that though atomic steps are found during small scale AFM scanning for sample grown at 370°C (R0387), but in large scale AFM scanning, the RMS roughness became even higher (23.48 nm) for this sample. For samples grown at 385°C (R0398) and 395°C (R0400), no atomic steps can be found in small scale AFM scanning and the surface became much worse at these growth temperatures. The layers are probably relaxed at these higher T_g.

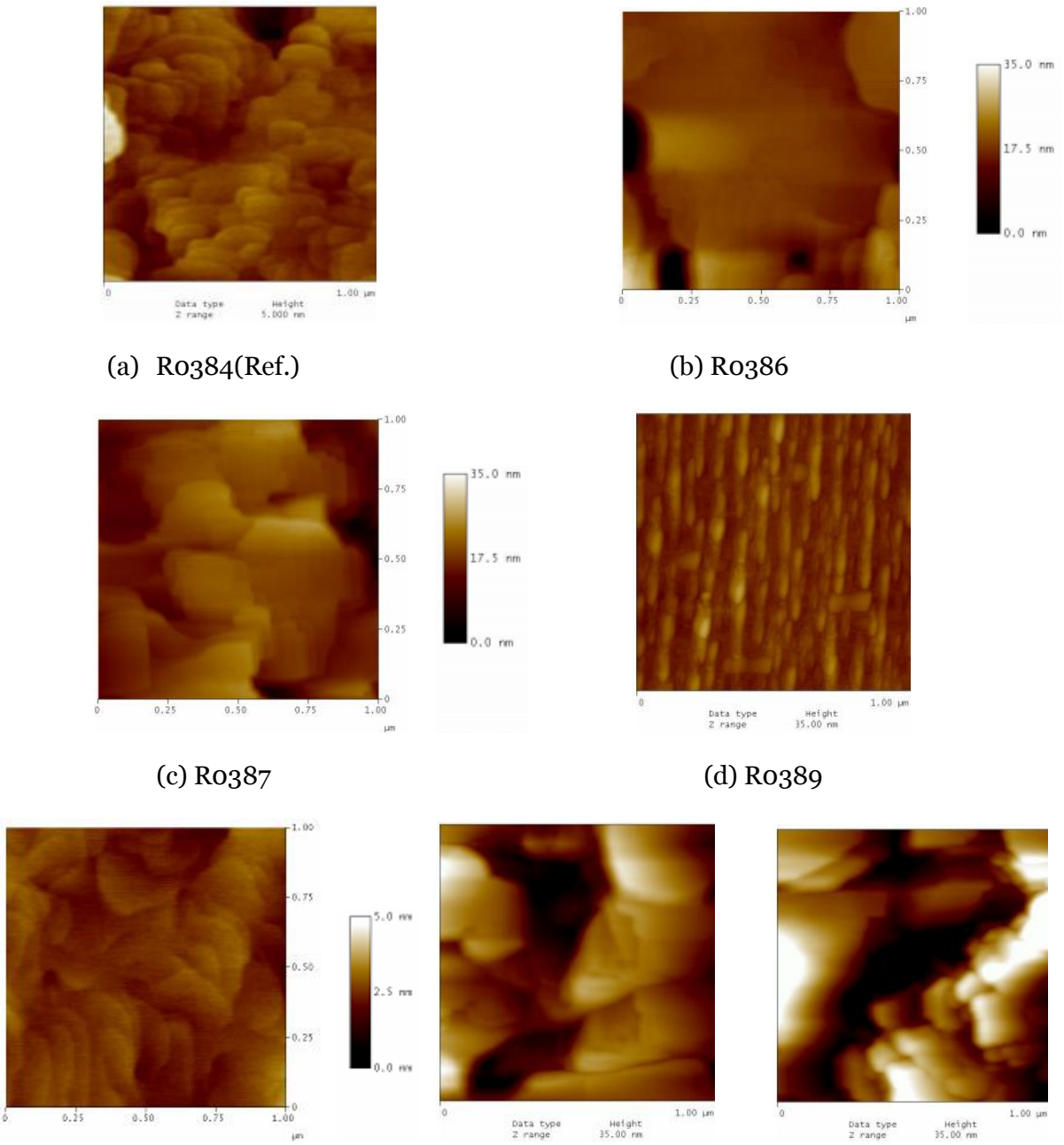

(a) R0384(Ref.) (b) R0386

(c) R0387 (d) R0389

(e) R0396 (f) R0398 (g) R0400

Figure 4.15: 1x1 μm² AFM height images of InSbBi (on GaAs substrate) materials grown at different growth temperatures showing different surface morphologies with 0.2 μm/h growth rate. Sample names are mentioned below each image (from (a) to (g)).

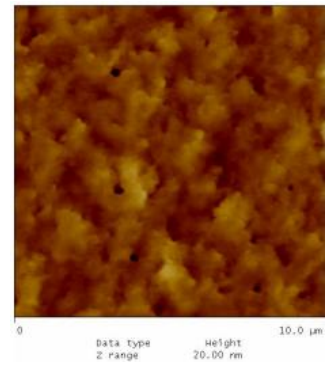

(a) R0384(Ref.)

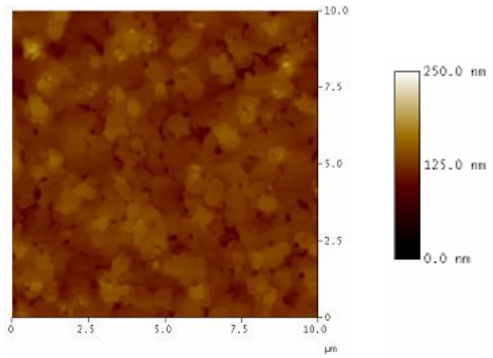

(b) R0386

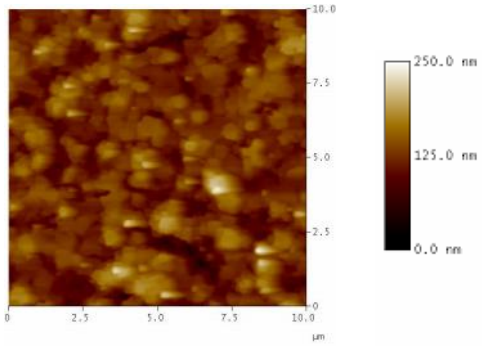

(c) R0387

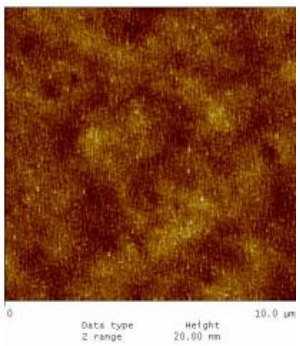

(d) R0389

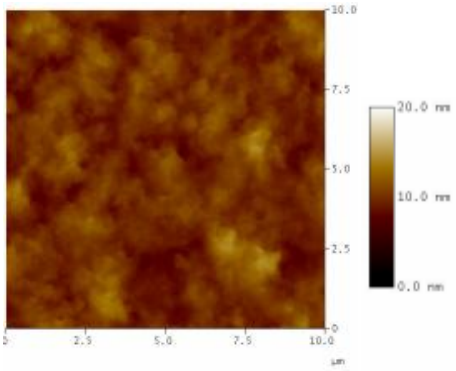

(e) R0396

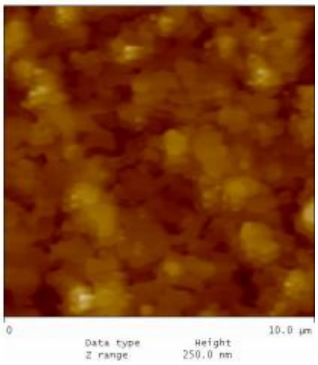

(f) R0398

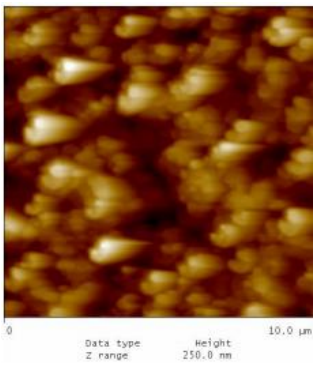

(g) R0400

Figure 4.16: 10x10 μm² AFM height images of InSbBi (on GaAs substrate) materials grown at different growth temperatures showing different surface morphologies with 0.2 μm/h growth rates. Sample names are mentioned below each image (from (a) to (g)).

Figure 4.17 shows the surface RMS roughness (in nm) of InSbBi samples on GaAs substrates for different growth temperatures (Tg in °C) for 1x1 μm² (indicated by blue) and 10x10 μm² (indicated by red) scan size. Surface RMS roughness of reference sample is also shown separately in this figure. From the below graph, it can easily be observable that the surface roughness is lowest for the sample 'R0396' grown at T_g = 355 °C from both small and large scale AFM characterizations. Surface roughness varies from 1.9 nm to 7.5 nm for small scale

scanning. It can also be pointed out from the 1x1 μm² curve that the roughness increases almost linearly with increasing T_g.

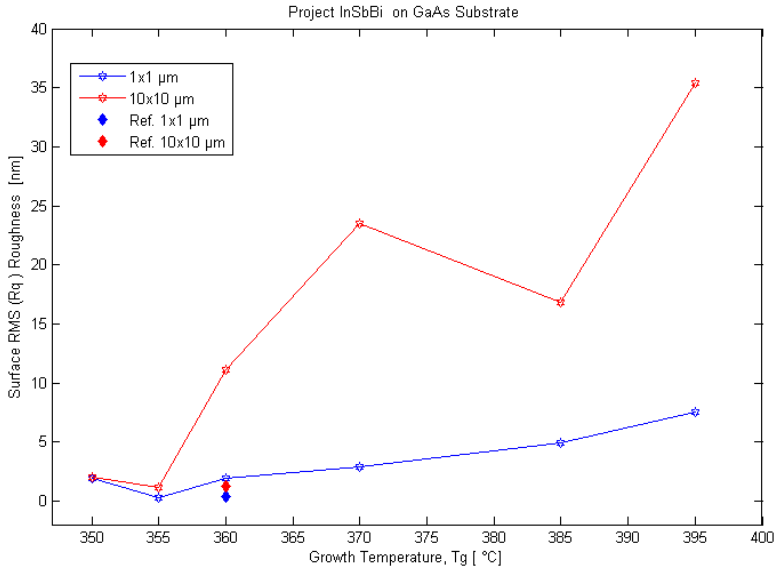

Figure 4.17: Surface RMS roughness (in nm) of InSbBi samples on GaAs substrates for different growth temperature (T_g in °C) for 1x1 μm² (blue) and 10x10 μm² (red) scan size. Surface RMS roughness of reference sample is also shown separately in above figure.

Figure 4.18 (a) shows XRD (004) rocking curves of InSbBi samples grown at different temperatures and Bi beam equivalent pressures (BEPs), which are mentioned to the right side of each curve. The graph is shown in logarithmic scale. Figure 4.18 (b) shows the separation between the InSbBi peak and the InSb peak vs. the Bi BEP.

In Figure 4.18 (a), the right most peaks are obtained from the GaAs substrate, middle peaks are from the GaSb buffer layers and the left most are from top InSbBi layer. From the XRD figure, it can be found that the intensities and lattice constants of GaAs substrate and GaSb buffer layers did not vary at all, i.e. same with different T_g, whereas it totally differs for each top InSbBi layer of the sample. This is because different amount of Bi is incorporated in different growth conditions. The lattice constants are higher in InSbBi layers than that of GaAs substrates layers. In comparison with GaSbBi samples grown on GaSb substrate, InSbBi samples has 10 times larger angle difference. When T_g increases from 350 °C to 360 °C, a quick and higher angle shift occurs to the 0^{th} peak and then it goes to saturation.

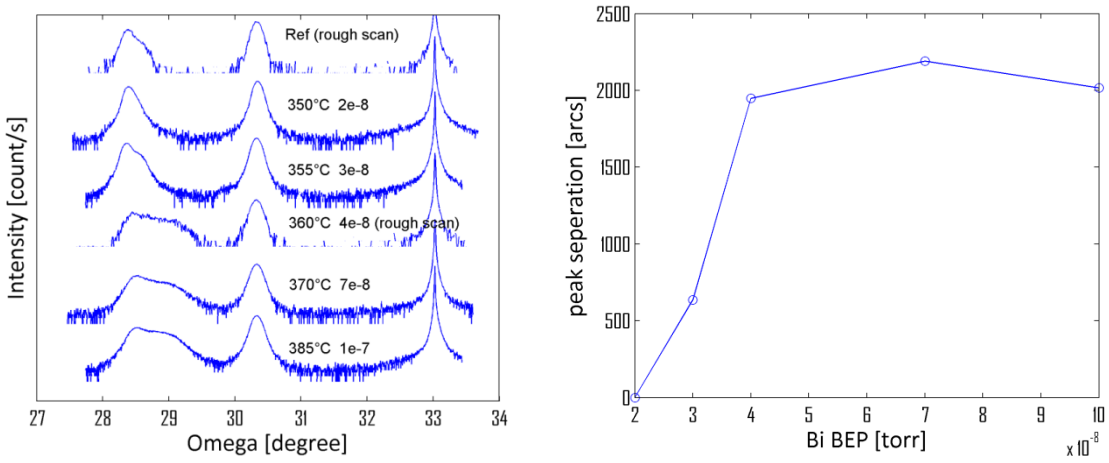

(a) (b)

Figure 4.18: a) XRD (004) rocking curves of InSbBi samples grown at different temperatures and Bi beam equivalent pressures (BEPs), which are mentioned to the right side of each curve. The graph is shown in logarithmic scale. (b) The separation between the InSbBi peak and the InSb peak vs. the Bi BEP.

4.2 Optical Properties of InGaAsBi QW material by Photoluminescence

4.2.1 Room Temperature PL (RTPL)

In order to understand the uniformity in wavelengths and PL intensities, RTPL has been performed at different positions on QW samples.

Figure 4.19 shows the schematic diagrams of (a) a reference InGaAs QW sample, 'R0296' and (b) a Bi-containing InGaAsBi QW sample 'R0297'. The reference InGaAs QW sample (R0296) is measured from top to bottom, indicated in Figure 4.19 (a) and Bi-containing InGaAsBi QW sample (R0297) is measured from right to left, indicated in Figure 4.19 (b). The measurement scales are also shown in this figure.

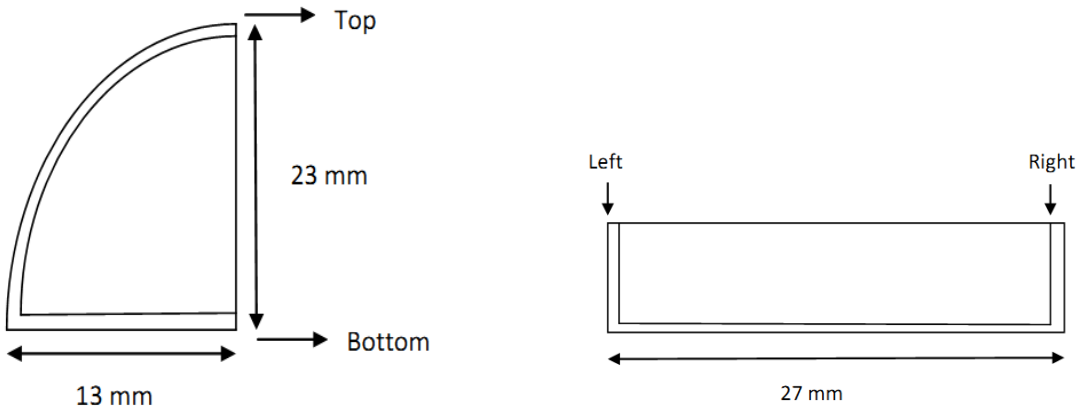

Figure 4.19: Schematic diagrams of (a) reference InGaAs QW sample: R0296 and (b) Bi-containing InGaAsBi QW sample: R0297.

Figure 4.20 shows comparison of wavelengths and PL intensities of two QW samples by RTPL: (a) reference InGaAs QW sample (R0296) and (b) Bi-containing InGaAsBi QW sample (R0297), showing different PL intensities at different wavelengths in position varying RTPL measurements. It is observable from Figure 4.20 (a) that at the top position of the reference 'R0296' sample, higher PL intensity is obtained; then the intensity decreases gradually. Wavelength is almost the same for all measured sample positions. And from Figure 4.20 (b), longer wavelength has been found at the right most position of R0297 that ensures the desired bandgap reduction. The measured maximum wavelength difference at different sample positions is shown in Figure 4.20 (b). Also 10 times higher PL intensity is obtained at the right most position of R0297 than the reference R0296 sample.

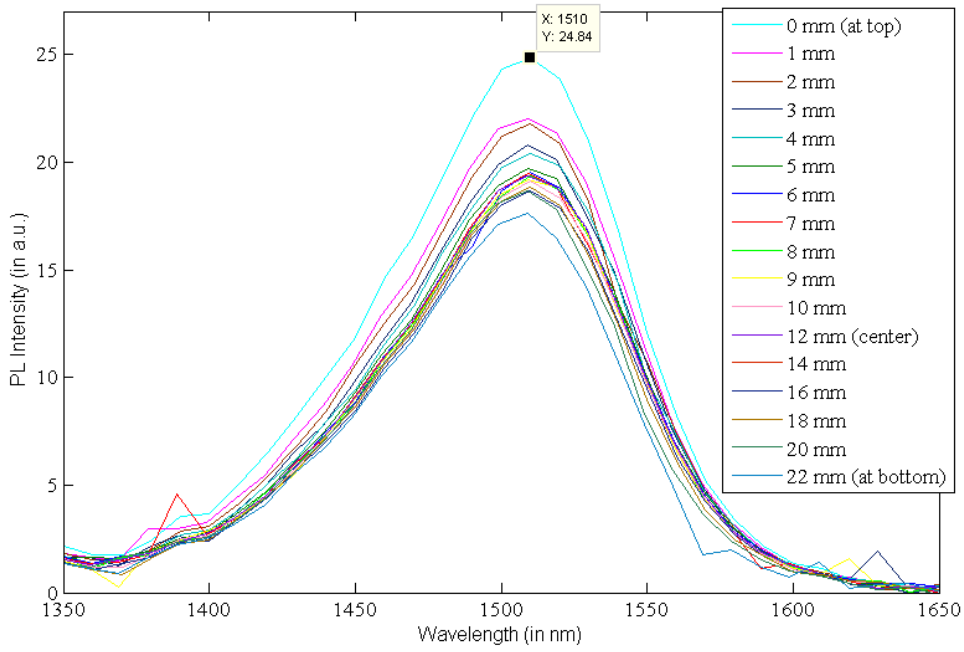

(a) R0296

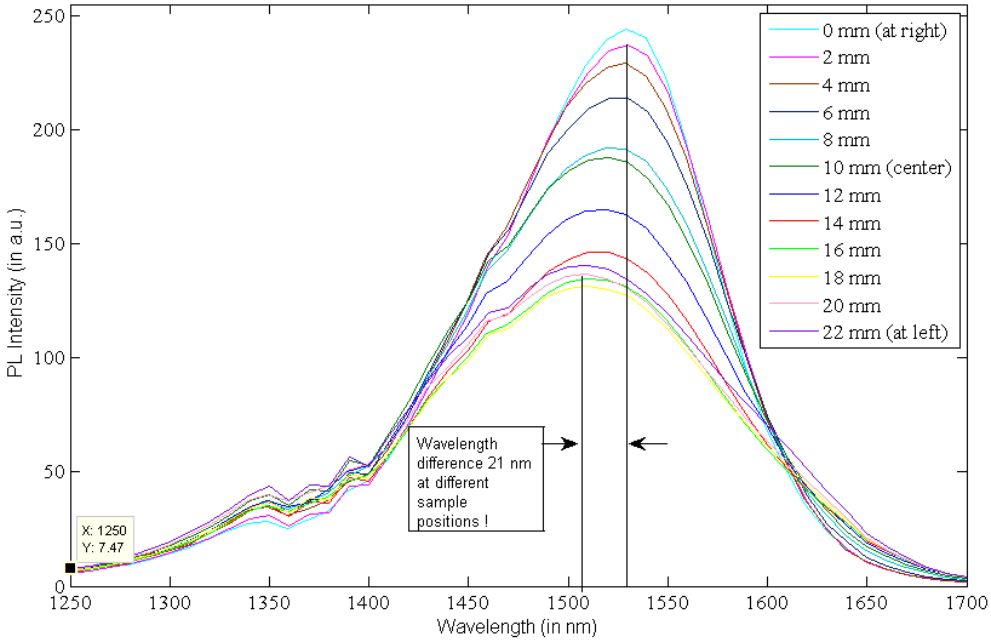

(b) R0297

Figure 4.20: Comparison of wavelengths and PL intensities of two QW samples by RT PL: (a) reference InGaAs QW sample (R0296) and (b) Bi-containing InGaAsBi QW sample (R0297), showing different PL intensities at different wavelengths in position varying RTPL measurements.

Figure 4.21 shows comparison of wavelengths between reference InGaAs QW 'R0296' (red) and InGaAsBi QW 'R0297' (blue) samples. For the reference 'R0296', uniformity is observed in wavelength, i.e, wavelength is almost the same (1510 nm) for all measured sample positions. For R0297, non-uniformity is found in wavelength, i.e., wavelength is different for different sample positions. Longer wavelength at 1530 nm is obtained at the right side of the sample, i.e., 20 nm longer than the ref. R0296 for some positions during RTPL characterization. But, no observable wavelength difference has been achieved at the left side of the sample. The possible reason can be that very little amount of Bi is incorporated in this part of the sample during MBE growth.

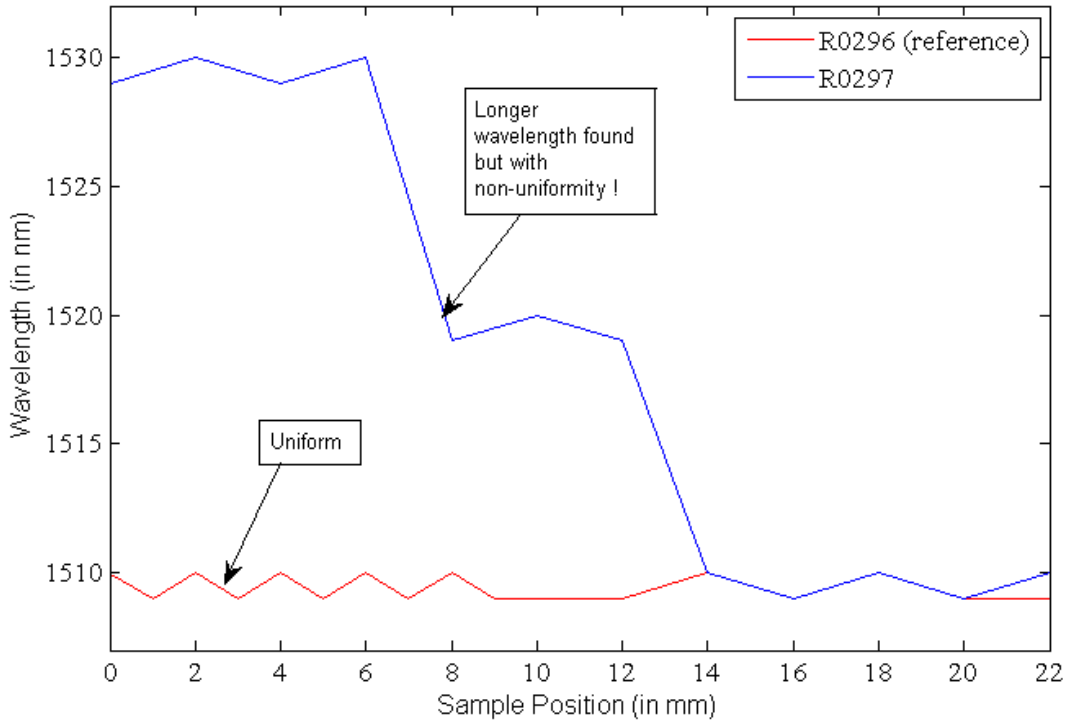

Figure 4.21: Comparison of wavelengths between reference InGaAs QW (R0296) and InGaAsBi QW (R0297) samples. R0297 shows non-uniform longer wavelength features at different sample positions.

Figure 4.22 shows comparison of PL intensities between reference InGaAs QW 'R0296' (red) and InGaAsBi QW 'R0297' (blue) samples. R0297 shows better intensity features at different sample positions than the ref. R0296. For some parts of the samples with long wavelengths thus high Bi concentration, 10 times higher intensity is found for R0297 than the ref. R0296 and at least 5 times or more higher intensity is observed for other parts of R0297 with short wavelengths. So, Bi-containing QW sample 'R0297' ensures better optical quality than the reference R0296.

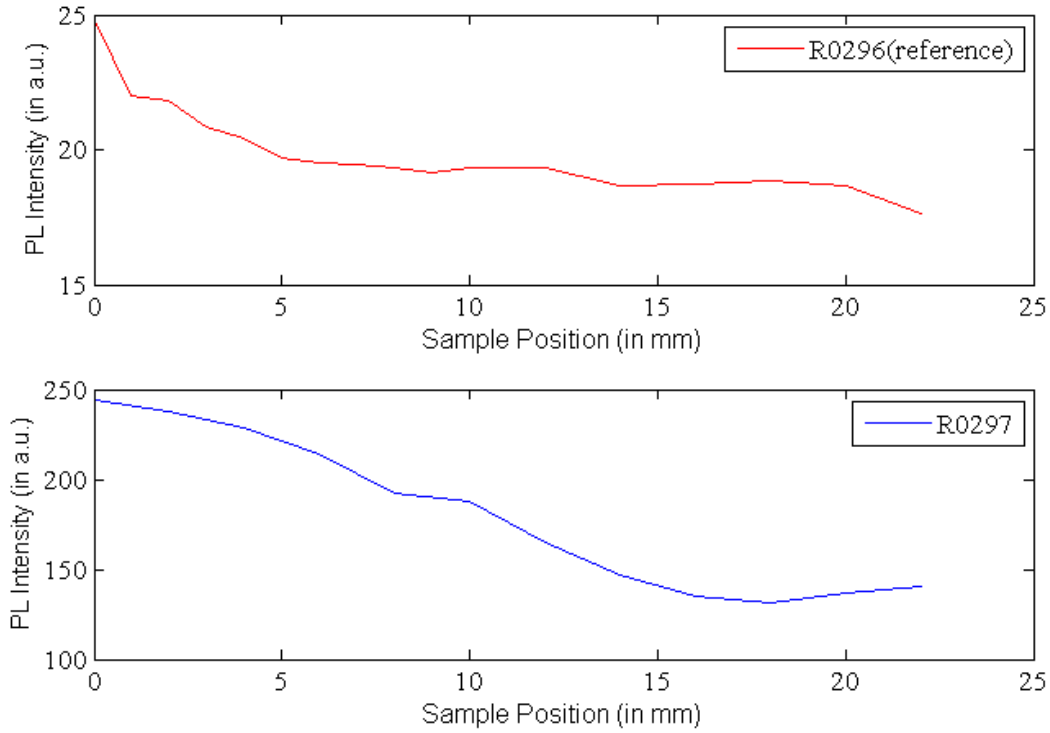

Figure 4.22: Comparison of PL intensities between reference InGaAs QW 'R0296' (red) and InGaAsBi QW 'R0297' (blue) samples. R0297 shows better intensity features at different sample positions than the ref. R0296.

4.2.2 Low Temperature PL (LTPL)

Low Temperature PL (LTPL) has been performed to investigate how the intensities and wavelengths, full width at half maximum (FWHM) energy and band gap energies change with temperature for InGaAsBi QW samples. For the reference InGaAs QW sample 'R0296', the temperature is varied from 47 Kelvin to 330 Kelvin and for the Bi-containing InGaAsBi QW sample, this temperature range was from 45 Kelvin to 330 Kelvin during LTPL characterizations.

Figure 4.23 shows the curves for comparison of wavelengths and PL intensities of two QW samples by LTPL measurement technique. From these two figures, it is found that PL intensities dropped and peak wavelength became longer gradually with increasing temperature. These two issues (PL intensity and wavelength) are discussed later.

At the lowest measured temperature, the shortest wavelength and the highest PL intensity are found for both QW samples. On the other hand, at the highest measured temperature, the longest wavelength and the lowest PL intensity are found for both QW samples. By observing

these curves, 10 times higher PL intensity has been obtained when Bi is incorporated into InGaAs QW material.

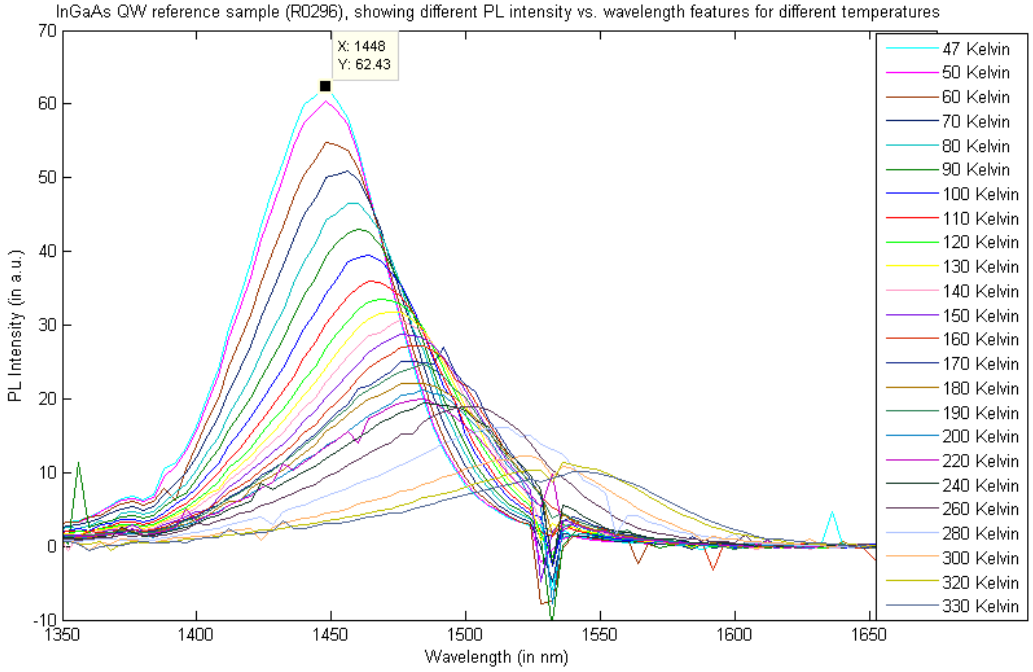

(a)

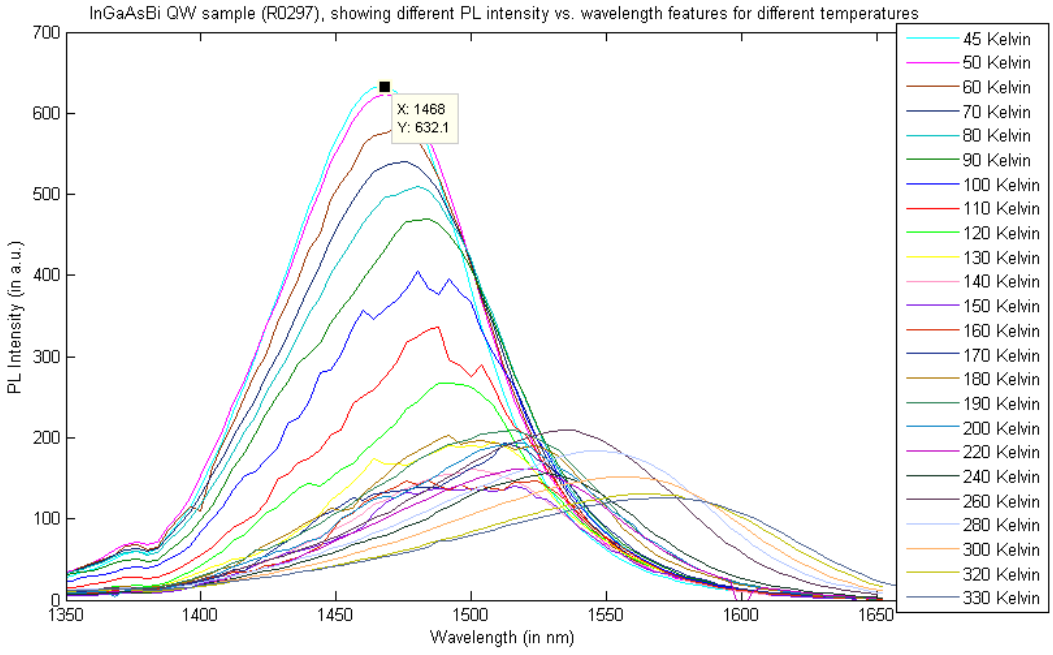

(b)

Figure 4.23: Comparison of wavelengths and PL intensities of two QW samples by LT PL: (a) reference InGaAs QW sample (R0296) and (b) Bi-containing InGaAsBi QW sample (R0297), showing different PL intensities at different wavelengths in temperature varying LTPL measurements.

Figure 4.24 shows comparison between two QW samples, reference 'R0296' (red) and Bi-containing 'R0297' (blue). Figure 4.24 (a) shows maximum PL intensity obtained at the lowest temperature and Figure 4.24 (b) shows maximum wavelength difference obtained at the highest measured temperature during LTPL characterization. From Figure 4.24 (a), the maximum PL intensity value of 632 a.u. is observable and the peak wavelength is found to be 1468 nm for R0297 at 45 Kelvin. At the similar temperature of 47 Kelvin, the 1448 nm peak wavelength and the maximum 62 a.u. PL intensity value are found for reference R0296. So the PL intensity difference is 10 times and the wavelength shift is 20 nm. Similarly from Figure 4.24 (b), the PL intensity difference is found by 12.5 times between the two samples and the maximum wavelength shift is 24 nm.

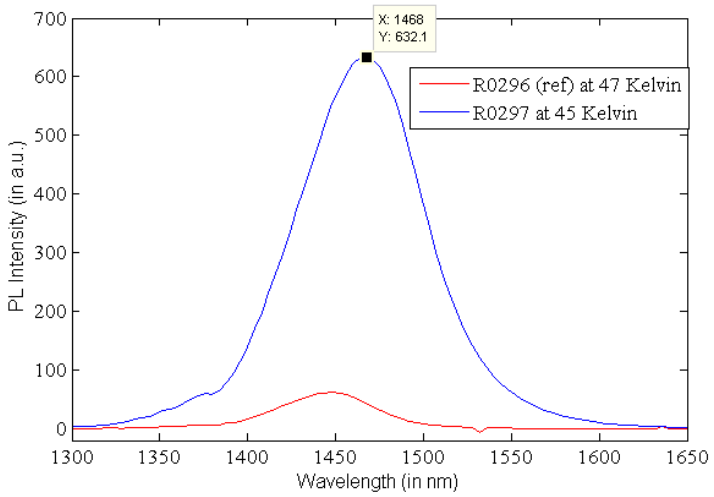

(a)

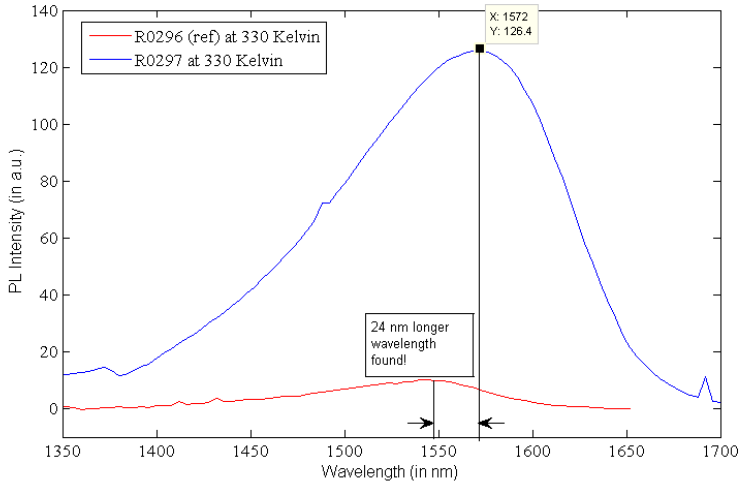

(b)

Figure 4.24: Comparison between two QW samples, reference 'R0296' (red) and Bi-containing 'R0297' (blue): (a) where maximum PL intensity obtained at the lowest temperature and (b) where maximum wavelength shift obtained at the highest measured temperature during LTPL measurement.

Figure 4.25 (a) and (b) shows comparison of reference InGaAs QW 'R0296' (red) and InGaAsBi QW 'R0297' (blue) samples by showing different wavelength and FWHM energy features for different measured temperatures, respectively. From Figure 4.25 (a), the difference in wavelengths between R0296 and R0297 at different measured temperatures is clearly observable, which is discussed before. Figure 4.25 (b) is achieved from Figure 4.25 (a), where FWHM energies are calculated from wavelength information and more fluctuations are observed in FWHM energies at higher measuring temperature when Bi is incorporated into QW material.

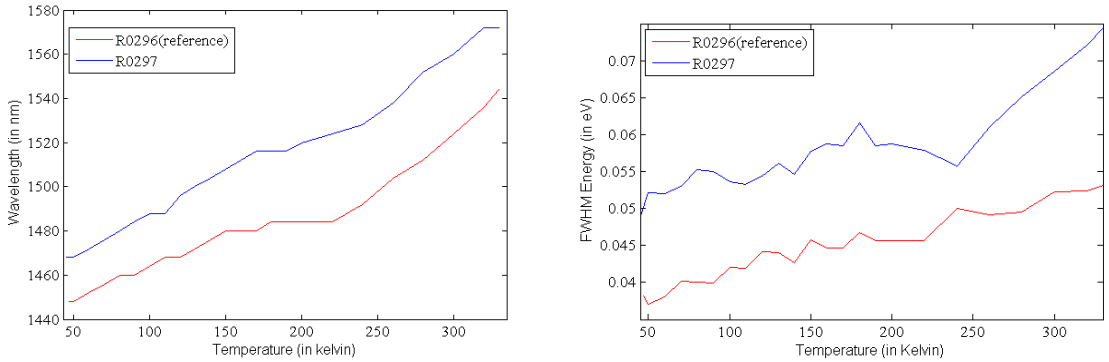

(a) (b)

Figure 4.25: Comparison of reference InGaAs QW 'R0296' (red) and InGaAsBi QW 'R0297' (blue) samples, showing different (a) wavelength and (b) FWHM energy features at different measured temperatures.

Generally, the relation between change of the band gap energy and measured different temperatures can be calculated from the *Varshni approximation* [31]:

$$E_g\,(T) = E_g\,(0) - \frac{AT^2}{B+T}\;(eV) \qquad (4.2.1)$$

Here, $E_g\,(T)$ is the temperature dependent bandgap energy, $E_g\,(0)$ is the bandgap energy at 0 Kelvin, T is the measuring temperature in Kelvin, A and B are two empirical material parameters. Equation 4.2.1 describes how the bandgap energy changes with temperature.

According to Karachevtseva et al. (1994) [32] [33], the bandgap energy equation for InGaAs is:

$$E_g\,(x,T) \cong E_g(0) - \frac{\{6(1-x)^2 - 8.6\times(1-x) + 5.2\}\times 10^{-4}\times T^2}{T + \{337(1-x)^2 - 455\times(1-x) + 196\}}\;(eV) \qquad (4.2.2)$$

Here, x is the Indium-composition of $In_xGa_{1-x}As$ alloy.

By comparing equation 4.2.2 with the *Varshni approximation* (eqn.: 4.2.1), the empirical material parameters, A and B, can be determined, i.e.,

$$A = \{6(1-x)^2 - 8.6 \times (1-x) + 5.2\} \times 10^{-4}, \quad (4.2.3)$$

$$B = 337(1-x)^2 - 455 \times (1-x) + 196. \quad (4.2.4)$$

And according to Goetz et al. (1983) [32] [34], the equation of band gap energy at 2 Kelvin is:

$$E_g(T = 2\ K) \cong 0.4105 + 0.6337\ (1-x) + 0.475(1-x)^2\ (eV) \quad (4.2.5)$$

Since 2 Kelvin is very near to 0 Kelvin, equation 4.2.5 can be considered to determine $E_g(0)$.

In this QW material project, $x = 0.45$ is used as the composition of Indium. By injecting the value of xx in the equations 4.2.3, 4.2.4 and 4.2.5, it can be determined that $A = 2.285 \times 10^{-4}$, $B = 47.6925$ and $E_g(0) \cong 0.9027\ eV$, respectively.

Now, the equation 4.2.2 becomes,

$$E_g\ (x = 0.45, T = 2\ K)\ \cong 0.9027 - \frac{2.285 \times 10^{-4} \times T^2}{T + 47.6925}\ (eV) \quad (4.2.6)$$

In Figure 4.26, the difference of band gap energies between calculated and measured values for QW materials are shown. The green line is plotted using Equation 4.2.6 for different measured temperatures (T). The band gap energies for electron and hole confinements are also included and considered as constant for the measured curves. So, the energy equation for the measured curves can be written as below.

$$E_{PL}(T) = E_g(T) + \Delta E_C(T) + \Delta E_V(T) \quad (4.2.7)$$

Here, $E_{PL}(T)$ is the temperature-dependant energy from PL measurements. $\Delta E_C(T)$ is the temperature-dependant band gap energy from the electron confinement in conduction band and $\Delta E_V(T)$ is the temperature-dependant band gap energy from the hole confinement in valence band, which are considered as constants for all measured temperatures. The red and blue curves in Figure 4.26 are obtained from the reference and Bi-containing QW materials, respectively.

In comparison with the calculated curve, similar patterned but lower valued energy-curves can be observed for both the measured curves from Figure 4.26. The difference in energy between calculated and measured (for the reference QW) curves vary from 0.039 eV to 0.026 eV, whereas, it varies from 0.052 eV to 0.043 eV for Bi-containing QW with increasing measuring temperature. Also reduced band gap energy has been observed in Bi-containing QW material compared to the reference one. On an average, 0.015 eV reduced band gap energy has been found, when Bi is incorporated into InGaAs QW.

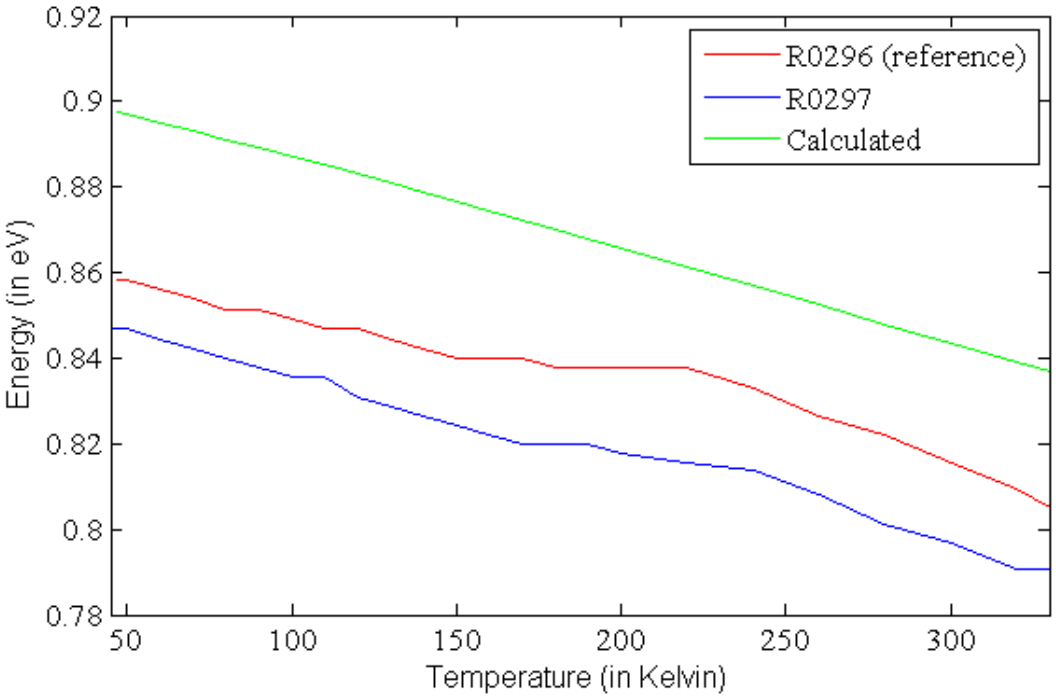

Figure 4.26: Comparison of band gap energies between calculated (green line, calculated from equation 4.2.6) and measured (red and blue) values for QW materials. Electron and hole confinements are also included for the measured values.

Figure 4.27 shows comparison of reference InGaAs QW 'R0296' (red) and InGaAsBi QW 'R0297' (blue) samples, where difference in PL intensities at different measured temperatures is shown separately for both QW samples. High PL intensity is observed at low temperatures and gradually decreases with increasing temperature. At low temperatures, the carrier lifetime is long resulting in high PL intensities. The carrier lifetime becomes short at room temperature or higher temperatures, and PL intensities dramatically drop.

After comparing these two QW samples, it is realized that 10 times higher PL intensity of Bi-containing QW sample (R0297) ensures better optical quality than the reference R0296 sample.

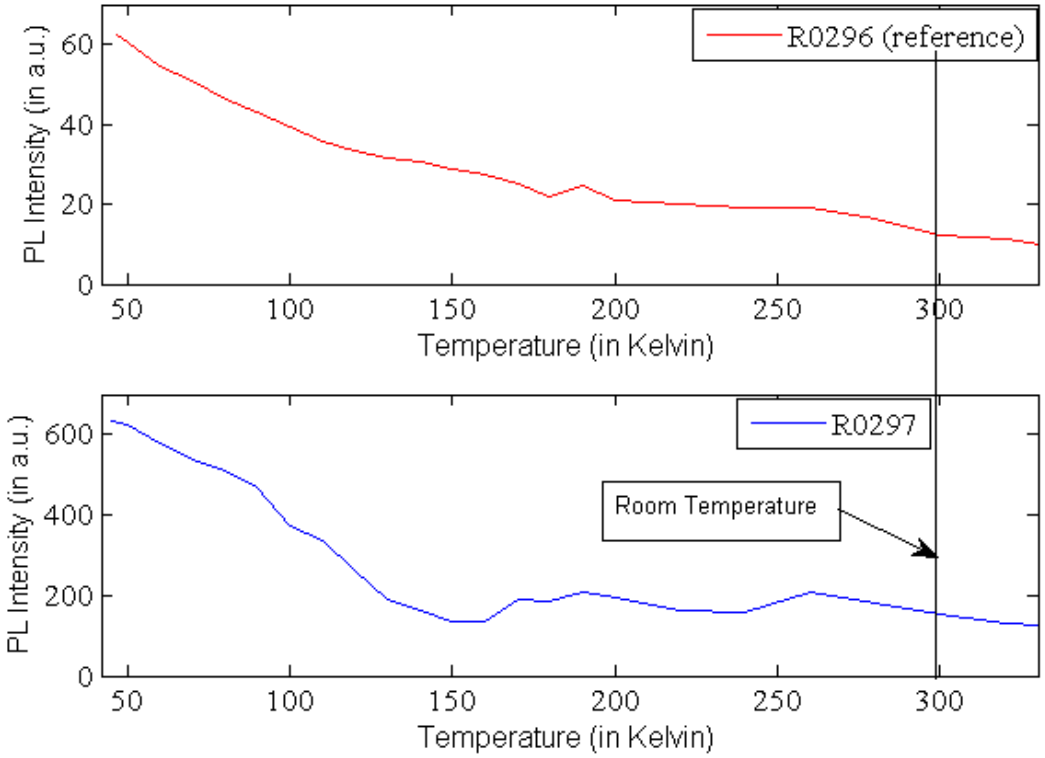

Figure 4.27: Comparison of reference InGaAs QW 'R0296' (red) and InGaAsBi QW 'R0297' (blue) samples, showing difference in PL intensities at different temperatures.

Chapter 5

5. Characterizations, results & analysis on Bi_2Te_3 by AFM and XRD

Depending on different growth temperature, growth method, growth time, thickness, substrate-type and flux ratio of the samples, the investigation on Bi_2Te_3 has been divided into three groups. Below is the discussion on MBE grown Bi_2Te_3 material considering all different growth conditions with the help of AFM and XRD characterization techniques. AFM and XRD are used to obtain surface morphology and structural properties of the samples, respectively. Step profiler is used to measure the thickness of the samples.

5.1 Group 1: Optimization of growth temperature

For these set of samples, growth methods were the same for the samples except growth temperature, T_g, varied from 200°C to 280°C with a step of 20°C. The doped Si(111)N+ conductive material is used as substrate for this sample-set.

Figure 5.1 shows AFM height images of a Bi_2Te_3 sample 'R0423' grown at 200°C obtained from (a) 1x1 μm² and (b) 10x10 μm² scan size. The measured top layer (i.e., Bi_2Te_3 layer) thickness is 150 nm. Though RMS roughness (mentioned above each image) is less in small scale, flake-like feature is found during the large scale scanning for this sample.

RMS roughness: 0.74 nm

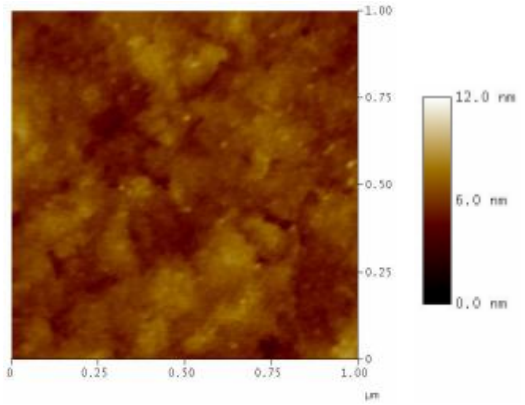

(a)

RMS roughness: 4.33 nm

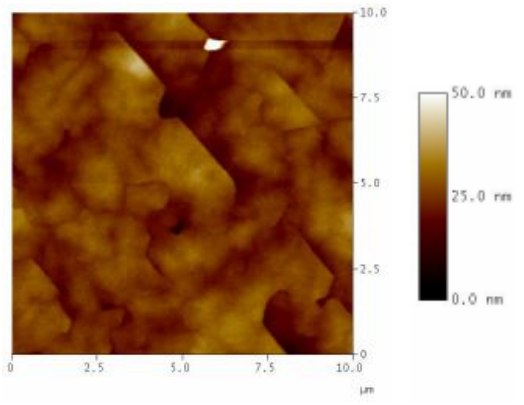

(b)

Figure 5.1: (a) 1x1 μm²and (b) 10x10 μm² AFM height images of a Bi_2Te_3 sample 'R0423' grown at 200 °C.

Figure 5.2 shows AFM height images of a Bi_2Te_3 sample 'R0424' grown at 220 °C obtained from scan size (a) 1x1 μm² and (b) 10x10 μm². In this case, the measured top layer (i.e., Bi_2Te_3 layer) thickness is 160 nm. Atomic steps are clearly observable with even better morphology from the small scale AFM image, which ensures higher quality material. But, flake-like feature is still present in the large scale scanning.

RMS roughness: 0.66 nm

RMS roughness: 6.25 nm

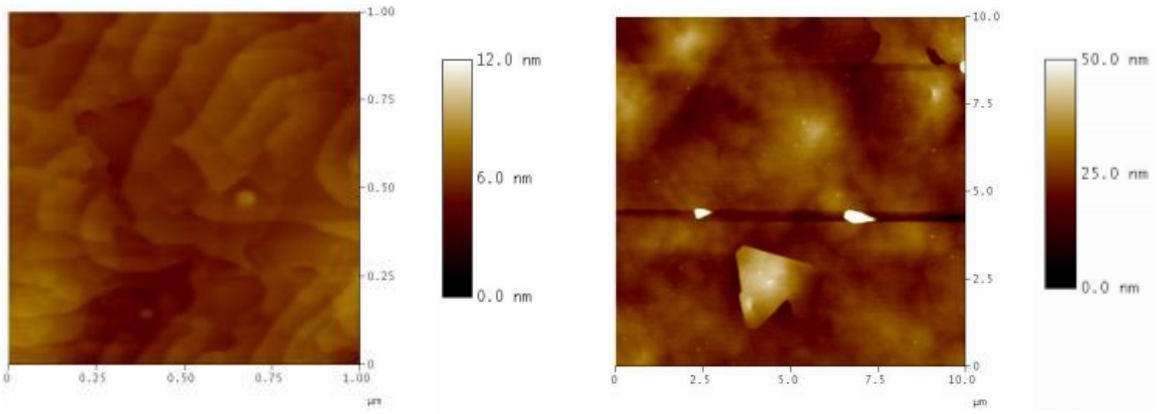

(a) (b)

Figure 5.2: (a) 1x1 μm²and (b) 10x10 μm² AFM height images of a Bi_2Te_3 sample 'R0424' grown at 220 °C.

Figure 5.3 shows AFM height images of a Bi_2Te_3 sample 'R0425' grown at 240 °C obtained from scan size (a) 1x1 μm² and (b) 10x10 μm². The measured top layer (i.e., Bi_2Te_3 layer) thickness is 165 nm. The lowest surface RMS roughness both in the small and the large scale are found from this sample, which ensures high quality material. Atomic steps can also be seen from the small scale morphology. However, holes are also pointed out from the hazy region of the sample.

RMS roughness: 0.46 nm

RMS roughness: 2.0 nm

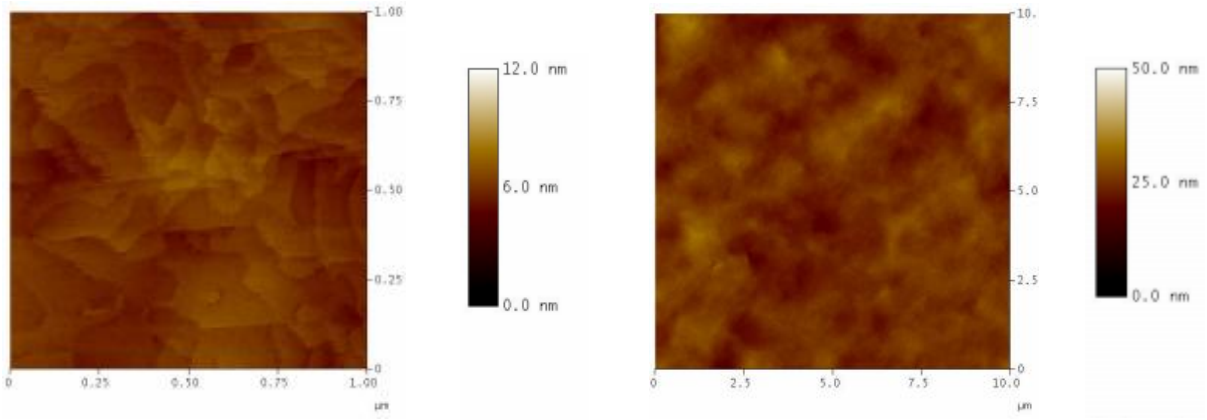

(a) (b)

Figure 5.3: (a) 1x1 μm²and (b) 10x10 μm² AFM height images of a Bi_2Te_3 sample 'R0425' grown at 240 °C.

Figure 5.4 shows AFM height images of a Bi_2Te_3 sample 'R0426' grown at 260 °C obtained from scan size (a) 1x1 μm² and (b) 10x10 μm². The measured top layer (i.e., Bi_2Te_3 layer) thickness is 100 nm. At this T_g, the sample surface became very rough. High density of small and different shaped droplets is also observed from the large scale AFM image. The reason for having it is not known yet.

RMS roughness: 11.87 nm

RMS roughness: 15.41 nm

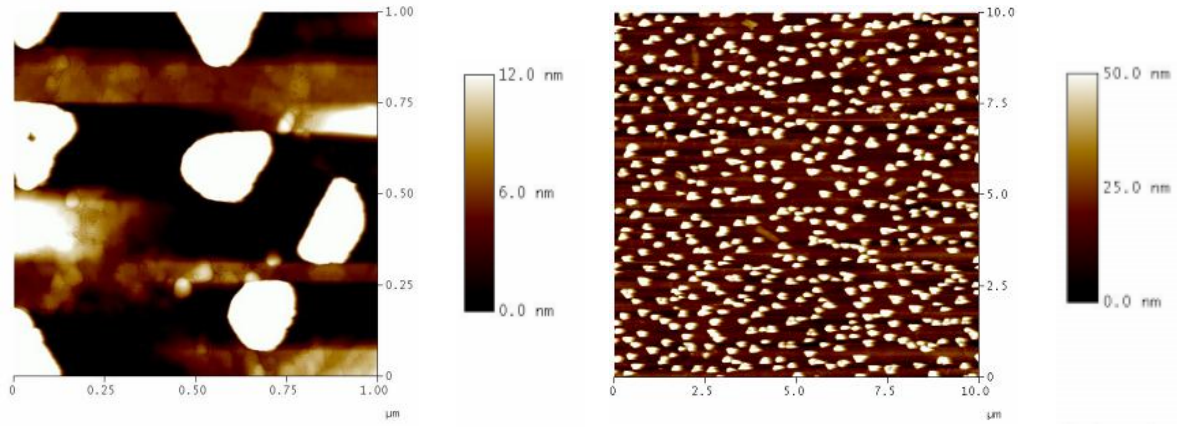

(a) (b)

Figure 5.4: (a) 1x1 μm²and (b) 10x10 μm² AFM height images of a Bi_2Te_3 sample 'R0426' grown at 260 °C.

Figure 5.5 shows AFM height images of a Bi_2Te_3 sample 'R0427' grown at 280 °C obtained from scan size (a) 1x1 μm² and (b) 10x10 μm². The measured top layer (i.e., Bi_2Te_3 layer) thickness is 30 nm. Better morphology with observable atomic steps in small scale scanning has been found for the sample grown at 280 °C compared to sample grown at 260 °C. The

surface RMS roughness is also lower at this T_g than at 260 °C. But high density of non-uniformed, different shaped holes is found during the large scale AFM scanning.

RMS roughness: 0.96 nm

RMS roughness: 10.87 nm

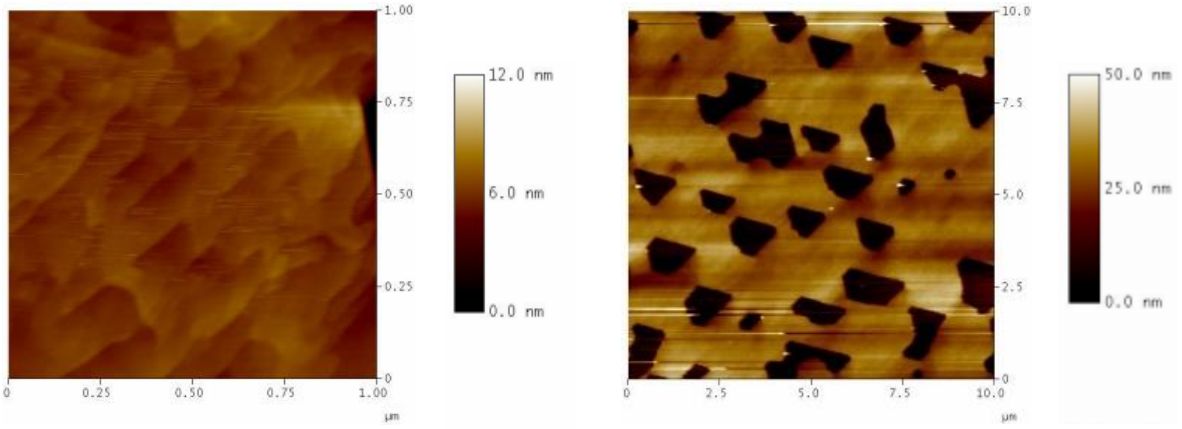

(a) (b)

Figure 5.5: (a) 1x1 µm²and (b) 10x10 µm² AFM height images of a Bi_2Te_3 sample 'R0427' grown at 280 °C.

Figure 5.6 shows the graph of surface RMS roughness of Bi_2Te_3 samples for different growth temperatures from 1x1 µm² (blue) and 10x10 µm² (green) AFM scanning. At around T_g 200 °C and 240 °C, almost flat surface has been found both in small and large scale scanning. And then the surface became very rough at 260 °C. From the graph below, it can be pointed out that the lowest surface RMS roughness is obtained from sample R0425 at T_g = 240 °C.

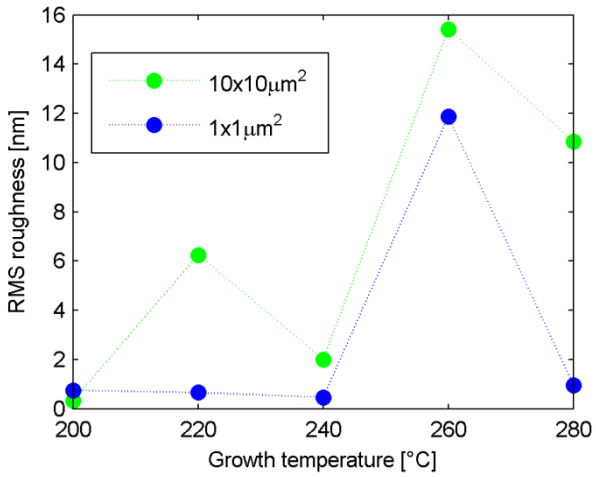

Figure 5.6: Surface RMS roughness (in nm) of Bi_2Te_3 samples grown at different growth temperatures (Tg in °C) for 1x1 µm² (blue) and 10x10 µm² (green) scan size.

Figure 5.7 describes XRD (111) rocking curves of Bi_2Te_3 samples comparing different growth temperatures. This graph shows (0015) peaks only, not the full range scanning. Considering

peak intensities and widths of the XRD curves, R0424 (red colored curve) and R0425 (green colored curve) samples which grown at 220 °C and 240 °C, respectively, have the best results. Both have higher peak intensities and narrower widths. The lowest peak intensities and large widths, i.e. the worst results, are found from R0426 and R0427 samples (magenta and cyan colored curves, respectively) in XRD characterization.

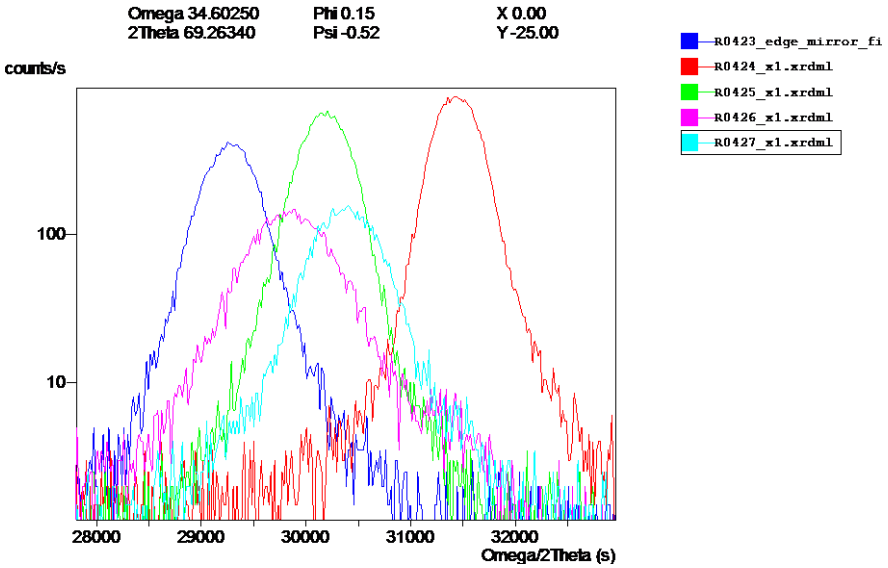

Figure 5.7: Comparison of XRD (111) rocking curves of Bi_2Te_3 samples at different growth temperatures, showing (0015) peaks only.

Finally it is realized that around 240 °C is the best growth temperature evaluated by both AFM and XRD characterizations.

5.2 Group 2: Comparison of different growth methods

Three different growth methods have been experimented for comparison, which are discussed here. Same growth method has been followed for the set of samples discussed in group 1 (R0423 to R0427). In this case, Bi_2Te_3 samples are grown at 200 °C or higher temperatures. But at first prior to the Bi_2Te_3 layer growing for 1 hour, Te soaked the substrate for 10 minutes and after that Bi and Te are co-deposited at low temperature. After this co-deposition, the samples are heated up and Bi_2Te_3 crystal layer started to form at around 200 °C. So for this set of samples, Bi_2Te_3 layer has been grown on it at this 200 °C or higher temperature (i.e., up to 280 °C). For sample 'R0428', Bi_2Te_3 was directly grown on Si(111)N+ substrate for 1 hour at same T_g for R0423, i.e., 200 °C with Te soaking. Based on R0425,

sample 'R0429' was grown. But in this case, Bi treatment has been used as a replacement of Te soaking prior to the Bi_2Te_3 growth.

Figure 5.8 (a) and (b) shows 1x1 μm^2 and 10x10 μm^2 AFM height images, respectively, of a Bi_2Te_3 sample 'R0428' where the Bi_2Te_3 layer is directly grown at 200 °C with Te soaking. Here, the measured top layer (i.e., Bi_2Te_3 layer) thickness is 90 nm only, which is smaller than its counterpart sample R0423. From the AFM images below, better surface morphology has been observed in comparison with R0423, grown at the same T_g. Atomic steps and holes can also be seen from the small scale and the large scale morphologies, respectively. Figure 5.8 (c) shows XRD (111) rocking curves of R0423 (blue) and R0428 (red) of Bi_2Te_3 samples to compare different growth methods. From this XRD rocking curves, it is examined that at T_g 200 °C, the directly grown Bi_2Te_3 sample (R0428) shows higher intensity than R0423. However, at higher temperature (e.g., 240 °C), no Bi_2Te_3 crystal layer has been found on sample surface if direct growth method followed. In this case, both Bi and Te are re-evaporated from the sample surface. So, when the growth temperature is higher than 200 °C, direct growth becomes unrealistic.

RMS roughness: 0.46 nm

RMS roughness: 2.79 nm

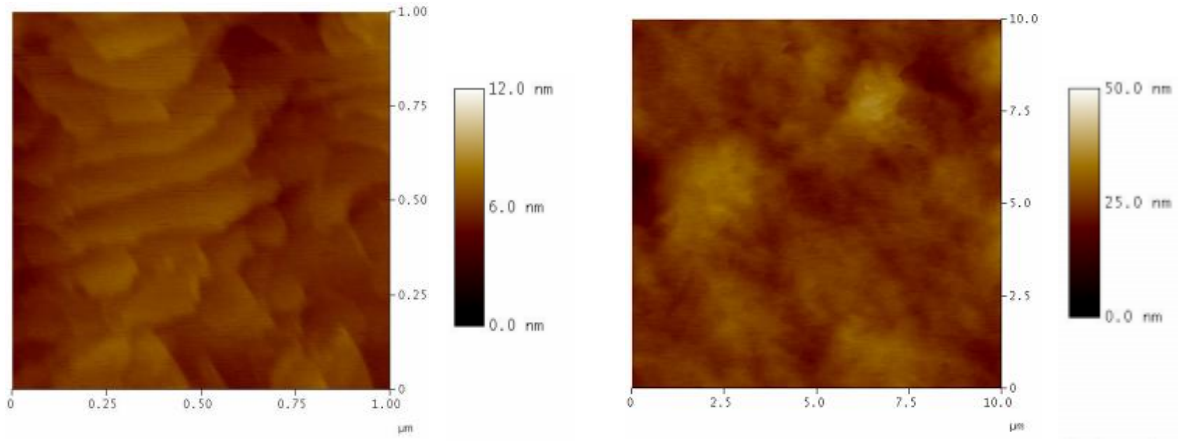

(a) (b)

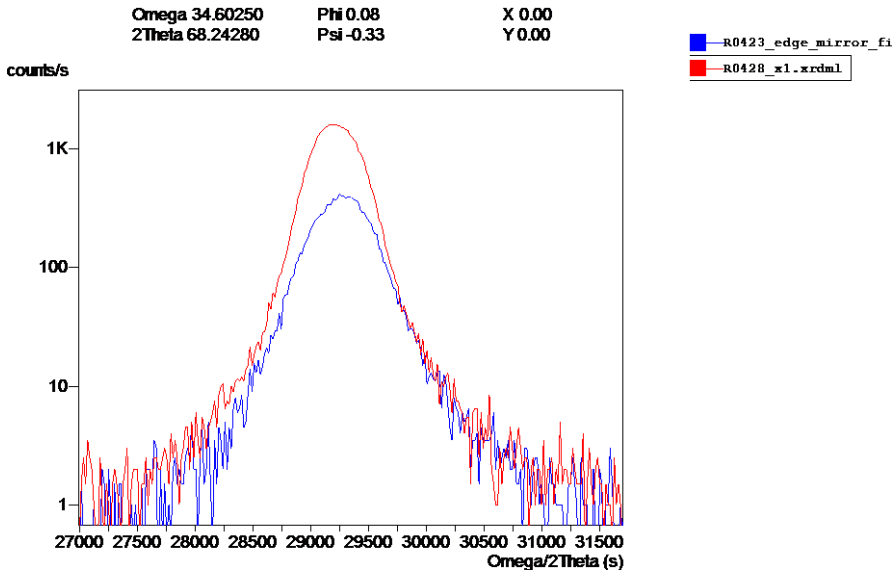

(c)

Figure 5.8: (a) 1x1 µm² and (b) 10x10 µm² AFM height images of a Bi_2Te_3 sample 'R0428' where the Bi_2Te_3 layer directly grown at 200 °C with Te soaking. (c) Comparison of XRD (111) rocking curves of R0423 (blue) and R0428(red) of Bi_2Te_3 samples at different growth methods, showing (0015) peaks only.

Figure 5.9 (a) and (b) shows 1x1 µm² and 10x10 µm² AFM height images, respectively, of a Bi_2Te_3 sample 'R0429' where Bi treatment is used instead of Te soaking in advance of the material growth at T_g = 240 °C. The measured top layer (i.e., Bi_2Te_3 layer) thickness is 210 nm. In comparison with R0425 at the same T_g = 240 °C, sample R0429 with Bi treatment has better surface (i.e., lower RMS roughness) in large scale. Atomic steps and holes are found from the small scale and the large scale morphologies, respectively. Figure 5.9 (c) shows XRD

(111) rocking curves for R0425 (blue) and R0429 (red) of Bi_2Te_3 samples to compare different growth methods. No obvious difference has been monitored in peak intensity or width from the XRD curves.

RMS roughness: 0.42 nm

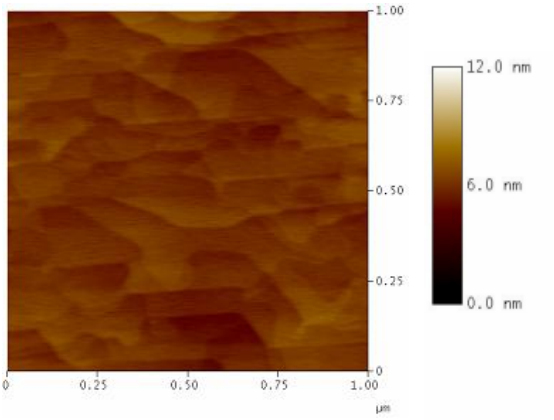

(a)

RMS roughness: 0.90 nm

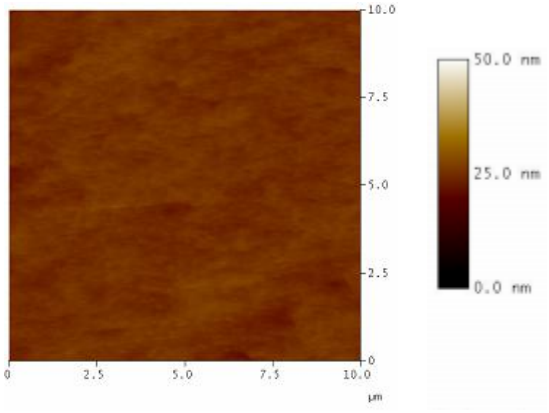

(b)

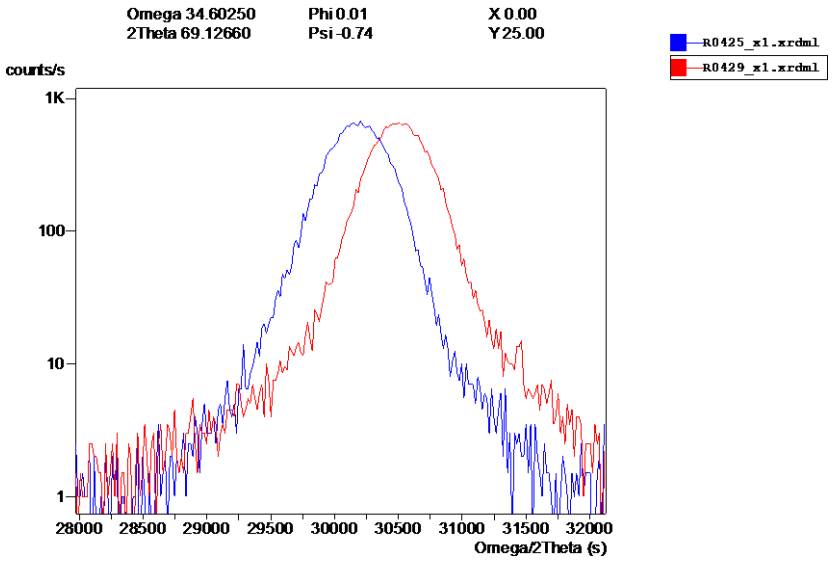

(c)

Figure 5.9: (a) 1x1 µm² and (b) 10x10 µm² AFM height images of a Bi_2Te_3 sample 'R0429' where Bi treatment is used instead of Te soaking in advance of the material growth at T_g = 240 °C. (c) Comparison of XRD (111) rocking curves of R0425 (blue) and R0429 (red) of Bi_2Te_3 samples at different growth methods, showing (0015) peaks only.

5.3 Group 3: Comparison of different flux ratio

Two samples (R0430 and R0431) are grown in order to compare the significant difference for different Bi/Te flux. For both samples, the top Bi_2Te_3 layer is grown for three hours at the same T_g = 200 °C. For this group of samples, semi insulating non-conductive Si (111) SI substrates are used. Higher Bi flux (i.e., higher beam equivalent pressure (BEP) for Bismuth) is used to grow sample R0431. The BEP of Bismuth for R0430 is $6x10^{-8}$, whereas, it is $1.2x10^{-7}$ for R0431.

Figure 5.10(a)–(d) shows AFM height images of two Bi_2Te_3 samples at T_g 200 °C with different Bi flux, where (a) and (b) are showing 1x1 μm² and 10x10 μm² scanning range for 'R0430' sample with Bi BEP $6x10^{-8}$, respectively, and (c) and (d) are showing 1x1 μm² and (d) 10x10 μm² scanning range for 'R0431' sample with Bi BEP $1.2x10^{-7}$, respectively. Sample R0423 and R0430 are grown at the similar condition; the only difference is growth time. For R0423, the growth time was 1 hour, whereas for R0430, it was 3 hours. From Figure 5.10(a) and (b), it is pointed out that though the surface RMS roughness is higher for R0430, but the morphology of this sample is not far from R0423. In Figure 5.10 (d), large scale AFM scanning ensures much rougher surface for R0431 than R0430. Also strong trenches in only one direction can be found for R0431. Figure 5.10(e) shows XRD (111) rocking curves of R0430 (blue) and R0431 (red), to compare the difference in peaks or widths. From the XRD figure, it is observed that peaks are not overlapped and sample R0431 has higher and narrower peak intensity than sample R0430. Here, top layer (i.e., Bi_2Te_3 layer) thickness of R0430 is very small in comparison with R0431. Generally, less thick samples give lower peaks and broader widths in XRD characterization. So in this case, the reason for having it could be the thickness difference of the top layer.

RMS roughness: 1.06 nm

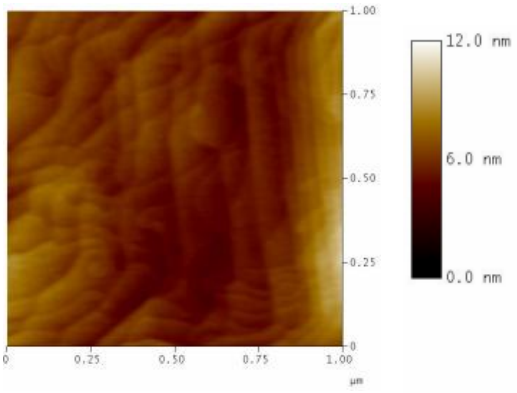

(a)

RMS roughness: 5.87 nm

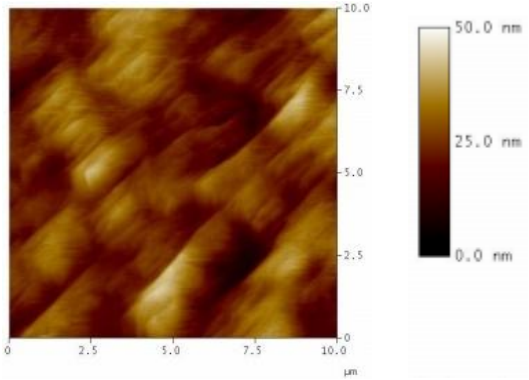

(b)

RMS roughness: 2.64 nm

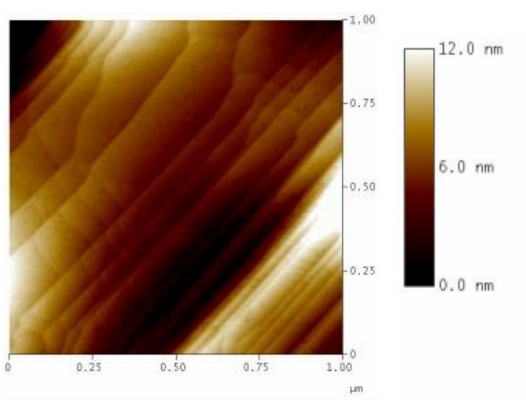

(c)

RMS roughness: 8.38 nm

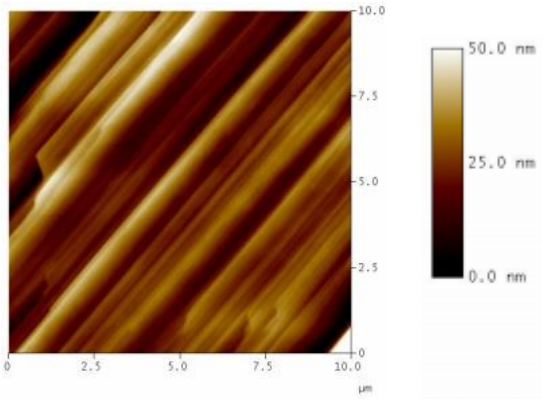

(d)

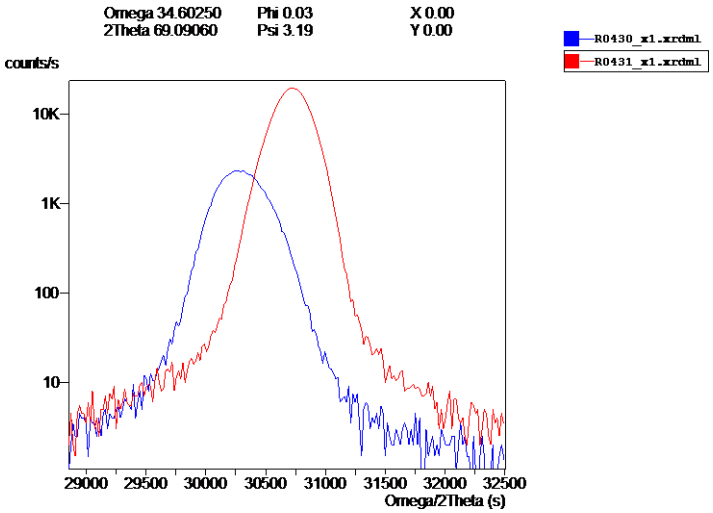

(e)

Figure 5.10: (a) – (d) AFM height images of two Bi_2Te_3 samples at T_g = 200 °C with different Bi flux: (a) 1x1 µm² and (b) 10x10 µm²scanning range, respectively, for 'R0430' sample with Bi BEP = $6x10^{-8}$; (c) 1x1 µm² and (d) 10x10 µm²scanning range, respectively, for 'R0431' sample with Bi BEP = $1.2x10^{-7}$. (e) XRD (111) rocking curves of R0430 (blue) and R0431 (red) of Bi_2Te_3 samples with different Bi flux to compare the difference in peaks or widths, curves showing (0015) peaks only.

Chapter 6

6. Summary and future direction

6.1 Summary

New semiconductor materials with more beneficial properties are continuously demanding for device applications. In this research project, different features have been found and studied for different Bi containing compounds. MBE grown Bismuth containing compounds GaSbBi, GaAsBi, InGaAsBi QW, InSbBi and also Bi_2Te_3 are investigated by Atomic Force Microscopy (AFM), X-ray diffraction (XRD) and Photoluminescence (PL) techniques and then surface morphologies, structural and optical properties are explored from these characterizations, respectively. Different growth methods have been applied to catch comparatively accurate Bi composition. The varying parameters were basically growth temperatures, growth rates and Bi flux.

So far, Bi is incorporated into GaAs for making GaAsBi. The MBE grown $GaSb_{1-x}Bi_x$ thin films are established for the first time. From XRD and AFM, better results have been obtained for growth temperature 370 ºC and then saturation occurs. Strategies have been taken care of to avoid the formation of Bi droplets and enhance Bi incorporation. GaSbBi Samples were grown on GaSb and GaAs substrates for comparison and rougher surface morphologies have been found for samples grown on GaAs substrates compare to that grown on GaSb substrate. InGaAsBi QW samples are characterized by PL at room temperature (RTPL) and also at low temperature (LTPL) for different positions and temperatures, respectively. When Bi is incorporated, 10 times higher relative intensity has been achieved comparing with the reference InGaAs QW sample. For Bi_2Te_3 samples, growth temperature of 240°C showed the best feature both in AFM and XRD characterizations. Though at 200°C, the direct grown sample showed better feature than samples grown with Te soaking prior to Bi_2Te_3 layer, but direct growth is not feasible at higher growth temperatures.

6.2 Future direction

Since this project on Bi-containing compounds is still under experimental demonstration, there is a lot to do for improving the material quality. At the current stage, lots of defects have been found in materials due to the vacancies or holes inside the materials. In future, this problem should be taken care of for having better quality materials with flat surfaces. One important future goal of this project is to establish the relation between the lattice constant and the Bi composition. Getting hold of improved quality Bi containing QW at 1.55 μm is another goal of this research in future. To obtain this challenging triumph, optimization of QW without Bi could be performed first. After having optimization of QW without Bi, perfect Bi containing QW can be achieved by incorporating Bi for different growth conditions.

References

1. S. Francoeur, M. J. Seong, A. Mascarenhas, S. Tixier, M. Adamcyk, and T. Tiedje, “Band gap of GaAs[sub 1-x]Bi[sub x], 0<x<3.6%”, *Applied Physics Letters*, vol. 82, no. 22, p. 3874, 2003.
2. K. Alberi, J. Wu, W. Walukiewicz, K. Yu, O. Dubon, S. Watkins, C. Wang, X. Liu, Y.-J. Cho, and J. Furdyna, “Valence-band anticrossing in mismatched III-V semiconductor alloys”, *Physical Review B*, vol. 75, no. 4, p. 045203, Jan. 2007.
3. S. J. Sweeney, Z. Batool, T. J. C. Hosea, and S. R. Jin, “The Potential of III-Bismides for Near- and Mid-IR Photonic Devices”, in *1st International Workshop on Bismuth-Containing Semiconductors: Theory, Simulation, and Experiment*, 2010.
4. G. E. Smith, R. Wolfe, “Thermoelectric Properties of Bismuth-Antimony Alloys”, *Journal of Applied Physics*, vol. 33, no. 3, pp. 841-846, 1962.
5. Y. C. Jung et al, “Material characteristics of metalorganic chemical vapor deposition of Bi_2Te_3 films on GaAs substrates”, *Journal of Crystal Growth*, vol. 290, no. 24, pp. 441-445, 2006.
6. T. Tiedje, E. C. Young, and A. Mascarenhaus, “Growth and properties of the dilute bismide semiconductor $GaAs_{1-x}Bi_x$ a complementary alloy to the dilute nitrides”, *International Journal of Nanotechnology*, vol. 5, no. 9/10/11/12, pp. 963-983, 2008.
7. Hase, US Patent no. 7, vol. 009, p. 225, 2006.
8. P. M. Asbeck, R. J. Welty, C. W. Tu, H. P. Xin, and R. E. Welser, “Heterojunction bipolar transistors implemented with GaInNAs materials”, *Semiconductor Science and Technology*, vol. 17, no. 18, p. 898- 906, 2002.
9. K. L. Lew, S. F. Yoon, H. Wang, S. Wicaksono, J. A. Gupta, and S. P. McAlister, “GaAsNSb-base GaAs heterojunction bipolar transistor with a low turn-on voltage”, *Journal of Vacuum Science and Technology B: Microelectronics and Nanometer Structures*, vol. 24, no. 3, pp. 1308- 1310 , May 2006.
10. C. Tarde, “RIBER Compact 21: the World Best Seller Molecular Beam Epitaxy System”, *in III National Conference on Nanotechnology,* Bezons, France, 2009.
11. Y. Song, “Optimization of Metamorphic Materials on GaAs Grown by MBE”, Thesis for the Degree of Licentiate of Engineering, Chalmers University of Technology, 2010.
12. J. Zilko, and J. Greene, “Growth of metastable $InSb_{1-x}Bi_x$ thin films by multitarget sputtering”, *Applied Physics Letters*, vol. 33, no. 3. AIP, p. 254, 1978.
13. K. Oe, S. Ando, and K. Sugiyama, “$InSb_{1-x}Bi_x$ Films Grown by Molecular Beam Epitaxy”, *Japanese Journal of Applied Physics*, vol. 20, no. 4, p. L303 LP – L306, 1981.

14. A. Noreika, W. Takei, M. Francombe, and C. Wood, “Indium antimonide-bismuth compositions grown by molecular beam epitaxy”, *Journal of Applied Physics*, vol. 53, no. 7, p. 4932, 1982.
15. K. Oe and H. Okamoto, “New Semiconductor Alloy $GaAs_{1-x}Bi_x$ Grown by Metal Organic Vapor Phase Epitaxy” *Japanese Journal of Applied Physics*, vol. 37, no. Part 2, No. 11A, p. L1283 LP – L1285, 1998.
16. S. Tixier, M. Adamcyk, T. Tiedje, S. Francoeur, A. Mascarenhas, P. Wei, F. Schiettekatte, “Molecular beam epitaxy growth of GaAs[sub 1-x]Bi[sub x]”, *Applied Physics Letters*, vol. 82, no. 14, p. 2245, 2003.

17. Yuxin Song, Shumin Wang, and Ivy Saha Roy, "Molecular Beam Epitaxy Growth of $GaSb_xBi_{1-x}$", *in 28th North American Molecular Beam Epitaxy Conference*, San Diego, USA, August 2011.
18. Shumin Wang, and Yuxin Song, "Bismuth Incorporation and Lattice Contraction in GaSbBi and InSbBi", *in International Workshop on Bismuth-Containing Semiconductors: Theory, Simulation and Experiment*, Surrey, UK, July 2011.
19. S. Tixier, M. Adamcyk, E. C. Young, J. H. Schmid, and T. Tiedje, “Surfactant enhanced growth of GaNAs and InGaNAs using bismuth”, *Journal of Crystal Growth*, vol. 251, no. 1-4, pp. 449-454, Apr. 2003.
20. E.C. Young, S. Tixier, and T. Tiedje, “Bismuth surfactant growth of the dilute nitride GaN_xAs_{1-x}”, *Journal of Crystal Growth, vol.* 279, no. 3-4, pp. 316-320, 2005.
21. R. R. Wixom, L. W. Rieth, and G. B. Stringfellow, “Sb and Bi surfactant effects on homo-epitaxy of GaAs on (001) patterned substrates”, *Journal of Crystal Growth*, vol. 265, no. 3-4, pp. 367-374, May 2004.
22. A. D. Howard, D. C. Chapman, and G. B. Stringfellow, “Effects of surfactants Sb and Bi on the incorporation of zinc and carbon in III/V materials grown by organometallic vapor-phase epitaxy”, *Journal of Applied Physics*, vol. 100, no. 4, pp. 044904-1 - 044904-8, 2006.
23. M. Yoshimoto, S. Murata, A. Chayahara, Y. Horino, J. Saraie, and K. Oe, “Metastable GaAsBi Alloy Grown by Molecular Beam Epitaxy”, *Japanese Journal of Applied Physics*, vol. 42, no. part 2, No. 10B, pp. L1235-L1237, October 2003.

24. “TE Technology, Inc.” [Online]. Available: http://www.tetech.com/techinfo.
25. “Thermoelectric-cooling.” [Online]. Available: http://searchnetworking.techtarget.com/definition/thermoelectric-cooling.
26. “Thermoelectric-cooling (TEC).” [Online]. Available: http://www.techopedia.com/definition/14769/thermoelectric-cooling-tec.

27. B.C. Sales, “Thermoelectric Materials: Smaller is Cooler”, *Science*, vol. 295. no. 5558, pp. 1248 – 1249, February 2002.
28. L. P. Caywood, and G. Miller, “Anisotropy of the constant energy surfaces in p-type Bi_2Te_3 and Bi_2Se_3 from galvanomagnetic coefficients”, *Physical Review B*, vol. 2, no. 8, pp. 3209-3220, 1970.
29. X. Chen et al, “Molecular Beam Epitaxial Growth of Topological Insulators”, *Advanced Materials*, vol. 23, no. 9, pp. 1162–1165, March 2011.
30. C. B. Satterthwaite, and R. Ure, “Electrical and Thermal Properties of Bi_2Te_3”, *Physical Review*, vol. 108, no. 5, pp. 1164-1170, 1957.
31. Anders Larsson, “Semiconductor Optoelectronics (Device Physics and Technologies)”, Course compendium: Optoelectronics course, Chalmers University of Technology, pp. 25, February 2010.
32. Yu. A. Goldberg, and N. M. Schmidt, *Handbook Series on Semiconductor Parameters*, vol. 2, M. Levinshtein, S. Rumyantsev and M. Shur, ed., pp. 62-88, 1999.
33. M. V. Karatchevtseva, A. S. Ignatiev, V. G. Mokerov, G. S. Nemtsov, V. A. Strakhov, N. G. Yaremenko, “Temperature-Dependence of the Photoluminescence of $In_xGa_{1-x}As$/GaAs Quantum-Well Structures”, *Semiconductors*, vol. 28, no.7, pp.691-694, 1994.
34. K. -H. Goetz, D. Bimberg, H. Jurgensen, J. Selders, A. V. Solomonov, G. F. Glinskii, M. Razeghi, “Optical and crystallographic properties and impurity incorporation of $Ga_xIn_{1-x}As$ ($0.44 \ll x \ll 0.49$) grown by liquid phase epitaxy, vapor phase epitaxy, and metal organic chemical vapor deposition” , *Journal of Applied Physics*, vol. 54, no.8, pp. 4543-4552, August 1983.

Paper [A] & [B]

Journal Papers

Paper [A]

Growth of $GaSb_{1-x}Bi_x$ by molecular beam epitaxy

Y. X. Song, S. M. Wang, I. S. Roy, P. X. Shi, and A. Hallen

J. Vac. Sci. Technol., B **30** (2), 02B114-7 (2012)

Growth of $GaSb_{1-x}Bi_x$ by molecular beam epitaxy

Yuxin Song (宋禹忻),[a] Shumin Wang,[b] and Ivy Saha Roy
Photonics Laboratory, Department of Microtechnology and Nanoscience, Chalmers University of Technology, SE-41296 Göteborg, Sweden

Peixiong Shi
DANCHIP, Technical University of Denmark, DK-2800, Lyngby, Denmark

Anders Hallen
ICT, Royal Institute of Technology, SE-16440 Kista, Sweden

(Received 20 September 2011; accepted 4 December 2011; published 18 January 2012)

Molecular beam epitaxy for $GaSb_{1-x}Bi_x$ is investigated in this article. The growth window for incorporation of Bi in GaSb was found. Strategies of avoiding formation of Bi droplets and enhancing Bi incorporation were studied. The Bi incorporation was confirmed by SIMS and RBS measurements. The Bi concentration in the samples was found to increase with increasing growth temperature and Bi flux. The position of $GaSb_{1-x}Bi_x$ layer peak in XRD rocking curves is found to be correlated to Bi composition. Surface and structural properties of the samples were also investigated. Samples grown on GaSb and GaAs substrates were compared and no apparent difference for Bi incorporation was found. © *2012 American Vacuum Society*. [DOI: 10.1116/1.3672025]

I. INTRODUCTION

Bismuth is the heaviest and least studied group V element. Incorporation of a small amount of Bi atoms in common III-V compounds; for example, arsenides and antimonides, is expected to lead to a large band gap reduction[1] and strong spin-orbit splitting.[2] To the contrary of dilute nitride, which is well-known for its large bandgap bowing effect by lowering the conduction band edge, the influence of Bi on band structure occurs only in the valence band.[3] This provides a new degree of freedom to engineer band structure of semiconductors for potential electronic and optoelectronic applications. Attempts to reach the narrowest possible band gap of III-V materials for long wavelength infrared detectors were carried out since the late 1970s by synthesizing $InSb_{1-x}$ Bi_x bulk materials.[4–6] Intensive research has also been implemented on $GaAs_{1-x}Bi_x$ and related materials after its first realization of epitaxial growth by metal organic vapor phase epitaxy in 1998 (Ref. 7) and by molecular beam epitaxy (MBE) in 2003.[8] The bandgap bowing effect[1] and the spin-orbit splitting effect[9] were experimentally observed afterwards, making $GaAs_{1-x}Bi_x$ closer to potential device applications. The valence band edge reduction can lead to a reduced temperature dependence of the band gap, which is attractive for fabricating temperature insensitive lasers, optical amplifiers and modulators for telecommunications. It is also proposed that the large spin-orbit splitting can suppress inter-valence band Auger recombination processes and thus increasing the characteristic temperature of 1.55 μm telecom lasers on GaAs.[10]

GaSb based III-V semiconductor compounds are very attractive for optoelectronic devices working at near- and mid-infrared range, such as lasers, detectors and modulators; as well as high speed electronic devices; for example, transistors.[11] Incorporation of Bi in Sb-related materials will have several potential benefits. First, Bi incorporation in GaSb can reduce the band gap more effectively than utilizing InGaSb, leading to less lattice mismatch for a required emission wavelength. Second, one major problem for >3 μm GaSb based type-I quantum well lasers is insufficient valence band offset[12] due to the use of heavily compressive strained InGaAsSb quantum wells, resulting in significant hole leakage. By employing Bi, a large band gap bowing in valence band could provide large valence band offset. Third, the utilization of spin-orbit splitting is much easier in $GaSb_{1-x}Bi_x$ than in $GaAs_{1-x}Bi_x$, since the value of spin-orbit splitting is already very close to the band gap.[13] By incorporating a much smaller amount of Bi in $GaSb_{1-x}Bi_x$ than that in $GaAs_{1-x}Bi_x$, a larger spin-orbit splitting than the band gap can be readily achieved to suppress Auger recombination processes in optoelectronic devices. So far, little work has been done on $GaSb_{1-x}Bi_x$. To the best of our knowledge, only two publications attempting to incorporate Bi in bulk GaSb ingots were found[14,15] using liquid phase growth methods. Both work were intended to use Bi as a dopant to reduce background p-doping in GaSb ingots.

In this paper, we investigate the growth conditions of $GaSb_{1-x}Bi_x$ thin films by MBE. The effects of parameters, such as growth rate, Bi/Sb ratio and growth temperature were studied.

II. EXPERIMENT

Samples were grown on undoped (100) GaSb and undoped (100) GaAs substrates in a Riber Compact21 MBE system equipped with a dual filament effusion cell for Ga, a single filament effusion cell for Bi and a valved cracker for Sb and As, respectively. Sample surface was *in situ* monitored by reflection high-energy electron diffraction (RHEED) during the growth. For samples grown on GaSb substrates, a very thin GaSb buffer layer (5 nm) was first grown at 510 °C (measured by a thermocouple, same for all temperatures in this paper) after deoxidation of the GaSb substrate at 580 °C. RHEED shows a sharp 1×3 pattern at this stage indicating smooth

[a]Electronic mail: yuxin.song@chalmers.se
[b]Electronic mail: shumin@chalmers.se

TABLE I. Description of the samples.

Name	Substrate	Growth temperature [°C]	Bi BEP [Torr]
A1	GaSb	340	1.2×10^{-7}
A2	GaSb	360	1.2×10^{-7}
A3	GaSb	380	1.2×10^{-7}
A4	GaSb	340	1.0×10^{-8}
A5	GaSb	360	1.0×10^{-8}
B_Ref	GaSb	370	
B1	GaSb	330	1.0×10^{-8}
B2	GaSb	360	4.0×10^{-8}
B3	GaSb	370	7.0×10^{-8}
B4	GaSb	380	1.0×10^{-7}
B5	GaSb	390	2.0×10^{-7}
C_Ref	GaAs	370	
C1	GaAs	360	4.0×10^{-8}
C2	GaAs	370	7.0×10^{-8}
C3	GaAs	380	1.0×10^{-7}
C4	GaAs	390	2.0×10^{-7}

growth front. Then, a 200 nm thick $GaSb_{1-x}Bi_x$ layer was grown with a growth rate in the range of $0.1 - 0.5$ μm/h at lower temperatures ranging between 280 and 390 °C. For samples grown on GaAs substrate, the substrate was first deoxided at 650 °C, and then cooled down to much lower temperatures ranging between 360 and 390 °C. A 200 nm $GaSb_{1-x}Bi_x$ layer was directly grown on the substrate. The measured beam equivalent pressure (BEP) of Ga for 0.5 μm/h and 0.1 μm/h is 5.5×10^{-8} Torr and 2.0×10^{-8} Torr, respectively. The BEP of Sb was chosen as 5.2×10^{-7} Torr and 8.8×10^{-8} Torr, correspondingly. The BEP of Bi ranges between 6×10^{-9} Torr and 2×10^{-7} Torr depending on other growth conditions. A description of all the samples with the key parameters are summarized in Table I.

Surface morphology is investigated by atomic force microscopy (AFM). High resolution x-ray diffraction (XRD) was employed as a quick tool to study structural properties following the growth of each sample. Rutherford backscattering spectroscopy (RBS) and secondary ion mass spectrometry (SIMS) were used as "post-analysis" tools to confirm Bi incorporation and study element distribution profiles. Because $GaSb_{1-x}Bi_x$ is a new material, the SIMS measurement parameters were first optimized using a Bi_2Te_3 thin film as a reference sample. Oxygen and cesium ions were tried. It was found that use of negative oxygen ions with an incident angle of 60° has the highest sensitivity on Bi detection. The Bi signal is possible to be interfered by Ga due to atomic mass superimposition (Ga69 + Ga70 + Ga70 = 209). However, no correlation can be found between the Ga isotopes and Bi curves (not shown here), proving the reliability of the Bi results.

III. RESULTS AND DISCUSSIONS

A. Bismuth incorporation in $GaSb_{1-x}Bi_x$

From previous experiences of GaAsBi and InSbBi growth, V/III ratio, growth rate and growth temperature (T_g), are very important parameters to enhance Bi incorporation. Due to the higher bonding energy of GaSb than that of GaBi, it is difficult for Bi to compete with Sb to be incorporated into the crystal lattice. Therefore, the Sb/Ga flux ratio should be kept close to the Ga-rich growth condition while the Bi flux should be as high as possible to facilitate Bi incorporation. However, the risk of a low Sb/Ga flux ratio is formation of Ga droplets. Bismuth is metallic that is different from other group-V elements. Excess Bi atoms on the growth surface will form Bi droplets if they are neither incorporated nor evaporated. Growth rate has influence on kinetic processes at the growth front. Fast growth rate would favor formation of stronger bonds than weak ones. A low growth rate is therefore positive for formation of Ga–Bi bonds but would lead to practical problems such as too long growth time for growing a thick layer. Surface migration, incorporation, desorption and droplet formation highly depend on growth temperature. A low growth temperature facilitates Bi staying on surface but can have a risk for formation of Bi droplets if not incorporated. A high growth temperature reduces such a risk but leads to less effective Bi incorporation and potential Ga droplets.

Based on the above considerations, a 0.5 μm/h growth rate and a growth temperature, T_g, of 380, 360, and 340 °C, which was lower compared with the normal growth temperature for GaSb, were chosen for the first batch of samples grown on GaSb substrates (A1–A3 in Table I). For a 0.5 μm/h growth rate of GaSb, the critical BEP of Sb was found to be 4.7×10^{-7} Torr, with the criterion of the surface reconstruction change judged by RHEED. The final Sb BEP was set to be 10% higher than the critical value, i.e., 5.2×10^{-7} Torr to secure surface from degradation due to formation of Ga droplets. The BEP of Bi was set to be 1.2×10^{-7} Torr. The thickness of the $GaSb_{1-x}Bi_x$ layer of these samples is 200 nm.

Figure 1 shows AFM images of the samples A1–A3. The surface of all of them is covered by three-dimentional (3D) structures. As the Sb BEP was tested to be enough for the growth of GaSb, these structures are most probably from residual Bi on the surface. There are two kinds of distinct features on the sample grown at 380 °C (A3). One is composed of large platelets with an average diameter of 2.5 μm and an average height of 20 nm. The top of them is not completely flat, but tend to show facets. The other one is rectangular shaped with an average size of 250×500 nm^2. The height is around 60 nm, which is about 3 times of the height of the large platelets. The side of these structures shows clear facets. Both structures are very different from conventional group III droplets which often are semisphere or domelike. Therefore we believe that those 3D features are related to excess Bi atoms. Surprisingly, when the T_g is decreased by 20 °C, the morphology of 3D structures looks very different. On the sample grown at 360 °C (A2), many dome shaped 3D droplets similar to Ga droplets are observed as shown in Fig. 1(b). However, if observed carefully in 1×1 μm^2 scans, these droplets are not round but also with clear facets, see the inset of Fig. 1(b). The average diameter of these Bi droplets is around 250 nm and the average height is 50 nm. On the sample grown at 340 °C (A1), similar 3D droplets are found but with a much larger size and a lower density. The

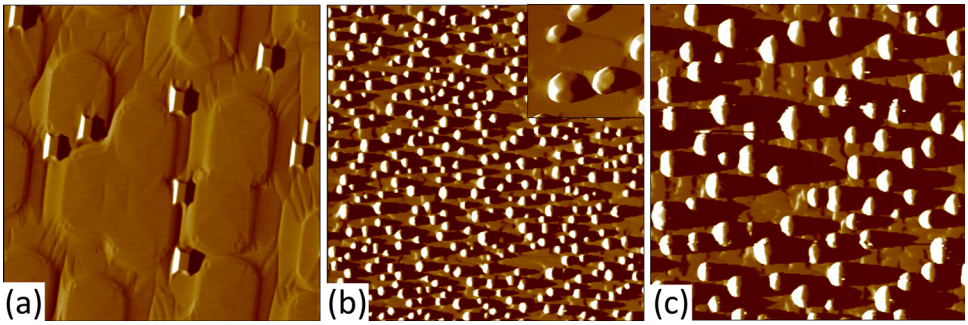

FIG. 1. (Color online) 10×10 μm^2 AFM amplitude images of samples A1, A2, and A3 grown with a 0.5 μm/h growth rate on GaSb substrates. The inset in (b) is a zoom-in image with a 1×1 μm^2 area.

average diameter and height are 800 and 180 nm, respectively.

The surface morphology the samples A1–A3 apparently indicates a too high Bi flux impinging onto the samples. In spite of poor surface quality (in contrary to flat surfaces), we expect excess Bi should enhance Bi incorporation at low growth temperatures. XRD measurements were implemented for these samples. The lattice constant of GaBi is predicted to be 6.324 Å (Ref. 16) which is larger than that of GaSb and a peak of $GaSb_{1-x}Bi_x$ to the left of the GaSb substrate peak is expected to be the signature of Bi incorporation. However, no such peaks in XRD (004) rocking curves were found for all the three samples, instead, shoulders at the right side of the substrate peak can be seen. The XRD (004) rocking curve of the sample A3 is shown as the red curve in Fig. 2. As will be discussed below, we find out that this shoulder is in fact related to the Bi incorporation, but the amount of incorporated Bi is expected to be very little.

For the next two samples A4 and A5, the BEP of Bi was reduced to 1×10^{-8} to avoid the Bi-related surface structures and the T_g was 340 and 360 °C, respectively. Flat surfaces with root mean square (RMS) roughness of 0.34 and 0.17 nm in 1×1 μm^2 AFM scans were obtained. However, with such a low Bi flux, even less feature was observed from XRD rocking curves.

In order to avoid formation of Bi droplets, excess Bi on the surface, which is not incorporated into the lattice, must be thermally evaporated. The evaporation process is highly dependent on temperature. The relation between Bi vapor pressure and temperature was calculated and plotted in Fig. 3. Considering that the real surface temperature is normally lower than the temperature read by the thermocouple, the actual vapor pressure versus the real sample surface temperature curve should be slightly lower than the curve in the figure. The BEP values of Bi for the above five samples are also indicated in red. The XRD results indicate that only a very small fraction of Bi can be incorporated. Thus the excess Bi atoms on the growth surface increases with decreasing T_g from the first batch samples. The metallic Bi adatoms are mobile at these temperatures leading to formation of large Bi metallic crystals as shown in Fig. 1. For a low Bi BEP, most impingent Bi atoms are re-evaporated rather than being incorporated as a result of the Sb/Bi competition. Therefore, to effectively enhance Bi incorporation but avoid Bi droplets at the same time, the Bi BEP should be chosen close to the vapor pressure relative to the substrate temperature. In order to reach a high Bi/Sb ratio, a high T_g, which can allow for a high Bi flux, and a low Sb BEP are preferred. The low Sb BEP can be readily realized by lowering the growth rate. One example is shown in Fig. 2. The two samples were grown at 380 °C, but the Bi/Sb BEP ratio is

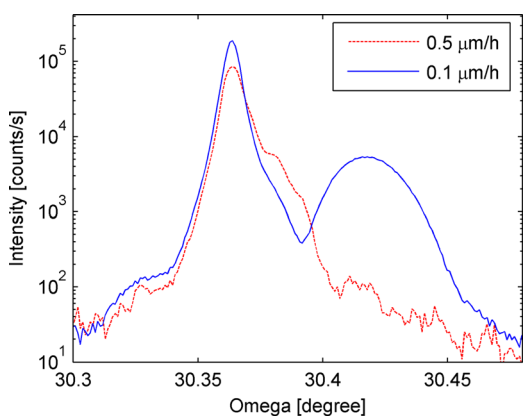

FIG. 2. (Color online) XRD (004) rocking curves of the sample A3 with a growth rate of 0.5 μm/h (red dashed curve) and the sample B4 at 0.1 μm/h (blue solid curve) at the same T_g, 380 °C on GaSb substrates.

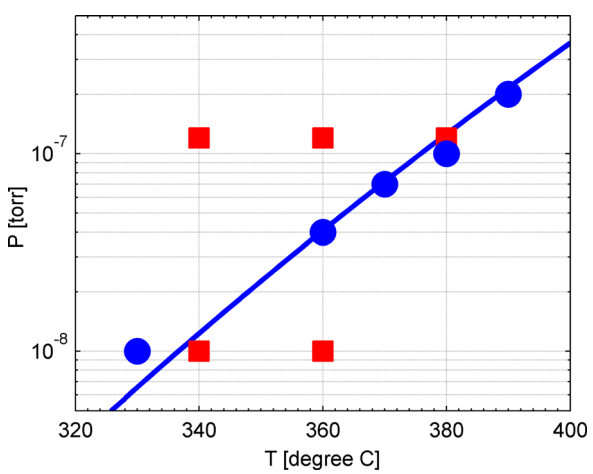

FIG. 3. (Color online) Bi vapor pressure vs temperature (blue line) and selected growth temperatures at particular Bi BEPs for the samples grown with 0.1 μm/h growth rate (blue round markers) and 0.5 μm/h (red square markers), respectively.

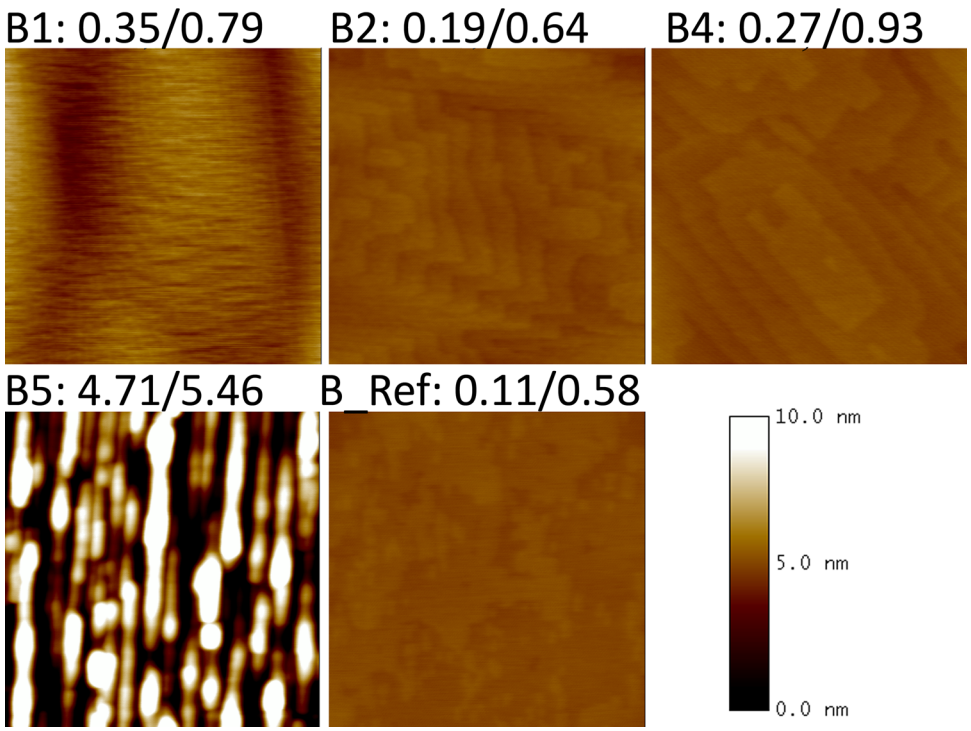

FIG. 4. (Color online) $1 \times 1\ \mu m^2$ AFM height images for the group B samples grown at 0.1 μm/h growth rate on GaSb substrates. RMS roughness in units of nm obtained from $1 \times 1\ \mu m^2$ and $10 \times 10\ \mu m^2$ scans is shown before and after the slash, respectively.

increased from 0.23 to 1.14 when the growth rate is decreased from 0.5 μm/h to 0.1 μm/h. Much greater Bi incorporation is indicated by XRD for a high Bi/Sb ratio. The later samples were all grown with a 0.1 μm/h growth rate.

B. Temperature dependence of $GaSb_{1-x}Bi_x$ growth

Based on 0.1 μm/h growth rate, five T_g-values were selected to study the temperature effect on Bi incorporation. The Bi BEP of these samples was chosen close to the vapor pressure as marked with blue round markers in Fig. 3, i.e., 1×10^{-8} Torr, 4×10^{-8} Torr, 7×10^{-8} Torr, 1×10^{-7} Torr and 2×10^{-7} Torr at 330, 360, 370, 380, and 390 °C, for the samples B1 to B5, respectively. The thickness of the $GaSb_{1-x}Bi_x$ layer of these samples is 200 nm. A reference sample without Bi was grown at 370 °C for comparison.

It can be found from Fig. 4 that, most samples have flat surface without any 3D structures seen in Fig. 1. The samples B1 to B4 show high quality surface with atomic steps and slightly larger RMS roughness than that of the B_Ref sample. For the samples gown at and 390 °C (B5), the surface shows elongated dots, leading to relative larger roughness, but still much smaller than that of the samples with droplets. It is not clear yet what caused such surface morphology, but it is probably related to excess Bi due to growth temperature fluctuation. The shape of the elongated dots indicates anisotropy of surface diffusion along the two orthogonal directions.

Figure 5(a) shows typical SIMS depth profiles for the sample B3. The dotted line marks the interface between the epilayer and the GaSb substrates. The results are similar for all other samples. The three key elements Ga (69), Sb (121), and Bi (209) are examined, as well as In (115) and As (75) which may remain in the MBE growth chamber as background dopants. The initial intensity changes within 20–25 nm are artifacts. A clear step of Bi intensity at the interface between the epitaxial $GaSb_{1-x}Bi_x$ layer and the GaSb substrate, evidencing Bi incorporation, can be found. The coincidence between the background As and In steps and the Bi step ensures the initiation of epitaxial growth and that the Bi signal is reliable although its intensity is relatively low. Normalized Bi intensity from SIMS measurements, which can be an indicator as Bi concentration, is calculated and shown in Fig. 5(b). It can be found that the Bi concentration increases with increasing T_g, as well as the Bi/Sb BEP ratio, and tends to saturate at high ratios.

RBS measurements were carried out in parallel with the SIMS measurements as antitheses. Bi incorporation in $GaSb_{1-x}Bi_x$ samples was also confirmed. From the simulations, the Bi concentration of 0.2, 0.7, and 0.7% is deduced for the $GaSb_{1-x}Bi_x$ samples B2, B3, and B5, respectively. All the XRD (004) rocking curves of the $GaSb_{1-x}Bi_x$ samples reveal clear peaks on the right side of the GaSb substrate peak, i.e., lattice contraction of the GaSbBi films grown on GaSb substrates. This is also true for (115) and (11-5) planes and azimuth rotation checks confirm that those peaks are not related to the tilting of the GaSbBi films relative to the GaSb substrate. Detail discussions of such lattice contraction will be published elsewhere. The calculated GaSbBi lattice constant from (115) and (11-5) measurements is shown in Fig. 5(c). Compared with the lattice constant of GaSb 6.096 Å, lattice contraction of 0.034, 0.061, 0.079, 0.084, and 0.041% were found for the samples B1–B5, respectively. We propose that the lattice contraction would

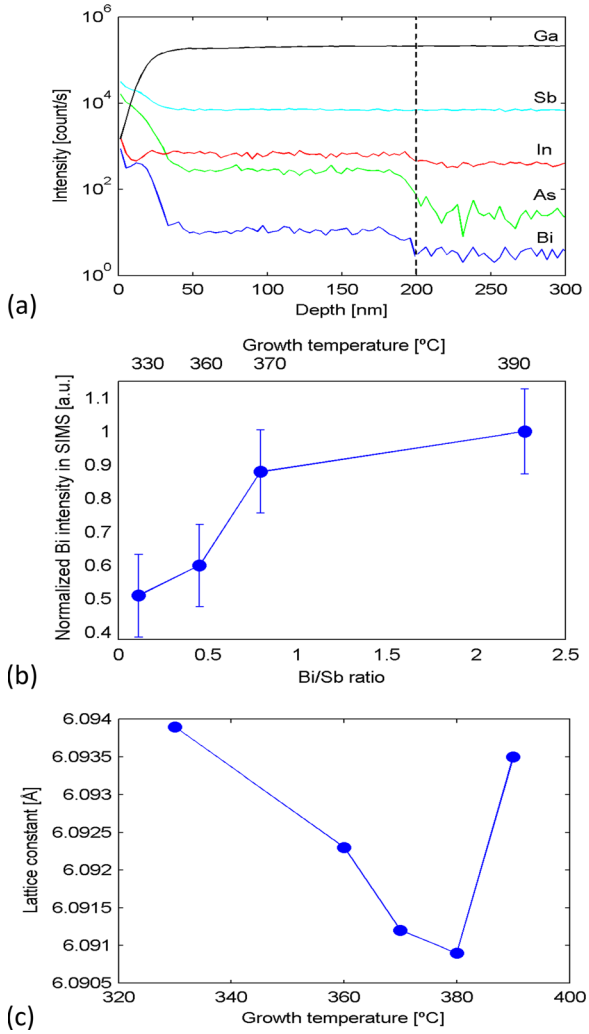

FIG. 5. (Color online) Structural property measurement results of the group B samples. (a) SIMS profile of different elements in the sample grown at 370 °C. (b) Normalized Bi intensity in SIMS profiles vs Bi/Sb ratio and T_g. (c) Lattice constant of $GaSb_{1-x}Bi_x$ layers extracted from XRD (115) and (11-5) series measurements.

be due to vacancies at group-V sites caused by Bi segregation. Higher Bi concentration leads to higher density of vacancies resulting in strong lattice contraction.

C. $GaSb_{1-x}Bi_x$ grown on GaAs

Group C samples with the same growth conditions were grown on GaAs substrate for comparison. As there is 7.8% lattice mismatch between GaSb and GaAs, the growth mode of $GaSb_{1-x}Bi_x$ on GaAs is different from that on GaSb. The evolution of RHEED pattern for the sample grown at 380 °C is shown in Fig. 6. The initial GaAs surface under Sb over pressure shows (2×8) reconstruction in Fig. 6(a). The pattern changed to dots upon the growth of $GaSb_{1-x}Bi_x$ within one monolayer (ML). Then, new streaks slowly appear, showing GaSb (1×3) like reconstruction, while the dots gradually dim, as shown in Figs. 6(b) and 6(c), respectively. At the end of the growth, a clear streaky pattern is observed. This $GaSb_{1-x}Bi_x$ growth process is similar to the GaSb grown on

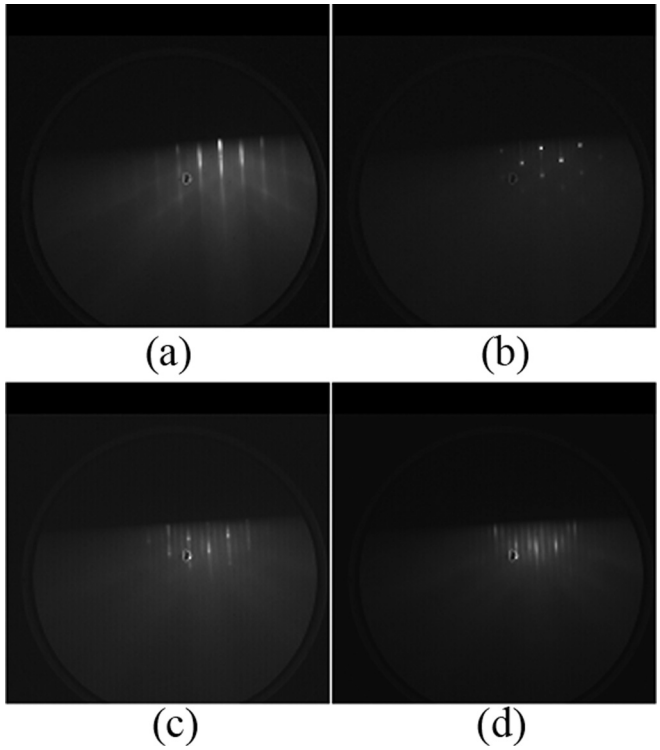

FIG. 6. RHEED pattern for the sample C4. (a) GaAs under Sb over pressure, (b) 9 nm $GaSb_{1-x}Bi_x$, (c) 27 nm $GaSb_{1-x}Bi_x$, and (d) growth 200 nm $GaSb_{1-x}Bi_x$. The black dot at the up-right of the image is from a damage of the phosphorus screen.

GaAs by the "interfacial misfit arrays."[17] However, it requires about 30 nm growth to recover a streaky pattern for a $GaSb_{1-x}Bi_x$ layer, which is much thicker compared with 3 nm observed for the reference sample without Bi.

Figure 7 shows the surface morphologies for the group C samples. Due to the strain relaxation, the surface roughness is in general higher than that of the counterpart samples grown on GaSb substrate. Except the one grown at 360 °C (C1), all other $GaSb_{1-x}Bi_x$ samples have relatively constant roughness but different morphologies. The sample C1 has only slightly rougher surface than the reference sample, with elongated features instead of the round features on the reference sample. Discrete platformlike features are found for all other $GaSb_{1-x}Bi_x$ samples in this group. The average area of platforms increases with T_g. This platformlike morphology can explain that, although the surface is rough, a relatively good RHEED pattern can still be observed. XRD rocking curves (not shown here) confirm the single crystal nature of these samples.

SIMS measurements were carried out for some of the samples. Figure 8(a) shows the element depth profiles of the sample C4. A clear interface between the GaAs substrate and the epilayer can be found by the step of different elements. A step of Bi can be found at the same position. However, the Bi intensity is not very uniform. Arsenic is found to diffuse into the $GaSb_{1-x}Bi_x$ layer. An increase of Bi concentration at the interface and a tail of Bi extending into the GaAs substrate can also be seen. This indicates that Bi may

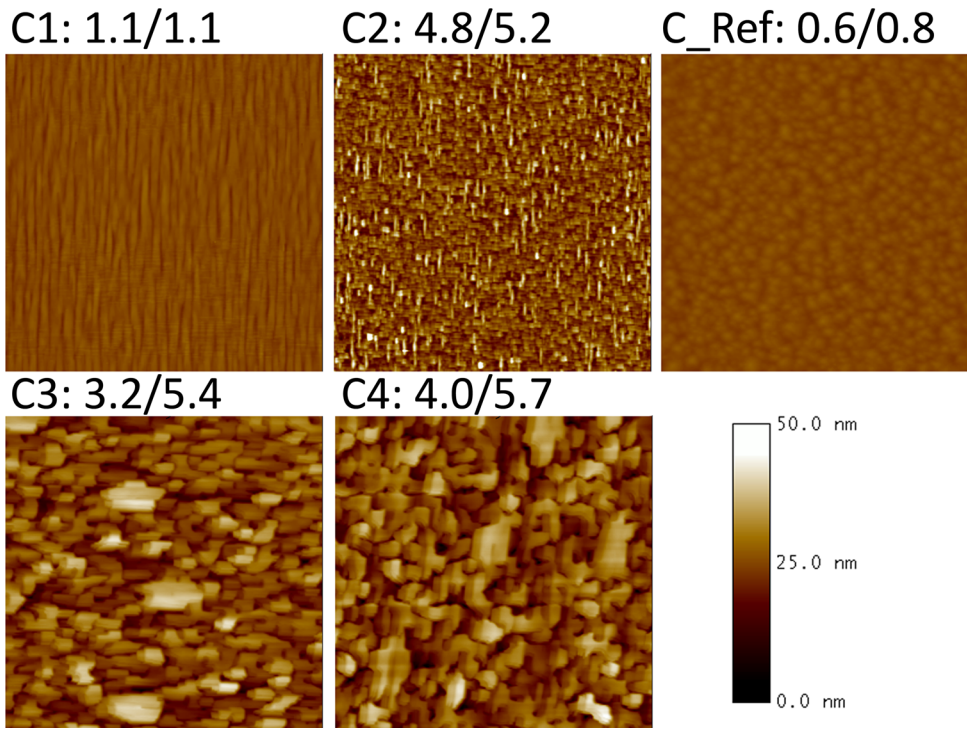

FIG. 7. (Color online) 10×10 μm^2 AFM height images for the group C samples grown on GaAs substrates. RMS roughness in units of nm obtained from 1×1 μm^2 and 10×10 μm^2 scans is shown before and after the slash, respectively.

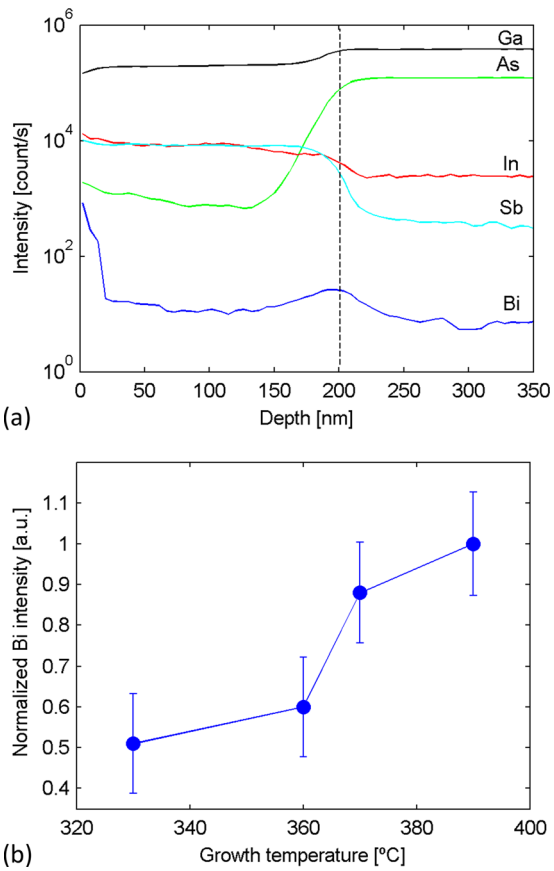

FIG. 8. (Color online) SIMS measurement results for the group C samples grown on GaAs substrates. (a) SIMS profile of different elements in the sample grown at 390 °C. The curves are smoothened by five-point averaging. (b) Normalized Bi intensity vs Bi/Sb ratio and T_g. The vertical axis scale is the same with Fig. 5(b).

be easier to be incorporated with the existence of As. Since the measurement time of this group of samples is shorter than that of the GaSb based samples, the fluctuation of the normalized Bi incorporation values is larger, as shown in Fig. 8(b). The normalized Bi intensity of the samples is close to that of the counterpart samples grown on GaSb substrates.

Comparing the samples grown on GaSb and GaAs substrates, no apparent difference in Bi incorporation was found within the accuracy of SIMS measurements. However, the surface of the samples grown on GaAs substrate is much worse than those grown on GaSb substrates.

IV. SUMMARIES

We have investigated the growth of $GaSb_{1-x}Bi_x$ by MBE. We firstly studied the growth window for incorporation of Bi in GaSb. Excess Bi related surface morphologies were found. Strategies of avoiding Bi accumulation and enhancing Bi incorporation were studied. The Bi incorporation was confirmed by SIMS and RBS measurements. The normalized Bi level in different samples was studied by comparing Bi intensity in SIMS measurements. It was found to increase with increasing growth temperature and Bi flux, and tends to saturate when T_g is higher than 370 °C. The position of $GaSb_{1-x}Bi_x$ layer peak in XRD rocking curves is found to be correlated to Bi composition in the samples. Lattice contraction, instead of dilation, was observed. Surface and structural properties of the samples were also investigated. Samples grown on GaSb and GaAs substrates were compared and no apparent difference for Bi incorporation was found.

ACKNOWLEDGMENT

The Swedish Research Council (VR) is acknowledged for financial support for this project.

[1]S. Francoeur, M. J. Seong, A. Mascarenhas, S. Tixier, M. Adamcyk, and T. Tiedje, Appl. Phys. Lett. **82**, 3874 (2003).
[2]K. Alberi, J. Wu, W. Walukiewicz, K. Yu, O. Dubon, S. Watkins, C. Wang, X. Liu, Y. J. Cho, and J. Furdyna, Phys. Rev. B **75**, 045203 (2007).
[3]K. Alberi, O. D. Dubon, W. Walukiewicz, K. M. Yu, K. Bertulis, and A. Krotkus, Appl. Phys. Lett. **91**, 051909 (2007).
[4]J. Zilko and J. Greene, Appl. Phys. Lett. **33**, 254 (1978).
[5]K. Oe, S. Ando, and K. Sugiyama, Jpn. J. Appl. Phys. **20**, L303 (1981).
[6]A. Noreika, W. Takei, M. Francombe, and C. Wood, J. Appl. Phys. **53**, 4932 (1982).
[7]K. Oe and H. Okamoto, Jpn. J. Appl. Phys. **37**, L1283 (1998).
[8]S. Tixier, M. Adamcyk, T. Tiedje, S. Francoeur, A. Mascarenhas, P. Wei, and F. Schiettekatte, Appl. Phys. Lett. **82**, 2245 (2003).
[9]B. Fluegel, S. Francoeur, A. Mascarenhas, S. Tixier, E. C. Young, and T. Tiedje, Phys. Rev. Lett. **97**, 67205 (2006).
[10]S. Sweeney, 1st International Workshop on Bismuth-Containing Semiconductors: Theory, Simulation, and Experiment, Michigan, USA, 2010 (unpublished).
[11]P. S. Dutta, H. L. Bhat, and V. Kumar, J. Appl. Phys. **81**, 5821 (1997).
[12]T. Hosoda, G. Kipshidze, G. Tsvid, L. Shterengas, and G. Belenky, IEEE Photonics Technol. Lett. **22**, 718 (2010).
[13]I. Vurgaftman, J. R. Meyer, and L. R. Ram-Mohan, J. Appl. Phys. **89**, 5815 (2001).
[14]P. Gladkov, E. Monova, and J. Weber, J. Cryst. Growth **146**, 319 (1995).
[15]A. Danilewsky, S. Lauer, J. Meinhardt, K. Benz, B. Kaufmann, R. Hofmann, and A. Dornen, J. Electron. Mater. **25**, 1082 (1996).
[16]A. Janotti, S. H. Wei, and S. B. Zhang, Phys. Rev. B **65**, 115203 (2002).
[17]S. H. Huang, G. Balakrishnan, A. Khoshakhlagh, A. Jallipalli, L. R. Dawson, and D. L. Huffaker, Appl. Phys. Lett. **88**, 131911 (2006).

Paper [B]

MBE growth and lattice contraction of $GaSb_{1-x}Bi_x$ thin films

Y. X. Song, S. M. Wang, I. S. Roy, P. X. Shi, and A. Hallen

Journal Manuscript

MBE growth and lattice contraction of $GaSb_{1-x}Bi_x$ thin films

*Yuxin Song [1, *], Shumin Wang[1, *], Ivy S. Roy[1], Peixiong Shi[2] and Anders Hallen[3]*

[1] Photonics Laboratory, Department of Microtechnology and Nanoscience, Chalmers University of Technology, SE-41296 Göteborg, Sweden

[2] DANCHIP, Technical University of Denmark, DK-2800, Lyngby, Denmark

[3] ICT, Royal Institute of Technology, SE-16440 Kista, Sweden

[*] Electronic mail: yuxin.song@chalmers.se, shumin@chalmers.se

ABSTRACT

MBE growth of GaSb1-xBix thin films is demonstrated for the first time. Bismuth incorporation is confirmed by RBS and SIMS measurements. The Bi composition increases following increasing the Bi flux and tends to saturate at growth temperature around 370 ºC, resulting in the highest Bi composition of 0.7% measured by RBS. Lattice contraction was observed from XRD measurements showing tensile strain rather than compressive strain when Bi is incorporated in GaSb. We propose that the lattice contraction is due to vacancies caused by Bi segregation.

Incorporation of a small amount of Bi atoms in common III-V compounds is expected to lead to a large bandgap reduction [1] and strong spin-orbit splitting [2], showing great potentials for electronic and optoelectronic applications. Attempts to reach the narrowest possible bandgap of III-V materials for long wavelength infrared photodetectors were carried out since the late 1970s by synthesizing $InSb_{1-x}Bi_x$ bulk materials [3, 4, 5]. Intensive research has also been implemented on $GaAs_{1-x}Bi_x$ and related materials after its first realization of epitaxial growth by metal organic vapor phase epitaxy (MOVPE) in 1998 [6] and by molecular beam epitaxy (MBE) in 2003 [7]. The band-gap bowing effect [1] and the spin-orbit splitting effect [8] were experimentally observed afterwards, making $GaAs_{1-x}Bi_x$ one step closer to potential device applications. The bandgap reduction occurs only in the valence band [9] leading to reduced temperature dependence of the bandgap, which is attractive for fabricating temperature insensitive lasers, optical amplifiers and modulators for telecommunications. It is also proposed that the large spin-orbit splitting can suppress inter-valence band Auger recombination processes and thus increasing the characteristic temperature of 1.55 μm telecom lasers on GaAs [10].

GaSb based III-V semiconductor compounds are very attractive for optoelectronic devices working at near- and mid-infrared range, such as lasers, detectors and modulators, as well as high speed electronic devices, for example, transistors [11]. Incorporation of Bi in Sb-related materials will have several potential benefits. First, Bi incorporation in GaSbBi can reduce the bandgap more effectively than use of InGaSb. Second, one major problem for >3 μm GaSb based lasers is insufficient valence band offset [12] due to the use of heavily compressively strained InGaAsSb quantum wells, resulting in significant hole leakage. By employing Bi, a large bandgap bowing in valence band could provide large valence band offset. Third, the utilization of spin-orbit splitting is much easier in $GaSb_{1-x}Bi_x$ than in $GaAs_{1-x}Bi_x$, since the value of spin-orbit splitting is already very close to the bandgap [13]. By incorporating a small amount of Bi in $GaSb_{1-x}Bi_x$, a larger spin-orbit splitting than the band gap can be readily achieved to suppress Auger recombination processes in optoelectronic devices. So far, to the best of our knowledge,

only two publications attempting to incorporate Bi in GaSb were found [14, 15]. Both work were intended to use Bi as a dopant to reduce background p-doping in GaSb bulks.

In this letter, we report growth of $GaSb_{1-x}Bi_x$ thin films using MBE. We employ special growth conditions based on previous knowledge on growth of $GaAs_{1-x}Bi_x$ and $InSb_{1-x}Bi_x$ to effectively incorporate Bi while minimize formation of both Ga and Bi droplets at the same time. Surface quality was *in-situ* monitored by reflection high-energy electron diffraction (RHEED) during the growth. Surface and structural properties of the samples are examined by atomic force microscopy (AFM) and X-ray diffraction (XRD). Incorporation of Bi in GaSb was confirmed by Rutherford backscattering spectroscopy (RBS) and secondary ion mass spectrometry (SIMS). Lattice contraction of $GaSb_{1-x}Bi_x$ thin films along the growth direction with respect to that of GaSb was observed, in contrary to the expectation of lattice dilation due to the larger covalent radius of Bi than that of Sb. This phenomenon is explained by vacancies induced by Bi segregation.

Samples were grown on undoped (100) GaSb substrates in a Riber Compact21 MBE system with a cluster tool, equipped with a dual filament effusion cell for Ga, a single filament effusion cell for Bi and a valved cracker for Sb. A very thin GaSb buffer layer (5 nm) was first grown at 510 ºC (measured by a thermocouple) after deoxidation of the GaSb substrate at 580 ºC. RHEED shows a sharp 1x3 pattern at this stage indicating smooth growth front. Then, A 200 nm $GaSb_{1-x}Bi_x$ layer was grown with a growth rate of 0.1 μm/h. From previous experiences of GaAsBi and InSbBi growth, V/III ratio and growth temperature, T_g, are two crucial parameters to enhance Bi incorporation. Due to the higher bonding energy of Ga-Sb than that of Ga-Bi, the Sb/Ga flux ratio should be kept low enough, close to the Ga-rich growth condition, while the Bi flux should be kept as high as possible to facilitate Bi incorporation. However, a low Sb/Ga flux ratio may cause formation of Ga droplets. Bismuth is also metallic which is different from other group-V elements. Excess Bi atoms on the growth surface will form Bi droplets if they are neither incorporated nor evaporated. All these processes including surface migration,

incorporation, desorption and droplet formation highly depend on growth temperature. Use of a low growth temperature facilitates Bi staying on surface but has a risk for formation of Bi droplets if Bi atoms are not incorporated. Use of a high growth temperature reduces such a risk but leads to less effective Bi incorporation due to the weak Ga-Bi bonding and potential Ga droplets. Based on the above discussions, our strategy is using a low growth rate and keeping a low constant Sb flux (beam equivalent pressure (BEP) of 8.8e-8 Torr), but varying the Bi BEP which is set to be close to the Bi vapor pressure at the particular growth temperature in the range of 330-390 ºC as shown in Fig. 1(a). In the later discussions, T_g will be used to designate the samples. A reference (Ref) sample of 200 nm thick GaSb without Bi was grown at 370 ºC for comparison. This growth strategy avoids Bi droplet formation and effective Bi incorporation is expected at a high Bi BEP. Since the high Bi BEP is coupled to the growth temperature shown in Fig. 1(a) and the weak Ga-Bi bonding limits the effective Bi incorporation at high growth temperatures, a maximum Bi incorporation is expected at a certain growth temperature. It should also be noted that a slightly higher Bi BEP than the Bi vapor pressure line in Fig. 1(a) can be used to further enhance Bi incorporation. Surface morphology was checked by atomic force microscopy (AFM). Samples are mirror like with clear atomic steps in 1×1 μm^2 AFM scans. The AFM images of the $GaSb_{1-x}Bi_x$ sample grown at 380 °C are taken as examples in Fig. 1 (b) and (c) for 1x1 and 10x10 μm^2, respectively. Triangle shaped features are found for all samples. Even with such features, the root-mean-square roughness in 10×10 μm^2 scans is only 0.4-0.7 nm for different samples.

Results of RBS measurements for four samples are summarized in Fig. 2 (a). Compared with the Ref sample, a peak/step-like signal can be observed at the channel value of around 480 and its intensity increases with T_g. This signal is a strong evidence of Bi incorporation. From the simulations, the Bi concentration of 0.2%, 0.7% and 0.7% is deduced for the $GaSb_{1-x}Bi_x$ samples grown at 360 ºC, 370 ºC and 390 ºC, respectively. A trend can be found that the Bi concentration in $GaSb_{1-x}Bi_x$ layer increases with Bi BEP and then saturates at 370 ºC. RBS channeling measurement was performed for the sample grown at 390 ºC. The channeled spectrum is compared with two random spectra as shown in Fig. 2 (b).

By evaluating the yield difference, about 65% of the incorporated Bi atoms are estimated to be at substitutional sites.

SIMS measurements were carried out in parallel with the RBS measurements as antitheses. Compared with RBS, SIMS shows the relative counts of elements following the depth in a sample. SIMS results measured by negative oxygen ions are shown in Fig. 2(c) and (d). The sample grown at 390 ºC is taken as an example in Fig. 2 (c). It is similar to all the other samples. The three key elements Ga (69), Sb (121) and Bi (209) are examined, as well as In (115) and As (75) which may remain in the MBE growth chamber as background dopants. The initial intensity changes within 20-25 nm are artifacts. A clear step of Bi intensity at the interface between the epitaxial $GaSb_{1-x}Bi_x$ layer and the GaSb substrate, evidencing Bi incorporation, can be found. The coincidence between the background As and In steps and the Bi step ensures the initiation of epitaxial growth and that the Bi signal is reliable although its intensity is relatively low. It is possible for the Bi signal to be interfered by Ga due to atomic mass superimposition (Ga^{69}+Ga^{70}+Ga^{70}=209). However, no correlation can be found between the Ga isotopes and Bi curves (not shown here), proving again the reliability of the Bi results. Background As is detected from the growth chamber. It is about one order of magnitude higher than the value found in GaSb substrates and is similar for both the Ref sample and the GaSbBi samples grown in the range of 330-390 ºC. Figure 2 (d) summarizes the Bi distribution profile in the measured four samples. All curves have a step for Bi intensity at the same position. Strong surface accumulation of Bi is clearly observed for the samples grown at 370 and 390 ºC. It can be found that the Bi level increases following T_g (also Bi BEP) up to the maximum growth temperature of 390 ºC. However, the difference between 370 ºC and 390 ºC is rather small, indicating saturation of Bi incorporation. This saturation is expected to be as a result of the balance between the increased Bi BEP, the weak Ga-Bi bonding and the enhanced Bi segregation at high growth temperatures as will be discussed later. Because there is no pure GaBi or $GaSb_{1-x}Bi_x$ material available with a known *x*-value as a reference, it is very difficult to obtain the exact Bi concentration in these samples. Comparisons are made relatively. For example, the average Bi level in

the $GaSb_{1-x}Bi_x$ layer grown at 370 ºC, excluding the surface region, is 1.45 times compared with that grown at 360 ºC. This difference is smaller than that deduced from the RBS measurement which is the sum of the surface and the incorporated Bi concentration. We can thus conclude that, by combining the results of RBS and SIMS measurements, Bi incorporation is demonstrated, Bi concentration in the $GaSb_{1-x}Bi_x$ layer increases with Bi BEP and tends to saturate at the growth temperature above 370 ºC.

Figure 3 (a) shows the XRD (004) rocking curves of the 200 nm thick samples. The highest peak of each curve is from the GaSb substrate. Compared with the Ref sample, all $GaSb_{1-x}Bi_x$ samples show a peak at a larger angle than that of the GaSb substrate peak, indicating a smaller lattice constant of $GaSb_{1-x}Bi_x$ thin films than that of GaSb along the growth direction. When the T_g increases from 330 ºC to 380 ºC (correspondingly the Bi BEP from 1e-8 Torr to 1e-7 Torr), the separation between the $GaSb_{1-x}Bi_x$ and the GaSb substrate peak increases as well. Clear interference fringes between the $GaSb_{1-x}Bi_x$ layer and the GaSb substrate can be found for samples with T_g lower than 380 ºC, indicating high interface quality. In order to rule out the possibility that this $GaSb_{1-x}Bi_x$ peak is an illusion caused by crystal plane tilting, XRD (004) scans with sample rotation angles of 0°, 90°, 180° and 270° were implemented. All the curves have exactly the same shape. XRD (115) and (11-5) scans with sample rotation angles of 0° and 180° were also carried out. Free standing lattice constants of the $GaSb_{1-x}Bi_x$ layer are estimated. Compared with the lattice constant of GaSb 6.096Å, lattice contraction of 0.034%, 0.061%, 0.079%, 0.084% and 0.041% were found for the sample grown at 330 ºC, 360 ºC, 370 ºC, 380 ºC and 390 ºC, respectively. Except for the sample grown at 390 ºC, the trend of lattice contraction well follows the Bi concentration deduced from RBS and SIMS measurements as shown in Fig. 3 (b). The lattice constant of $GaSb_{1-x}Bi_x$ layer reduces with increasing T_g/Bi BEP and increases when T_g is above 380 ºC.

Similar lattice contraction phenomenon was also observed in $InSb_{1-x}Bi_x$ [16, 17], $InTl_xAs_{1-x}$ [18] and $InTl_xSb_{1-x}$ [19], and several possible explanations were proposed. Lanthanoid contraction was attributed

to the lattice contraction in $InTl_xAs_{1-x}$ and $InTl_xSb_{1-x}$. Although Tl has a larger atomic number than In, the 4*f* valence electrons in a Tl atom have a weak screening effect against the Coulomb force of the nuclei. As a result the bond length of TlAs and TlSb is smaller than that of InAs and InSb. It would be similar for Bi compared with Sb. However, even though the covalent radius of Bi (148±4 pm) is quite similar to that of Sb (139±5 pm), it is still slightly larger than Sb. Therefore, Lanthanoid contraction should not be the reason for $GaSb_{1-x}Bi_x$. For $InSb_{1-x}Bi_x$, Lee *et al.* in ref [16] believed that the lattice contraction is due to lattice transformation from zincblende to tetragonal structure. Theoretical calculations reveal that natural InBi has a tetragonal PbO structure with a lattice constant $a = 5.005$ Å and $c = 4.771$ Å, all smaller than that of InSb. However, GaBi favors zincblende structure according to theory [20]. Consequently, $GaSb_{1-x}Bi_x$ is unlikely to change its crystal structure. Wagener *et al.* in ref [17] attribute the lattice contraction in $InSb_{1-x}Bi_x$ grown on GaAs to the As/ Sb intermixing due to As diffusion from the GaAs substrate to the epi-layer. The observed $InSb_{1-x}Bi_x$ peak with a smaller lattice constant compared with InSb was in fact $InAs_xSb_{1-x-y}Bi_y$. This should not be the case in our $GaSb_{1-x}Bi_x$ samples since the $GaSb_{1-x}Bi_x$ layer was grown on GaSb sample, no possible group-V intermixing is expected. Although background As doping was found from SIMS measurements as stated above, we can rule out this possibility by the following reasons. Firstly, the amount of As is very little. From the rocking curve of Ref sample grown at 370 ºC in Fig. 3 (a), no peak other than the GaSb substrate peak is observed. A seemingly shoulder at the right side of the GaSb peak can be found which could be due to very small As incorporation in the epitaxially grown GaSb layer. However, the obvious $GaSb_{1-x}Bi_x$ peaks in the $GaSb_{1-x}Bi_x$ samples are definitely different from the Ref sample. Secondly, sticking coefficient of background As atoms on the growing surface increases with decreasing growth temperature. This implies that the As-incorporation induced lattice constant change should be enhanced at low growth temperatures, which is opposite to the observed trend shown in Fig. 3(a). Finally, the measured As level by SIMS is very close for all the samples and is only about 10 times of that found in

GaSb substrates. This indicates that the incorporated As is at most at the doping level. Thus we conclude that the observed lattice contraction is certainly due to the Bi incorporation.

We propose that the lattice contraction would be due to vacancies at group-V sites caused by Bi segregation. Surface segregation is a well known phenomenon for group-III elements in ternary III-III-V compounds [21]. For example, In in $In_xGa_{1-x}As$ tends to segregate to the surface forming In rich growth front and broadening interface. Likewise, segregation of group-V elements in III-V-V system, like Sb in $GaAs_xSb_{1-x}$, has also observed and studied [22]. Compared with Sb, Bi is metallic and has a larger atomic radius, larger atomic mass and weaker bonding energy with group-III elements. It is also a well known surfactant for InGaAs with a complete layer of Bi atoms floating on the growing surface to minimize the system energy [23]. Therefore, Bi atoms should be very easy to segregate to the surface during the growth if the Bi surface coverage is less than a monolayer. As a result, there is significant surface accumulation of Bi atoms and the SIMS results from the GaSbBi samples grown at 370 °C or above shown in Fig. 2(d) support this assumption. As mentioned above, in order to realize Bi incorporation, a very low Sb flux must be used, leading to a quasi-Ga-rich growth condition for $GaSb_{1-x}Bi_x$. When a certain amount of the incorporated Bi atoms are segregated to the surface, there are no enough excess Sb atoms to fill in the vacant sites left by the segregated Bi atoms. Then, there are three possibilities, Ga and background As atoms will take the sites forming Ga_v anti-site defects or GaAsSbBi, respectively, or the vacancies will be buried in the $GaSb_{1-x}Bi_x$ layer. All the cases will lead to a smaller lattice constant as it would be for $GaSb_{1-x}Bi_x$. Vacancies are the most effective in reducing the lattice constant than the other two possibilities. If the amount of vacancies is considerably high, they can eventually compensate the incorporated Bi causing lattice contraction. Background As atoms could also be possible to fill in the vacancies and results in lattice contraction. However, this shouldn't be the major factor, because the measured As level by SIMS in all these samples are similar and very low as discussed above.

Surface segregation effect is usually enhanced at high growth temperatures. Figure 3 (b) compares the trend of Bi concentration obtained from SIMS measurements and the deduced lattice constant of the $GaSb_{1-x}Bi_x$ samples from XRD. When T_g increases from 330 ºC up to 380 ºC, we expect that Bi segregation increases as well, leading to more vacancies and stronger lattice contraction. Bi segregation also depends on surface coverage of Bi atoms. From SIMS results in Fig. 2 (d), Bi surface accumulation increases with growth temperature and is the highest for the sample grown at 390 ºC. A large Bi surface coverage will suppress the Bi segregation, which is the case for the T_g=390 ºC sample. From the SIMS measurement, the Bi level in this sample is similar to that of the sample grown at 370 ºC, but the lattice constant of the $GaSb_{1-x}Bi_x$ layer increases. This implies that the suppressed Bi segregation induces fewer vacancies which can't effectively compensate the incorporated Bi atoms in this particular sample. The incorporated Bi will thus stay at the lattice sites in the $GaSb_{1-x}Bi_x$ layer leading to smaller lattice contraction.

A 500 nm thick $GaSb_{1-x}Bi_x$ layer was grown under the identical growth conditions as the 200 nm thick sample grown at 380 ºC. To the contrary, the $GaSb_{1-x}Bi_x$ layer peak appears at the left side of the GaSb substrate, which is shown as the top curve in Fig. 3(c), indicating a larger lattice constant as expected. To evaluate the evolution of lattice constant with GaSbBi layer thickness, we etched down the sample at four different depths. As found in Fig. 3(c), the $GaSb_{1-x}Bi_x$ peak moves towards the GaSb substrate peak and eventually to the right side and becomes lower and broader at the same time when the $GaSb_{1-x}Bi_x$ layer thickness is reduced. The interference fringes are observed in the un-etched sample, but lost in the etched samples due to the rough etched surface. This observation supports the model discussed above. Bi segregation occurs in the beginning of the GaSbBi growth leading to lattice contraction. It becomes weak with the film thickness and eventually stops when the Bi surface accumulation is high enough. For later growth, the incorporated Bi atoms will occupy lattice sites causing lattice dilation as expected.

In conclusion, MBE growth of $GaSb_{1-x}Bi_x$ thin films is demonstrated for the first time. Bi incorporation is confirmed by RBS and SIMS measurements. The Bi composition increases with increasing Bi flux/T_g and tends to saturate above 370 ºC. The highest Bi composition is 0.7% measured by RBS. Lattice contraction was observed from XRD measurements. The lattice constant of the $GaSb_{1-x}Bi_x$ layer decreases with T_g up to 380 ºC with maximum tensile strain of 0.084%, although the incident Bi BEP increases at the same time. We propose that the lattice contraction is due to vacancies caused by Bi segregation.

ACKNOWLEDGMENT

The Swedish Research Council (VR) is acknowledged for financial support for this project.

REFERENCES

1 Francoeur, S.; Seong, M. J.; Mascarenhas, A.; Tixier, S.; Adamcyk, M.; Tiedje, T. *Appl. Phys. Lett.* **2003**, 82, 3874-3876.

2 Alberi, K.; Wu, J.; Walukiewicz, W.; Yu, K.; Dubon, O.; Watkins, S.; Wang, C.; Liu, X.; Cho, Y. J.; Furdyna, J. *Phys. Rev. B* **2007**, 75, 045203.

3 Zilko, J.; Greene, J. *Appl. Phys. Lett.* **1978**, 33, 254-256.

4 Oe, K.; Ando, S.; Sugiyama, K. *Jpn. J. Appl. Phys.* **1981**, 20, L303-L306.

5 Noreika, A.; Takei, W.; Francombe, M.; Wood, C. *J. Appl. Phys.* **1982**, 53, 4932-4937.

6 Oe, K.; Okamoto, H. *Jpn. J. Appl. Phys.* **1998**, 37, L1283-L1285.

7 Tixier, S.; Adamcyk, M.; Tiedje, T.; Francoeur, S.; Mascarenhas, A.; Wei, P.; Schiettekatte, F. *Appl. Phys. Lett.* **2003**, 82, 2245-2247.

8 Fluegel, B.; Francoeur, S.; Mascarenhas, A.; Tixier, S.; Young, E. C.; Tiedje, T. *Phys. Rev. Lett.* **2006**, 97, 67205.

9 Alberi, K.; Dubon, O. D.; Walukiewicz, W.; Yu, K. M.; Bertulis, K.; Krotkus, A. *Appl. Phys. Lett.* **2007**, 91, 051909.

10 Sweeney, S. 1st International Workshop on Bismuth-Containing Semiconductors: Theory, Simulation, and Experiment, Michigan, USA, **2010**

11 Dutta, P. S.; Bhat, H. L.; Kumar, V. *J. Appl. Phys.* **1997**, 81, 5821-5870.

12 Hosoda, T.; Kipshidze, G.; Tsvid, G.; Shterengas, L.; Belenky, G. *IEEE Photonics Technol. Lett.* **2010**, 22, 718-720.

13 Vurgaftman, I.; Meyer, J. R.; Ram Mohan, L R. *J. Appl. Phys.* **2001**, 89, 5815-5875.

14 Gladkov, P.; Monova, E.; Weber, J. *J. Cryst. Growth* **1995**, 146, 319-325.

15 Danilewsky, A.; Lauer, S.; Meinhardt, J.; Benz, K.; Kaufmann, B.; Hofmann, R.; Dornen, A. *J. Elec. Mater.* **1996**, 25, 1082-1087.

16 Lee, J.; Razeghi,J. M. *Opto-Electron. Rev.* **1998**, 6, 25-36.

17 Wagener, M. C.; Botha, J. R.; Leitch, A. W. R. *J. Cryst. Growth* **2000**, 213, 51-56.

18 Kajikawa, Y.; Asahina, S.; Kanayama, N. *Jpn. J. Appl. Phys.* **2001**, 40, 28-33.

19 Karam, N.; Sudharsanan, R.; Parodos, T.; Dodd, M. *J. Elec. Mater.* **1996**, 25, 1209-1214.

20 Ferhat, M.; Zaoui, A. *Phys. Rev. B* **2006**, 73, 115107.

21 Moison, J. M.; Guille, C.; Houzay, F.; Barthe, F.; Rompay, M. V. *Phys. Rev. B* **1989**, 40, 6149-6162.

22 Kaspi, R. K.; Evans, R. *J. Cryst. Growth* **1997**, 175-176, 838-843.

23 Tixier, S.; Adamcyk, M.; Young, E. C.; Schmid, J. H.; Tiedje, T. *J. Cryst. Growth* **2003**, 251, 449-454

Figure captions:

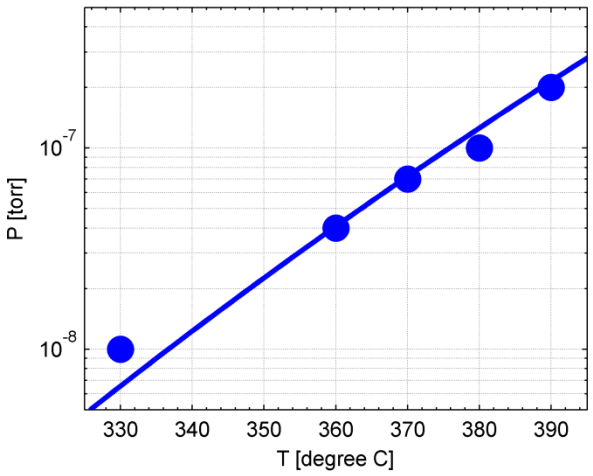

(a)

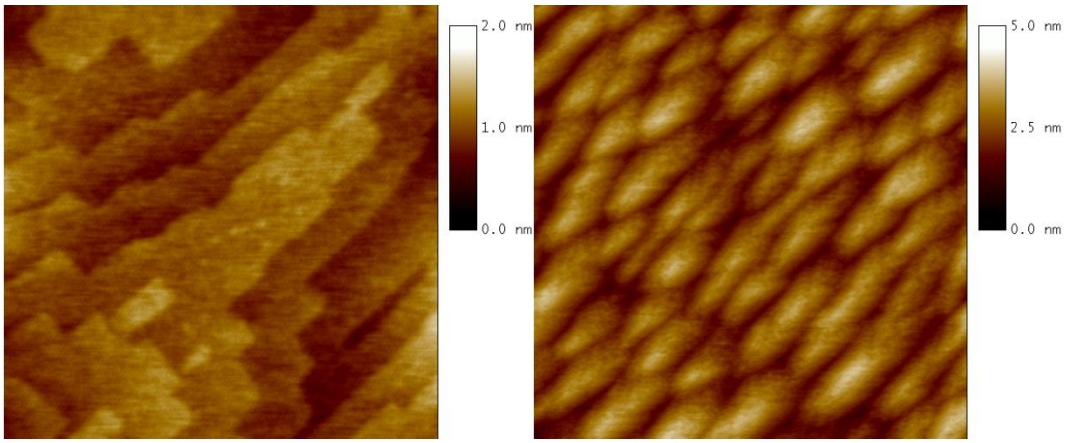

(b) (c)

Figure 1. (a) Bi vapor pressure vs. temperature (line) and selected growth temperatures at particular Bi BEPs for the samples (round dots). AFM image of $GaSb_{1-x}Bi_x$ sample grown at 380°C: (b) 1×1 μm^2 and (c) 10×10 μm^2.

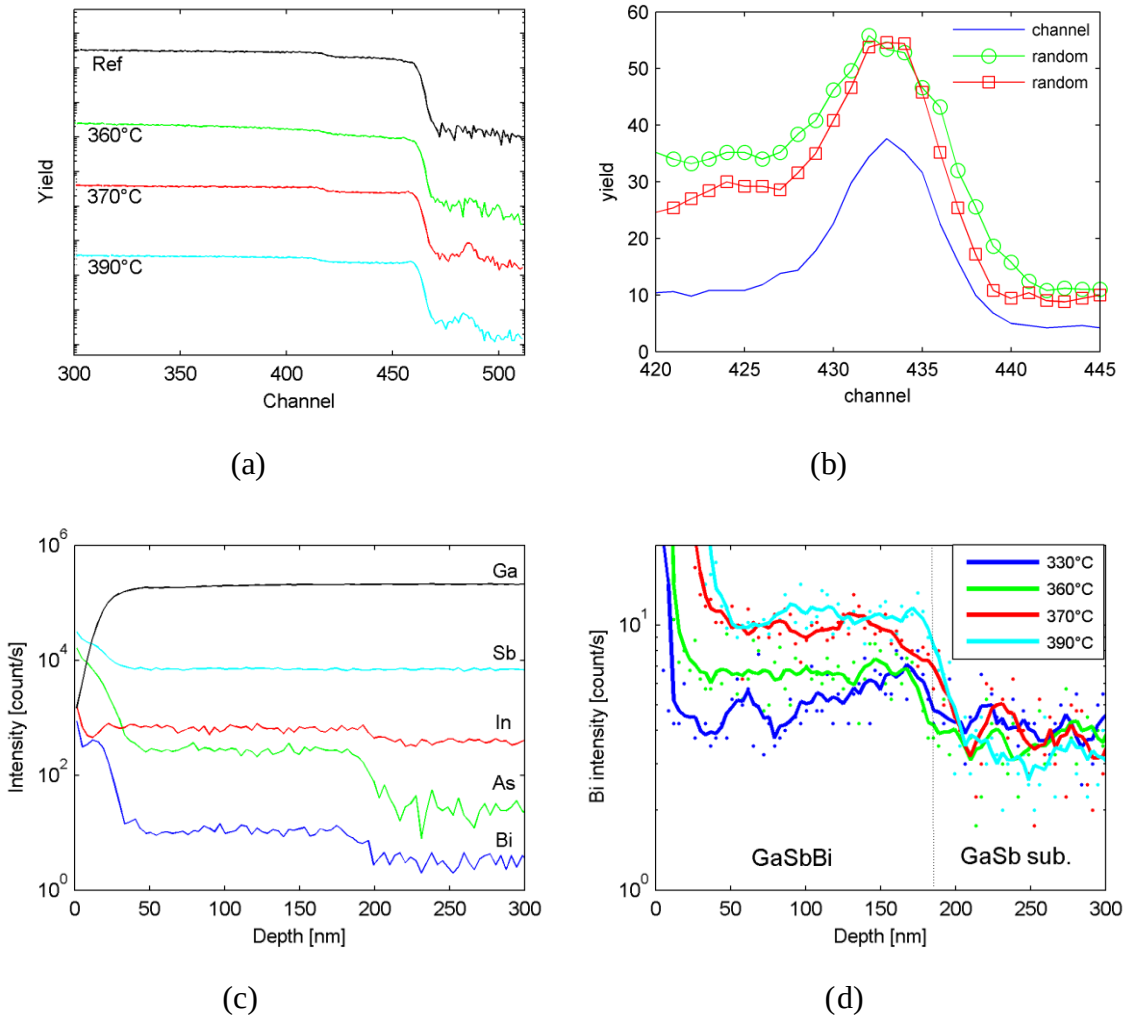

Figure 2. (a) RBS spectra of the Ref sample and the samples grown at 360 ºC, 370 ºC and 390 ºC. (b) RBS channeling result (focusing on the Bi signal) for the sample grown at 390 ºC. The green circled and red squared curves are from two random measurements and the blue solid curve is from the channeled measurement. (c) SIMS profiles of different elements in the sample grown at 390 ºC. (d) Bi profiles from SIMS in the $GaSb_{1-x}Bi_x$ samples. Dots are measurement data and the solid curves are obtained from five-point-smoothening of the measurement data.

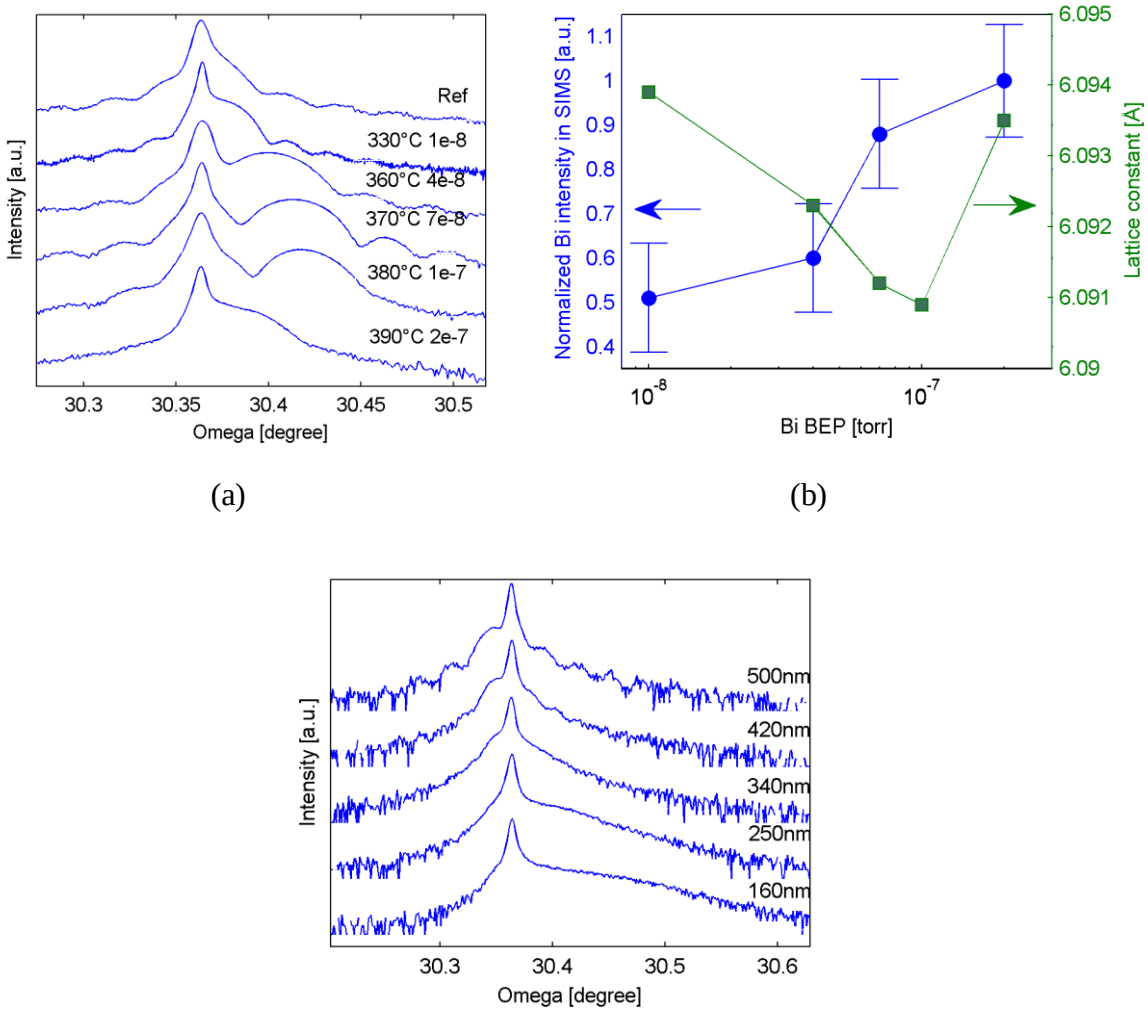

Figure 3. (a)XRD (004) rocking curves of the samples (logarithmic scale). Labels to the low-right of each curve indicate the growth temperature and the Bi BEP. (b) Trends of Bi concentration obtained from SIMS measurements and the lattice constant of the $GaSb_{1-x}Bi_x$ samples deduced from XRD. (c) XRD (004) rocking curves of a thick sample (500 nm) with different etching depths. The labels above each curve indicate the remaining layer thickness from the interface.